

The role of interception in the hydrological cycle

Miriam GERRITS

The role of interception in the hydrological cycle

Proefschrift

ter verkrijging van de graad van doctor
aan de Technische Universiteit Delft,
op gezag van de Rector Magnificus prof. ir. K.C.A.M. Luyben,
voorzitter van het College voor Promoties

in het openbaar te verdedigen op dinsdag 14 september 2010 om 10:00 uur

door

Anna Maria Josephina GERRITS

Civiel ingenieur
geboren te Haarlem

Dit proefschrift is goedgekeurd door de promotor:

Prof. dr. ir. H.H.G. Savenije

Samenstelling promotiecommissie:

Rector Magnificus, *voorzitter*

Prof. dr. ir. **H.H.G. Savenije**, *Technische Universiteit Delft, promotor*

Prof. **G. Jewitt**, *University of KwaZulu-Natal, South Africa*

Prof. dr. **L.A. Bruijnzeel**, *Vrije Universiteit Amsterdam*

Prof. dr. ir. **R. Uijlenhoet**, *Universiteit Wageningen*

Prof. dr. **S. Uhlenbrook**, *Technische Universiteit Delft en UNESCO-IHE*

Prof. dr. **W.G.M. Bastiaanssen**, *Technische Universiteit Delft*

Dr. **L. Pfister**, *Gabriel Lippmann Research Center, Luxembourg*

Prof. dr. ir. **N.C. van de Giesen**, *Technische Universiteit Delft*

Dr. L. Pfister heeft als begeleider in belangrijke mate aan de totstandkoming van het proefschrift bijgedragen.

The research described in this dissertation was performed at the Water Resources Section, Faculty of Civil Engineering and Geosciences, Delft University of Technology, and at the Gabriel Lippmann Research Center, Luxembourg. The Ministry of Culture, Higher Education and Research of Luxembourg (FNR) and Delft Cluster, the Netherlands are thanked for providing financial support.

Copyright by A.M.J. Gerrits, 2010

Published by VSSD, Delft, the Netherlands

All rights reserved. No part of this publication may be reproduced, stored in a retrieval system, or transmitted, in any form or by any means, electronic, mechanical, photo-copying, recording, or otherwise, without the prior written permission of the publisher.

ISBN: 978-90-6562-248-8

Keywords: canopy interception, forest floor interception, evaporation, Budyko curve, hillslope hydrology

Preface

Most people who know me think that my joy in field work started with the first field course to the Maisbich in Luxembourg in 2002. However, they are a bit wrong: the credits belong to my old high school geography teacher Van Ingen, who organised a one week field trip to Orvelte in Drenthe (the Netherlands) to ‘experience’ the characteristics of the Dutch sand landscape. Soil profiles were taken, ground water levels and surface topography were measured, the flora was described and the relation with the current spatial landscape organisation was made. Besides the social aspects, that I liked, I noticed that it increased my understanding and that the theory assimilated much better. I was happy that during my university studies I ended in a department that encourages field work.

Although I realise that the social and didactic aspect is personal, field work has an added value for all hydrological studies. Every hydrological question starts with ‘which processes do influence my problem, how do they work, and how do they interact with each other?’. Even if the processes are theoretically known, a modeller with field experience is better able to understand the hydrological system, knows the value of his input and output data, and has better insight in his model behaviour.

Experimental work was also the basis for this thesis. To answer the question what role interception plays in the hydrological cycle, measuring was a logical first step. Especially, since we did not want to investigate only the often studied canopy interception. We also wanted to look at interception on the forest floor and the interaction between the two interception types. Three locations were equipped to measure interception with the focus on forest floor interception. The grass and moss setup in Westerbork (Netherlands) was the first one in October 2004, shortly followed by the beech leaves setup in the Huewelerbach (Luxembourg), both built by Udo Brandt. Two years later the setup in the botanical garden (Netherlands) with cedar needles was born. With the three setups the most dominant vegetation species in Europe were covered, but the world is bigger... By the end of 2007 two new setups were installed in Harare, Zimbabwe to investigate Thatching grass and Msasa leaf interception in a Savannah climate.

So after the equipment was in place, I was ready to collect my data for analysing and modelling, but unfortunately I had to learn a hard lesson first: the practical implementation of Murphy’s Law. It appeared that lots of things that can go wrong also will go wrong. Except for storm

Xynthia in February 2010. She damaged a tree inside the plot that collapsed and missed the forest floor device by just one meter. After dealing with Mr Murphy, I finally obtained my first data records.

All efforts of driving 60.000 km to the field sites, carrying heavy batteries, reading out the data loggers with my favorite laptop, digging in frozen soils, reading out and cleaning the 81 manual throughfall collectors, constructing a ten meter high meteorological tower with an immense concrete foundation, and replacing almost all components, resulted just in eight figures in this thesis. This seems to be limited and is also much less then I expected at the beginning of my PhD. However, the field experiments taught me to understand the interception process and provided me data to test my hypotheses. Furthermore by regularly visiting the field sites I observed new things that explained my measurements.

In the end, the three setups enabled me to study interception at a small temporal and spatial scale and I discovered the dominant drivers of interception. By applying different model concepts at different scales, based on field observations, I investigated the way interception influences the water balance.

I hope that my thesis helps to make modellers aware of the importance of interception and the consequences of neglecting interception. It is the first process after rainfall in the hydrological cycle and therefore has an impact on all subsequent processes. Although percentage-wise the interception flux may be small, it still can influence other processes significantly due to non-linearities in the rainfall-runoff system. This thesis hopefully contributes to the understanding of interception and shows the influence it has on the subsequent processes.

Miriam Gerrits

Delft, June 2010

<http://www.interception.citg.tudelft.nl/>

Summary

Interception is the part of the rainfall that is intercepted by the earth's surface and which subsequently evaporates. In this definition the earth's surface includes everything that becomes wet after a rainfall event and that dries out soon after. It includes: vegetation, soil surface, litter, build-up surface, etc. How much of the precipitation evaporates depends on land cover characteristics, rainfall characteristics, and on the evaporative demand. Interception can amount up to 15-50% of precipitation, which is a significant part of the water balance. One can distinguish many types of interception, which can also interplay with each other. For example canopy, forest floor, fog, snow, and urban interception. This study we focus on canopy and forest floor interception. We measured interception of three dominant European vegetation types at three locations. In the Huewelerbach (Luxembourg) a beech forest has been investigated, in Westerbork (the Netherlands) grasses and mosses, and in the Botanical Garden (Delft, the Netherlands) a Cedar tree. Canopy interception is determined by the difference between gross precipitation and the sum of throughfall and stemflow. To measure forest floor interception a special device has been developed. It consists of two aluminium basins which are mounted above each other. The upper basin is permeable and contains the forest floor. By weighing both basins simultaneously, evaporation from interception can be calculated.

For the beech forest we found that canopy interception has a clear seasonal trend ranging from 15% of rainfall in summer to 7% in winter. On the other hand, forest floor interception appears to be constant over the year and evaporates on average 22% of precipitation. Evaporation from the Cedar needle floor is only a bit lower: 18%, although the storage capacity is significantly lower: 1.0 mm for the needle floor compared to 1.8 mm for beech leaves.

Both interception thresholds have a coefficient of variation as high as $\pm 100\%$. However, the interception process is not sensitive to this variability, resulting only in 11% variation of evaporation estimates for the beech forest. Hence the number of raindays and the potential evaporation are stronger drivers of interception. Furthermore, the spatial correlation of the throughfall and infiltration has been investigated with semi-variograms and time stability plots. Within 6-7 m distance throughfall and infiltration are correlated and the general persistence is weak.

The effect of spatial variability of interception on subsurface storm flow has also been investigated with a virtual experiment. A virtual experiment is a numerical experiment driven by collective

field intelligence. It provides a learning tool to investigate the effect of separated processes in a complex system. We used this approach to better understand the generation and behaviour of subsurface stormflow (SSF) at the hillslope scale, because this is still poorly understood. Interactions between the permeable soil and the less permeable bedrock may cause non-linearity in subsurface flow depending on several hillslope attributes such as soil depth, slope angle, and bedrock permeability. It is known that the size of storm events also controls subsurface flow generation. The objectives of this study were three-fold: 1) to investigate if and how different configurations of throughfall patterns change the SSF behaviour; 2) to investigate the interplay between the spatially variable input and the hillslope attributes (slope angle and soil depth) on the generation of SSF; and 3) to investigate a geo-statistical tool that uses semi-variogram characteristics to analyse if soil moisture patterns during an event are dominated by throughfall patterns or by bedrock topography patterns.

In our virtual experiment we combined spatial throughfall data from the Huewelerbach catchment in Luxembourg with the topography characteristics of the Panola hillslope in Georgia, USA. We used HYDRUS-3D as a modeling platform. The effect of the spatial throughfall pattern appears to be large on both SSF generation and the spatial variability of SSF along the hillslope, but only marginal on total SSF amounts. The spatial variability of SSF along the hillslope appears to be closely related to the drainage pattern of the bedrock. The geo-statistical analysis indicates that during the event soil moisture distribution reflects throughfall patterns, whereas after the event, during the drainage of the hillslope, the bedrock topography increasingly dominates soil moisture patterns.

Furthermore, we found that on a daily time scale, interception is a typical threshold process. We used this characteristic to upscale daily interception to an annual evaporation model and found similarities with the Budyko curve. The Budyko curve is often used to estimate the actual evaporation as a function of the aridity index in a catchment. Different empirical equations exist to describe this relationship; however, these equations have very limited physical background. Our model concept is physically based and uses only measurable parameters. It makes use of two types of evaporation: interception and transpiration. Interception is modeled as a threshold process at a daily time scale. If multiplied with the rainfall distribution function, integrated, and multiplied with the expected number of rain days per month, the monthly interception is obtained. In a similar way, the monthly interception can be upscaled to annual interception. This results in a Budyko-type equation. Analogous to the interception process, transpiration can be modeled as a threshold process at a monthly time scale and can be upscaled by integration and multiplication with the expected number of rain months. The expected rain days per month are modeled in two ways: as a fixed proportion of the monthly rainfall and as a power function based on Markov properties of rainfall. The latter is solved numerically. It appears that on an annual basis the analytical model does not differ much from the numerical solution. Hence, the analytical model is used and applied on 10 locations in different climates. We show that the empirical Budyko curve can be constructed on the basis of measurable parameters representing

evaporation threshold values and the expected number of rain days and rain months and, in addition, a monthly moisture carry-over amount for semi-arid zones.

Overall, we can conclude that interception has different roles in the hydrological cycle. The most important role is as a rainfall reducer, causing a significant amount of rainfall to be directly fed back to the atmosphere which is not available for infiltration. Second, interception influences the spatial distribution of infiltration. This has large influences on the soil moisture pattern and on subsurface flow paths. Finally, interception redistributes the water flows in time. Due to the filling of the spatial variable storage capacity and rainfall, the delay time is not homogeneous in space.

This thesis shows that interception is a key process in the hydrological cycle. It involves significant fluxes in the water balance and influences the subsequent processes both in quantity and timing. It is an important cause for non-linear behaviour of catchments. The role of interception in the hydrological cycle is crucial.

Samenvatting

Interceptie is dat deel van de neerslag dat onderschept wordt door het aardoppervlak en vervolgens verdampt. Volgens deze definitie bestaat het aardoppervlak uit alles dat nat wordt na een regenbui en snel weer opdroogt. Het bevat: vegetatie, de bovenste laag van de bodem, de strooisellaag, de bebouwde omgeving, etc. De hoeveelheid neerslag die verdampt hangt af van het landgebruik, regenkarakteristieken en van de verdampingsvraag. Vijftien tot vijftig procent van de neerslag kan verdampen door interceptie, wat een significant deel van de waterbalans is. Men kan verschillende interceptietypes onderscheiden die elkaar ook kunnen beïnvloeden. Voorbeelden van interceptietypes zijn: boomkruin, strooisellaag (bosondergrond), mist, sneeuw, verhard oppervlak en stedelijke interceptie. Deze studie richt zich op interceptie door de boomkruin en de strooisellaag. We hebben voor drie overheersende Europese vegetatietypes interceptie gemeten op drie verschillende locaties. In de Huewelerbach (Luxemburg) is een beukenbos onderzocht, in Westerbork (Nederland) gras en mos en in de botanische tuin (Delft, Nederland) een Ceder boom. Interceptie van bomenkruinen wordt bepaald door het verschil tussen de bruto neerslag en de som van de doorval en de neerslag die via de boomstam afstroomt. Voor het meten van interceptie van de strooisellaag is een speciale meetopstelling ontwikkeld. Deze bestaat uit twee aluminium bakken die boven elkaar hangen. De bovenste bak is waterdoorlatend en bevat de strooisellaag. Door beide bakken gelijktijdig te meten kan de interceptieverdamping worden berekend.

Voor het beukenbos hebben we gevonden dat de interceptie van bomen een duidelijke seizoenstrend heeft variërend van 15% van de neerslag in de zomer tot 7% in de winter. Daarentegen blijkt dat interceptie van de strooisellaag constant over het jaar is met gemiddeld 22% van de neerslag. Verdamping van het Ceder naaldendek is iets lager: 18%, hoewel de bergingscapaciteit beduidend lager is: 1.0 mm voor het naaldendek vergeleken met 1.8 mm voor de beukenbladeren.

Beide interceptiedrempels hebben een variatie-coëfficiënt van maar liefst $\pm 100\%$. Echter het interceptieproces is niet gevoelig voor deze variabiliteit en resulteert daarom slechts in 11% spreiding in verdampingsschattingen voor het beukenbos. Het aantal regendagen en de potentiële verdamping zijn dus sterkere invloedsfactoren op interceptie. Verder is de ruimtelijke correlatie van de doorval en infiltratie onderzocht met semi-variogrammen en persistentiegrafieken. Binnen 6-7 m afstand zijn doorval en infiltratie gecorreleerd en is de algemene persistentie zwak.

Het effect van ruimtelijke variabiliteit op de ondiepe grondwaterstroming (subsurface flow, SSF) is ook onderzocht met een virtueel experiment. Een virtueel experiment is een numeriek experiment dat wordt gedreven door collectieve veldkennis. Het is een leerinstrument dat het mogelijk maakt om effecten van verschillende processen in een complex systeem te kunnen onderzoeken. Deze aanpak is gebruikt om het ontstaan en het gedrag van SSF op hellingsschaal beter te begrijpen, omdat dit nogsteeds slecht begrepen wordt. Interactie tussen de doorlatende bodem en de minder doorlatende moedergesteente kunnen niet-lineairiteiten veroorzaken in de SSF afhankelijk van verschillende eigenschappen van de helling, zoals bodemdiepte, hellingshoek en doorlatendheid van het moedergesteente. Het is bekend dat de grootte van regenbuien ook het ontstaan van SSF controleert. Het doel van deze studie is drievoudig: 1) onderzoeken of en hoe verschillende configuraties van doorvalpatronen het gedrag van SSF veranderen; 2) onderzoek naar de interactie tussen ruimtelijke variabele invoer en de hellingseigenschappen (hellingshoek en bodemdiepte) op het ontstaan van SSF; en 3) onderzoek naar een geo-statistische analyse die gebruik maakt van semi-variogramkarakteristieken om te analyseren of bodemvochtpatronen tijdens een bui worden gedomineerd door doorvalpatronen of door de topografie van het moedergesteente.

In ons virtueel experiment hebben we ruimtelijke doorval van het Huewelerbach stroomgebied in Luxemburg gecombineerd met de topografiekenarakteristieken van de Panola-helling in Georgia, VS. HYDRUS-3D is gebruikt als modelplatform. Het effect van het ruimtelijk doorvalpatroon blijkt voor zowel het ontstaan van SSF als voor de ruimtelijke spreiding van SSF groot, maar slechts marginaal op het totale SSF volume. De ruimtelijke spreiding van SSF blijkt nauw gerelateerd aan het afstroompatroon van het moedergesteente. De geo-statistische analyse geeft aan dat tijdens een bui de verdeling van het bodemvocht het doorvalpatroon volgt, waar na de bui de topografie van het moedergesteente belangrijker wordt.

Verder hebben we gevonden dat op dagbasis interceptie een typisch drempelproces is. Gebruik makend van dit kenmerk hebben we dagelijkse interceptie opgeschaald naar een jaarlijks verdampingsmodel en hebben overeenkomsten gevonden met de Budyko curve. De Budyko curve wordt vaak gebruikt om de actuele verdamping als functie van de droogte-index te schatten voor een stroomgebied. Verschillende empirische vergelijkingen bestaan voor het beschrijven van deze relatie, echter deze vergelijkingen hebben een beperkte fysische grondslag. Ons modelconcept is fysisch gebaseerd en maakt alleen gebruik van meetbare parameters. Het model bestaat uit twee verdampingstypes: interceptie en transpiratie. Interceptie wordt op dagbasis gemodelleerd als een drempelproces. Als dit wordt vermenigvuldigd met de distributiefunctie van de regen, geïntegreerd en vermenigvuldigd met het verwachte aantal regendagen per maand, krijgt men de maandelijkse interceptieverdamping. Op eenzelfde manier kan de maandelijkse interceptie worden opgeschaald naar jaarlijkse interceptie. Dit resulteert in een Budyko-achtige vergelijking. Analooq aan het interceptieproces kan transpiratie op maandbasis worden gemodelleerd als een drempelproces en kan vervolgens worden opgeschaald door te integreren en te vermenigvuldigen met het aantal verwachte regenmaanden. Het aantal verwachte regendagen per jaar maand is

op twee manieren gemodelleerd: als een vast percentage van de maandelijkse neerslag en als een machtsfunctie op basis van de Markov eigenschappen van neerslag. Deze laatste is numeriek opgelost. Het blijkt dat op jaarbasis het analytische model niet veel verschilt van de numerieke oplossing. Dus hebben we het analytische model gebruikt en toegepast op tien locaties in verschillende klimaten. We laten zien dat de empirische Budyko curve kan worden verkregen op basis van enkel meetbare parameters: verdampingsdrempels, aantal verwachte regendagen en regenmaanden en nog een maandelijkse vochtsoverdrachtsfunctie voor de semi-aride gebieden.

Samenvattend kunnen we concluderen dat interceptie verschillende rollen heeft in de hydrologische kringloop. De meest belangrijke rol is die van regenverminderaar, wat tot gevolg heeft dat een aanzienlijke hoeveelheid regen direct terug wordt gebracht naar de atmosfeer en dus niet beschikbaar is voor infiltratie. Ten tweede beïnvloedt interceptie de ruimtelijke spreiding van infiltratie. Dit heeft grote invloed op het bodemvocht patroon en op de stroompaden van ondiepe grondwaterstroming. Tenslotte herverdeelt interceptie het water in de tijd. Door het vullen van de ruimtelijk variabele bergingscapaciteit van de neerslag is de vertraging ruimtelijk niet homogeen.

Dit proefschrift laat zien dat interceptie een sleutelproces in de hydrologische kringloop is. Het is een belangrijke flux in de waterbalans en beïnvloedt opvolgende processen zowel in hoeveelheid als in timing. Het is een belangrijke reden voor niet-lineair gedrag in stroomgebieden. De rol van interceptie in de hydrologische kringloop is cruciaal.

List of Symbols

A	Monthly moisture carry over for transpiration ($L T^{-1}$)
b	Constant in Rutter (1971) model (L^{-1})
B	Slope of relation between monthly effective rainfall and monthly transpiration (-)
B_r	Bowen ratio (-)
c	Canopy coverage (-)
c	Sill in Ch. 3 and 4 (-)
c_p	Specific heat ($L M T^{-3} K^{-1}$)
d	Constant in Rutter model for drainage (L^{-1})
D	Drainage rate from the canopy ($L T^{-1}$)
D_i	Interception threshold ($L T^{-1}$)
D_t	Transpiration threshold ($L T^{-1}$)
D_0	Constant drainage rate ($L T^{-1}$)
E	Actual evaporation ($L T^{-1}$)
E_i	Interception evaporation ($L T^{-1}$)
$E_{i,c}$	Interception evaporation from canopy ($L T^{-1}$)
$E_{i,c}^l$	Evaporation from leaves (without trunk) ($L T^{-1}$)
$E_{i,c}^t$	Evaporation from the trunk ($L T^{-1}$)
$E_{i,f}$	Interception evaporation from forest floor ($L T^{-1}$)
E_l	Evaporation from lower basin ($L T^{-1}$)
E_o	Open water evaporation ($L T^{-1}$)
E_p	Potential evaporation ($L T^{-1}$)
E_s	Soil evaporation ($L T^{-1}$)
E_t	Transpiration ($L T^{-1}$)
f	Constant in Rutter model for infiltration (L^{-1})
F	Infiltration ($L T^{-1}$)
F_0	Constant infiltration rate ($L T^{-1}$)
G	Ground heat flux ($M T^{-3}$)
h	Lag (L)
H	Sensible heat flux ($M T^{-3}$)
I	Interception process ($L T^{-1}$)
I	Irradiance in Ch. 3 ($M T^{-3}$)
k	Extinction coefficient (-)
L	Number of elemental surface areas per unit ground (L^{-2})
LAI	Leaf Area Index (-)
m	Mean number of raindrops striking an element (-)
n	Mean number of drops retained per element (-)
n	Number of measurement pairs in Ch. 3 and 4 (-)
n_a	Months within year (= 12) (-)
n_m	Days within a month (= 30.5) (-)
$n_{nr,m}$	Number of net rain months per year (-)
$n_{r,d}$	Number of rain days per month (-)

$n_{r,m}$	Number of rain months per year (-)
N	Throughfall or infiltration per interval ($L T^{-1}$)
p	Throughfall coefficient (-)
p_t	Trunk fraction coefficient (-)
P	Precipitation ($L T^{-1}$)
P_g	Gross precipitation ($L T^{-1}$)
P'_g	Gross precipitation necessary for canopy saturation ($L T^{-1}$)
P''_g	Gross precipitation necessary for trunk saturation ($L T^{-1}$)
Q	Discharge ($L^3 T^{-1}$)
q	Specific humidity in Ch. 1 ($M T^{-1} L^{-1}$)
q	Maximum amount of rain drops on element in Ch. 1 (-)
q	Constant in Ch. 5
r	Amount of rain drops on element in Ch. 1 (-)
r	Range in Ch. 3 and 4 (L)
r	Power in Ch. 5
R_n	Net radiation ($M T^{-3}$)
S	Storage (L)
S_b	Available soil moisture content at the boundary between moisture constrained transpiration and potential transpiration (L)
S_c	Storage of canopy (L)
S_c^l	Storage of leaves (without trunk) (L)
S_c^t	Storage of trunk (L)
S_f	Storage of forest floor (L)
S_i	Interception storage (L)
S_l	Storage of the lower basin (L)
S_u	Storage of the upper basin (L)
T	Temperature ($^{\circ}C$)
T_f	Throughfall ($L T^{-1}$)
T_s	Stemflow ($L T^{-1}$)
u	Constant in Ch. 5
v	Mean volume of raindrops in Ch. 1 (L^3)
v	Power in Ch. 5
z	Height (L)
β	Scaling factor for daily rainfall ($L T^{-1}$)
γ	Time scale for transpiration ($=S_b/D_{t,m}$) (T)
γ	Variance in Ch. 3 and 4 (-)
ϵ	Constant in Rutter (1971) model (-)
θ	Potential temperature (K)
κ_i	Scaling factor for monthly interception ($L T^{-1}$)
κ_m	Scaling factor for monthly rainfall ($L T^{-1}$)
κ_n	Scaling factor for monthly net rainfall ($L T^{-1}$)
λ	Latent heat of vaporization coefficient ($L^2 T^{-2}$)

ρ	Density of water (M L^{-3})
ϕ	Aridity index (-)

List of Subscripts

a	annual
d	daily
max	maximum
m	monthly
n	net
p	potential

Contents

Preface	v
Summary	vii
Samenvatting	xi
List of Symbols	xiv
1 Introduction	1
1.1 <i>Background</i>	2
1.2 <i>Importance of interception</i>	3
1.3 <i>Interception storage types</i>	4
1.3.1 Canopy interception	4
1.3.2 Forest floor interception	8
1.4 <i>Special interception cases</i>	8
1.4.1 Agricultural interception	8
1.4.2 Fog interception	8
1.4.3 Snow interception	11
1.4.4 Urban interception	11
1.5 <i>Methods to measure interception</i>	12
1.5.1 Canopy	12
1.5.2 Forest floor	13
1.6 <i>Interception models</i>	14
1.6.1 Conceptual Rutter model	14
1.6.2 Analytical Gash model	16
1.6.3 Stochastic interception models	18
1.7 <i>Consequences of underestimating interception for hydrological modelling and water resources assessment</i>	21
1.8 <i>Problem definition and study objectives</i>	22
1.9 <i>Thesis outline</i>	23
2 Methods and materials	25
2.1 <i>Instrumentation</i>	26
2.1.1 Throughfall	26
2.1.2 Stemflow	26

2.1.3	Leaf Area Index (LAI)	27
2.1.4	Forest floor interception device	28
2.2	<i>Study areas</i>	31
2.2.1	Huewelerbach	31
2.2.2	Westerbork	32
2.2.3	Botanical Garden	33
3	Spatial and temporal variability of canopy and forest floor interception	35
3.1	<i>Introduction</i>	36
3.2	<i>Methodology</i>	37
3.3	<i>Temporal variation in interception measurements</i>	40
3.3.1	Canopy interception	40
3.3.2	Forest floor interception	41
3.4	<i>Temporal variation in storage capacity</i>	43
3.4.1	Canopy interception	44
3.4.2	Forest floor interception	45
3.5	<i>Effect of variability in storage capacity on Rutter model predictions</i>	48
3.6	<i>Daily threshold model</i>	53
3.7	<i>Spatial variation in throughfall and infiltration</i>	54
3.8	<i>Conclusions</i>	57
4	The effect of spatial throughfall patterns on soil moisture patterns and the generation of subsurface stormflow	61
4.1	<i>Introduction</i>	62
4.2	<i>Method and materials</i>	63
4.2.1	Approach	63
4.2.2	Study sites and selected rainstorm event and pattern	65
4.2.3	Model description of base case scenario	67
4.3	<i>Results and discussion</i>	69
4.3.1	Pattern configuration	69
4.3.2	Interplay hillslope attributes on subsurface storm flow	71
4.3.3	Spatial pattern of soil moisture content	74
4.4	<i>Conclusions</i>	79
5	Analytical derivation of the Budyko curve based on rainfall characteristics and a simple evaporation model	81
5.1	<i>Introduction</i>	82
5.2	<i>Methodology</i>	85
5.2.1	Data	86
5.3	<i>Analytical derivation without Markov properties</i>	86
5.3.1	Monthly interception equation (analytical)	86
5.3.2	Annual interception equation (analytical)	88
5.3.3	Annual transpiration equation (analytical)	90

5.3.4	Total evaporation (analytical)	93
5.4	<i>Numerical derivation with Markov properties</i>	94
5.4.1	Monthly interception equation (analytical/numerical)	94
5.4.2	Annual interception equation (numerical)	96
5.4.3	Annual transpiration equation (numerical)	96
5.4.4	Total evaporation (numerical)	96
5.5	<i>From evaporation model to Budyko curve</i>	98
5.6	<i>Discussion</i>	99
5.7	<i>Conclusions</i>	101
6	Conclusions and Recommendations	105
6.1	<i>The role of interception in the hydrological cycle</i>	106
6.2	<i>Outlook</i>	109
	Acknowledgements	123
	Curriculum Vitae	125

Chapter 1

Introduction

.....

Interception is the part of the rainfall that is intercepted by the earth's surface and which subsequently evaporates. In this definition the earth's surface includes everything that becomes wet after a rainfall event and that dries out soon after. It includes: vegetation, soil surface, litter, build-up surface, etc. How much of the precipitation evaporates depends on land cover characteristics, rainfall characteristics, and on the evaporative demand. Interception can amount up to 15-50% of precipitation, which is a significant part of the water balance. One can distinguish many types of interception which can also interplay with each other. In this chapter rainfall interception of the canopy and forest floor are described and special interception cases like agricultural, fog, snow and urban interception are described. Also different techniques to measure canopy and forest floor interception are described. To model interception three kinds of models are explained. First, the conceptual Rutter model and its revised sparse canopy version. Second, the often used analytical Gash (original and revised sparse canopy version) model, and finally three stochastically based models are explained. We end with the consequences of underestimating interception in hydrological modelling and water resources assessments.

.....

Based on: Gerrits, A. M. J., Savenije, H. H. G., 2010 (in press)b. Treatise on Water Science. Elsevier, Ch. Interception; and Gerrits, A. M. J., Savenije, H. H. G., 2010 (in press)a. Forest Hydrology and Biogeochemistry. Springer-Verlag, Ch. Forest floor interception

1.1 Background

When it rains the entire surface becomes wet: trees, shrubs, grass, forest floor, footpaths, etc. Also in urban areas roads and roofs become wet, sometimes forming pools of stagnant water. After rainfall has ceased these surfaces soon become dry again. This process is called interception. It is the part of the rainfall that is captured by surface storage (i.e. vegetation, roofs, etc.) before it can runoff or infiltrate into the soil. The intercepted water generally evaporates during the event and shortly after the rainfall ceased, so that it can repeat its function during the next rainfall event.

In the literature, interception is defined in different ways: sometimes as a stock, sometimes as a flux or more appropriately, as the entire interception process (Savenije [2005]). If only interception storage (S_i [L]) is considered, interception is defined as the amount of rainfall which is temporarily stored on the earth's surface. Actually, this is the interception capacity or water holding capacity. If interception is defined as a flux, then it is the intercepted water which evaporated over a certain time [L T^{-1}] during and after the event. When interception is considered as a process (I [L T^{-1}]), it is defined as the part of the rainfall flux which is intercepted on the wetted surface after which it is fed back to the atmosphere. The interception process equals the sum of the change of interception storage (S_i) and the evaporation from this stock (E_i):

$$I = \frac{dS_i}{dt} + E_i \quad (1.1)$$

The time scale of the interception process is in the order of one day. After one day, it is fair to assume for most climates that the first term on the right hand side in Equation 1.1 approaches zero, and $I = E_i$. Of course in the case of snow under cold climates this may take longer.

How much of the precipitation is intercepted depends on several factors, which can be divided into three groups:

- **Vegetation characteristics.** Large vegetation types, like trees, have a high aerodynamic roughness, causing high potential evaporation rates. Grasses, crops, or bushes on the other hand have a much lower roughness and thus do not have as high potential evaporation rates. The storage capacity also depends on the vegetation type. The shape of the leaves, the thickness, the density (Leaf Area Index), and the configuration of the branches determine how much water can be stored. For example the capacity of a coniferous or a deciduous tree is different (e.g., Rutter et al. [1975], Baird and Wilby [1999], Bryant et al. [2005], Toba and Ohta [2005]). Although intuitively one might think that a deciduous tree can hold more water in its bucket-like leaves, a coniferous tree can hold much more water by adhesion. Furthermore, it is also important to take the seasonality into account. Deciduous trees lose their leaves in the dormant season, causing a large reduction in the canopy storage capacity. Vegetation also determines the amount of understorey growth and forest floor. The forest floor of different vegetation types can have

significantly different interception behaviour (e.g., a thick needle layer or a thin leaf litter layer).

- **Rainfall characteristics.** Rainfall has a large influence on the interception process. The rainfall frequency is a major determining factor. It makes a big difference if rainfall falls as one continuous storm or as a sequence of several small events with dry spells in between. Even if the total rainfall depth is the same, the last scenario intercepts much more rainwater, because between the events the storage can be (partly) emptied by evaporation and thus more storage is available. Second, the rainfall intensity is important, although there is no consensus in literature. Horton [1919] and Wang et al. [2007] concluded that the interception capacity is lower at higher intensity because high rainfall intensities cause splashing and shaking of leaves. On the other hand, Aston [1979] and Keim et al. [2006a] found the opposite: high rainfall intensities coincide with high storage capacities, due to dynamic storage.
- **Evaporative demand.** If the potential evaporation (i.e. open water evaporation) is high the intercepted water can evaporate more easily during and after the event. Wind plays an important role in removing moisture from the surface providing a higher vapour deficit, particularly in the canopy. Moreover, the roughness of the vegetation increases the evaporative power, by causing turbulence which makes it easier to take up the intercepted water. However, wind can also reduce the amount of interception by reducing the storage. Horton [1919], Klaassen et al. [1996], and Hörmann et al. [1996] found that with increasing wind speed the measured storage capacity is less, due to the fact that the wind shakes the rain water off the leaves. The intercepted water can also evaporate more easily when there is supply of advected energy. Several studies have shown the possible importance of advected energy as an additional source of energy (e.g., Shuttleworth and Calder [1979], Wallace and McJannet [2006]), although quantification of advected energy remains speculation (Schellekens et al. [2000]). For mountainous regions also the topography becomes importance, since the airflow alters the aerodynamic resistance (Raupach and Finnigan [1997]).

Of the above three factors the rainfall characteristics are most dominant for evaporation from interception. Although both the storage capacity (mainly vegetation characteristic) and the available energy form a constraint to the evaporation flux per event, the number of events is a more important factor. This is confirmed by the sensitivity analysis of Gerrits et al. [2009b].

1.2 Importance of interception

Although most surfaces can store only a few millimeters of rainfall, which is often not much in comparison to other stocks in the water balance, interception is generally a significant process. The impact becomes evident at longer time scales. Although interception storage is generally small, the number of times that the storage is filled and depleted can be so large that the interception flux is generally of the same order of magnitude as the transpiration flux (Savenije [2004]). In addition, the interception process smooths the rain intensities, causing more gradual

infiltration. Interception also redistributes the rainfall. Some parts of a field receive less water due to interception, while other parts receive more due to funneling of the vegetation (e.g., Germer et al. [2006] and Gerrits et al. [2009a]). Subsequently, this has an influence on the soil moisture patterns, and this is again important for flood generation (Roberts and Klingeman [1970]).

Besides the hydrological effects, there are influences on the nutrient cycle of a forest, and on agricultural applications. For example, interception affects the efficiency of insecticides and fertilizers (Aston [1979]). But also fire retardants are more effective if they are stored by vegetation. Finally, interception may reduce soil erosion by preventing rain drops to directly hit and erode the soil layer (Walsh and Voigt [1977]), although in the case of canopy interception the opposite can be true due to the formation of larger rain drops with a higher impact on the forest floor (Hall and Calder [1993]).

1.3 Interception storage types

As already stated in the introduction, it is possible to define an infinite number of interception storages. In principle, every surface that can store water can be considered as an ‘interception storage type’. In this chapter we focus on the major types, mainly occurring in a natural environment, plus some special mechanisms. However, more often than not, it is a combination of mechanisms. For example in a forest, it is likely that a part of the rainfall is intercepted by the canopy of a tree, while the remaining part can be intercepted by epiphytes on the branches and/or bark, and finally the understorey and forest floor intercept the throughfall before infiltration starts.

In this section we focus on two interception types: canopy and forest floor interception. The bare soil and the build-up surface can also intercept rainwater, but is not described here.

1.3.1 Canopy interception

Canopy interception is the rainwater that is stored on the leaves and branches of a tree which is subsequently evaporated. Canopy interception can be calculated by measuring rainfall above the trees or measured in an open area nearby (gross rainfall P) and subtract the throughfall (T_f) and stemflow (T_s) (Figure 1.1):

$$E_{i,c} + \frac{dS_c}{dt} = P_g - T_f - T_s \quad (1.2)$$

Many research studies have been carried out on canopy interception. In Table 1.1 an overview is given. We can see in this table and also in tables in Kittredge [1948], Zinke [1967], and Breuer et al. [2003] that there is a large difference in the canopy interception by deciduous and coniferous trees (e.g., Kittredge [1948], Bryant et al. [2005], and Toba and Ohta [2005]). Not only

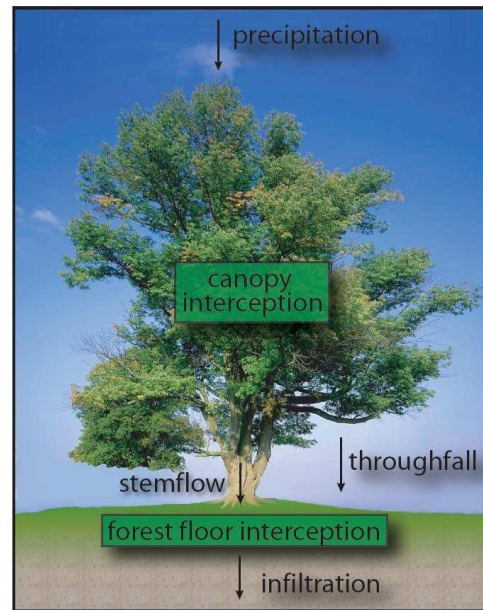


Figure 1.1: Two major interception types in the natural environment.

because deciduous trees lose their leaves, but also because the leaf area of coniferous trees is much larger than of deciduous trees, coniferous trees can store much more water. Furthermore, leaves may swing over when they become too heavy, causing a (sudden) decrease of the storage capacity. However, Herbst et al. [2008] found counterintuitive results, where higher evaporation rates were found in deciduous trees in winter caused by rougher aerodynamics of the bare canopy and deeper penetration of the wind.

In most cases the storage of water on the branches is small, however, in some environments the branches can be overgrown by epiphytes. Pypker et al. [2006] showed that in a Douglas fir forest the canopy water storage can potentially be increased by >1.3 mm and Hölscher et al. [2004] found that epiphytes can account for 50% of the storage capacity. However, this large increase in storage capacity is not necessarily resulting in high interception values (storage + evaporation), because the water uptake and release by the epiphytes is delayed. It takes a while to saturate the epiphytes, and already before saturation, runoff generation can take place. Successively, after wetting, the drying of the epiphytes takes much longer than drying of the canopy, causing less storage to be available.

Source	Specie	Location	$S_{c,max}$ [mm]	$E_{i,c}$ [%]
Aussenac [1968]	<i>Abies grances</i>	France	3.8	42
	<i>Picea abies</i>	France	3.1	34
	<i>Pinus silvestris</i>	France	3.0	30
	<i>Fagus sylvatica</i> & <i>Carpinus betulus</i>	France	1.9	19 (♣) 15 (‡)
Bultot et al. [1972]	Spruce (<i>Picea Abies</i>)	Belgium		15-40
	Beech (<i>Fagus sylvatica</i>)	Belgium		10-20
Rutter et al. [1975]	Corsian pine (<i>Pinus nigra</i>)	United Kingdom	1.05	35
	Douglas fir (<i>Pseudotsuga menziesii</i>)	United Kingdom	1.2	39
	Norway spruce (<i>Picea abies</i>)	United Kingdom	1.5	48
	Hornbeam (<i>Carpinus betulus</i>)	United Kingdom	1.0 (♣) 0.65 (‡)	36
	Oak (<i>Quercus robur</i>)	United Kingdom	0.88 (♣) 0.28(‡)	18
Gash and Morton [1978]	Scots pine (<i>Pinus sylvestris</i>)	United Kingdom	0.8	
Aussenac and Boulangeat [1980]	Douglas fir (<i>Pseudotsuga menziesii</i> Mirb)	France	3.7	32-36
	Beech (<i>Fagus sylvatica</i> L.)	France	1.7	21 (♣) 6 (‡)
Gash et al. [1980]	Sitka spruce (<i>Picea sitchensis</i>)	United Kingdom	0.75-1.2	27-32
	Scots pine (<i>Pinus sylvestris</i>)	United Kingdom	1.02	42
Rowe [1983]	Beech (<i>Nothofagus</i>)	New Zealand	1.5 (♣) 1.2 (‡)	35 (♣) 22 (‡)
Bruijnzeel and Wiersum [1987]	<i>Acacia auriculiformis</i>	Indonesia	0.5-0.6	11-18
Viville et al. [1993]	Norway spruce (<i>Picea abies</i>)	France		34.2
Hörmann et al. [1996]	Beech (<i>Asperulo-fagetum</i>)	Germany	1.28 (♣) 0.84 (‡)	18
Valente et al. [1997]	<i>Pinus pinaster</i>	Portugal	0.41	10.8
	<i>Eucalyptus globulus</i>	Portugal	0.21	17.1
Navar et al. [1999]	Tamaulipan thornscrub	Mexico		18.9

continued on next page

continued from previous page

Source	Specie	Location	$S_{c,max}$ [mm]	$E_{i,c}$ [%]
Bryant et al. [2005]	Loblolly (<i>Pinus taeda</i>) & shortleaf pine (<i>Pinus echinata</i>)	USA (GA)	1.97	22.3
	Longleaf pine (<i>Pinus palustris</i>)	USA (GA)	1.70	17.6
	Scrub oak (<i>Quercus berberidifolia</i>)	USA (GA)	1.40	17.4
	White oak (<i>Quercus alba</i>) & shortleaf pine (<i>Pinus echinata</i>) & loblolly pine (<i>Pinus palustris</i>)	USA (GA)	1.58	18.6
	Hardwood	USA (GA)	0.98	17.7
Toba and Ohta [2005]	Larch (<i>Larix cajanderi</i>)	Siberia		29
	Red pine (<i>Pinus sylvestris</i>)	Siberia		36
	Red pine (<i>Pinus densiflora</i>)	Japan		13-17
	Sawtooth oak (<i>Quercus acutissima</i>)	Japan		24
	Oak (<i>Quercus serrata</i>)	Japan		18
Cuartas et al. [2007]	Rain forest	Brazil	1.0	13-22

Table 1.1: Canopy interception values in literature, with $S_{c,max}$ the water storage capacity and $E_{i,c}$ the interception evaporation as percentage of gross precipitation. See also tables in Kittredge [1948], Zinke [1967], and Breuer et al. [2003] (♣ = leafy; ‡ = leafless).

1.3.2 Forest floor interception

Forest floor interception is the part of the throughfall that is temporarily stored in the top layer of the forest floor and successively evaporated within a few hours or days during and after the rainfall event. The forest floor can consist of short vegetation (like grasses, mosses, bushes, creeping vegetation), litter as described by Hoover and Lunt [1952] as the litter and fermentation (L & F) layer (i.e., leaves, twigs, small branches (still recognizable as origin material)), or bare soil. Although the latter seems to have an overlap with soil evaporation, we distinguish them by the fact that soil evaporation refers to the water that is stored in the root zone (De Groen and Savenije [2006]).

In Table 1.2 some results are presented of previous work on forest floor interception.

1.4 Special interception cases

1.4.1 Agricultural interception

A special case of canopy interception is interception by agricultural crops. In essence there is no difference between crops and other vegetation types. They both can store water up to a certain threshold and then drain water to the floor as throughfall. However, whereas vegetation has a gradual seasonal pattern (summer versus winter), crops have a phenological growth cycle (seeding to harvesting) which is therefore more abrupt. Hence when modelling crop interception the appropriate description of the variation in the storage capacity is important.

1.4.2 Fog interception

A special case of interception is fog interception or cloud interception. Vegetation cannot only intercept rain, but also moisture (in the form of small water droplets) from the air. Fog can occur due to different processes. Bruijnzeel et al. [2005] distinguished nine types: radiation fog, sea fog, stream fog, advection fog, ice fog, coastal fog, valley fog, urban fog, and mountain fog.

Fog interception is mainly important in tropical montane environments (table in Bruijnzeel [2005]: 6-53% of rainfall), but can also play a significant role in semi-arid regions near the coast (e.g., Hursh and Pereira [1953], Hutley et al. [1997], Hildebrandt et al. [2007]). In both environments the main problem with fog interception studies is to measure precipitation and throughfall (Equation 1.2), which is especially important because fog deposition can be twice as high as ‘normal’ rainfall. Since conventional rain gauges are not suitable to measure fog deposition, special fog collectors have been developed with often wire-meshes to intercept the moisture. These instruments suffer from various limitations. An overview of fog collectors can be found in Bruijnzeel et al. [2005].

Source	Forest floor type	Location	$S_{f,max}$ [mm]	$E_{i,f}$ [%]
Haynes [1940]	Kentucky bluegrass (<i>Poa pratensis</i>)	?		56 ¹
Kittredge [1948]	Californian grass (<i>Avena</i> , <i>Stipa</i> , <i>Lolium</i> , <i>Bromus</i>)	USA (CA)		26 ¹
Beard [1956]	<i>Themeda</i> & <i>Cymbopogon</i>	South Africa		13 ¹
Helvey [1964]	Poplar	USA (NC)		34
Brechtel [1969]	Scots pine	USA (NY)		21
	Norway spruce	USA (NY)		16
	Beech	USA (NY)		16
	Oak	USA (NY)		11
Pathak et al. [1985]	<i>Shorea robusta</i> & <i>Mallotus philippensis</i>	India		11.8
	<i>Pinus roxburghii</i> & <i>Quercus glauca</i>	India		7.8
	<i>Pinus roxburghii</i>	India		9.6
	<i>Quercus leucotrichophora</i> & <i>Pinus roxburghii</i>	India		10.6
	<i>Quercus floribunda</i> & <i>Quercus leucotrichophora</i>	India		11.0
	<i>Quercus lanuginosa</i> & <i>Quercus floribunda</i>	India		11.3
Clark [1940] in Thurow et al. [1987]	Blue stem <i>Andropogon gerardi</i> Vitman	USA (TX)		57-84
Walsh and Voigt [1977]	Pine (<i>Pinus sylvestris</i>)	United Kingdom	0.6-1.7	
	Beech (<i>Fagus sylvaticus</i>)	United Kingdom	0.9-2.8	
Pitman [1989]	Bracken litter (<i>Pteridium aquilinum</i>)	United Kingdom	1.67	
Miller et al. [1990]	Norway spruce	Scotland		18 ¹
	Sitka spruce	Scotland		16 ¹
Thamm and Widmoser [1995]	Beech (<i>Asperulo-Fagetum</i>)	Germany	2.5-3.0	12-28
Putuhen and Cordery [1996]	<i>Pinus radiata</i>	Australia	2.78	

continued on next page

continued from previous page

Source	Forest floor type	Location	$S_{f,max}$ [mm]	$E_{i,f}$ [%]
	Eucalyptus	Australia	1.70	
Schaap and Bouten [1997]	Douglas fir	Netherlands		0.23 mm d ⁻¹
Li et al. [2000]	Peble mulch (5-9cm)	China	0.281	11.5 ¹
	Peble mulch (2-6cm)	China	0.526	17.4 ¹
Sato et al. [2004]	<i>Cryptomeria japonica</i>	Japan	0.27-1.72	
	<i>Lithocarpus edulis</i>	Japan	0.67-3.05	
Guevara-Escobar et al. [2007]	Grass (<i>Aristida divaricata</i>)	Mexico	2.5	
	Woodchips (<i>Pinus</i>)	Mexico	8	
	Poplar leaves (<i>Populus nigra</i>)	Mexico	2.3	

Table 1.2: Forest floor interception values in literature, with the water storage capacity $S_{f,max}$ and the interception evaporation $E_{i,f}$ as percentage of net precipitation (i.e., throughfall).

1. percentage of gross precipitation instead of net precipitation

1.4.3 Snow interception

Snowfall is also intercepted by trees. Especially, coniferous trees can store so much snow, that they collapse under its weight. As an example, Storck et al. [2002] found in a Douglas fir dominated forest that up to 60% of the snowfall was intercepted, equalling 40 mm of snow water equivalent.

The storage of snow on the canopy is different from rain. For rainfall interception the storage capacity is mainly a function of the leaf surface area, whereas for snow interception the branch strength and canopy shape is more important (Ward and Trimble [2004]). Furthermore, the snow storage is also dependent on the temperature. If snow falls with temperatures close to freezing point, the cohesion of snow is higher causing more snow to be accumulated on the canopy (Ward and Trimble [2004]).

Another difference between rainfall interception and snow interception, is the way in which interception storage is depleted. Rainfall interception is a real threshold process, whereby throughfall starts when the storage capacity is exceeded. The storage capacity is then emptied by evaporation. Snow, on the other hand, can only be removed from the canopy by three ways: sublimation, mechanical removal (sliding leading to mass release), and melt water drip (Miller [1966]).

1.4.4 Urban interception

Most hydrological studies focus on natural environments and not on urbanised areas, which is also the case for interception studies. However, recently with the increasing interest for alternative sources of water for non-potable domestic use (so-called ‘grey water’), water balance studies on (interception) evaporation in urban areas have increased (Grimmond and Oke [1991], Ragab et al. [2003], Gash et al. [2008], Nakayoshi et al. [2009]).

The difference between urban and rural interception is not only that the typical storage capacities of buildings, roads, etc, are unknown, but that the entire energy balance is different in a city. Oke [1982] discovered the so called ‘Urban Heat Island’, i.e higher temperatures in urban areas compared to the surrounding rural areas. The Urban Heat Island is mainly caused by the (relatively warm) buildings, that block the cold night sky. Furthermore, the thermal properties of a city are different: concrete and asphalt have much higher heat capacities than forests and also the surface radiative properties differ (e.g., albedo and emissivity). The lack of vegetation in urban areas, which reduces cooling by transpiration, also causes a difference in the energy balance.

1.5 Methods to measure interception

1.5.1 Canopy

There exist already a lot of methods to measure canopy interception. The most often used method is to measure rainfall above the canopy and subtract throughfall and stemflow ([e.g., Helvey and Patric, 1965]). However, the problem with this method is that the canopy is not homogeneous, which causes it to be difficult to obtain representative throughfall data. Using multiple rain gauges under the canopy (Helvey and Patric [1965], Keim et al. [2005], Gerrits et al. [2009a]) reduces this problem. Sometimes the collectors are moved to achieve a better representation of throughfall (e.g., Lloyd and Marques [1988], Tobón-Marín et al. [2000], Manfroi et al. [2006], Ziegler et al. [2009]). Another method to avoid the problem with the spatial distribution of the canopy was introduced by Calder and Rosier [1976] and applied by e.g., Shuttleworth et al. [1984], Calder et al. [1986], and Calder [1990]. They covered the forest floor with plastic sheets and collected the throughfall. The disadvantage of this method is that for long periods irrigation is required, because otherwise in the end the trees will dry out and may even die due to water shortage. The method by Hancock and Crowther [1979] avoided these problems, by making use of the cantilever effect of branches. If leaves on a branch hold water, it becomes more heavy and will bend. By measuring the displacement, it is possible to determine the amount intercepted water. Huang et al. [2005] refined this method by making use of strain gauges. However, the disadvantages of these methods is that only information about one single branch is obtained and it is quite laborious to measure an entire tree. Edwards [1986], Fritschen and Kinerson [1973], and Storck et al. [2002] made use of weighing lysimeters with trees. Although interception of a whole tree is measured with this method, the big disadvantage of this method is that it is expensive and destructive. Friesen et al. [2008] developed a non-destructive method to measure canopy interception of a whole tree. With mechanical displacement sensors Friesen et al. [2008] measured the stem compression due to interception water, which is an integration of the whole canopy. However, although this method looks promising it is still under development.

A totally different way of measuring canopy interception of a forest plot, is to make use of ray attenuation. Calder and Wright [1986] used the attenuation of gamma rays. They transmitted from a tower gamma rays through the canopy at different heights and measured the gamma ray density at a receiving tower. The ratio between transmitted and received gamma ray density during dry conditions is successively compared to this ratio during a rainfall event. This gives an estimate of the amount of water stored on the canopy over time. Although the method gives interception estimates of an entire forest, the method becomes inaccurate under windy conditions. Furthermore, safety standards prohibits unattended use of this method. Bouten et al. [1991] overcame this problem, by making use of microwave attenuation. It appears to be a suitable method to measure canopy wetness, although it is an expensive method.

Evaporation can also be measured by flux measurements. By measuring temperature (θ) and specific humidity (q) at several heights (z) above the canopy one can calculate the Bowen ratio

(B_r), which is the sensible heat flux, H , divided by the latent heat flux (λE):

$$B_r = \frac{H}{\rho \lambda E} = \frac{c_p \delta \theta / \delta z}{\lambda \delta q / \delta z} \quad (1.3)$$

Combined with the energy balance, evaporation can be calculated (Gash and Stewart [1975]). The main difficulty with the Bowen ratio method is to measure the humidity gradient accurately enough (Stewart [1977]). Another method is the eddy covariance technique, where the net upward or downward flux is determined by fast-response 3D wind speed measurements combined with a ‘concentration’ measurement. This concentration can be humidity, temperature, or CO₂-concentrations (Amiro [2009]).

1.5.2 Forest floor

In the literature, little can be found on forest floor interception, although some researchers have tried to quantify the interception amounts. Generally these methods can be divided into two categories (Helvey and Patric [1965]):

1. Laboratory methods, whereby field samples are taken to the lab and successively the wetting and drying curves are determined by measuring the moisture content.
2. Field methods, whereby the forest floor is captured into trays or where sheets are placed underneath the forest floor.

An example of the first category is that of Helvey [1964], who performed a drainage experiment on the forest floor after it was saturated. During drainage, the samples were covered and after drainage had stopped (24 hours), the samples were taken to the lab, where the samples were weighed and successively dried until a constant weight was reached. By knowing the oven dry weight of the litter per unit area and the drying curve, the evaporation from interception could be calculated. In this way they found that about 3% of the annual rainfall evaporated from the litter. Similar work was done by Bernard [1963], Walsh and Voigt [1977], and Sato et al. [2004]. However, what they all measured was not the flux, but the storage capacity.

Another example of laboratory experiments was carried out by Putuhena and Cordery [1996]. First, field measurements were carried out to determine the spatial variation of the different forest floor types. Second, storage capacities of the different forest floor types were measured in the laboratory using a rainfall simulator. Finally, the lab experiments were extrapolated to the mapping step. In this way Putuhena and Cordery [1996] found average storage capacities of 2.8 mm for pine and 1.7 mm for eucalyptus forest floors. Also Guevara-Escobar et al. [2007] made use of a rainfall simulator.

Examples of the second category are carried out by Pathak et al. [1985], who measured the weight of a sample tray before and after a rainfall event. They found litter interception values of 8-12% of the net precipitation. But also here, they measured the storage capacity, rather than the flux. Schaap and Bouten [1997] measured the interception flux by the use of a lysimeter and

Main author	Model type	Interception element:				Time scale
		canopy	stem	forest	floor	
Rutter	Conceptual	x	x			\leq hourly
Gash	Analytical	x	x			event
Calder	Stochastic	x				\leq hourly
De Groen	Concept./Stoch.	x	x		x	monthly
Keim	Concept./Stoch.	x				6-hourly

Table 1.3: Characteristics of interception models.

found that 0.23 mm d^{-1} evaporated from a dense Douglas fir stand in early spring and summer. Also Brechtel [1969] and Thamm and Widmoser [1995] made use of lysimeters. Brechtel [1969] measured manually the infiltrated water and Thamm and Widmoser [1995] developed an automatic and more sophisticated method, whereby the suction under the forest floor is controlled by a tensiometer.

Measurements with sheets were done for example by Li et al. [2000], who found that pebble mulch intercepts 17% of the gross precipitation. Miller et al. [1990] found comparable results (16-18%) for a mature coniferous plantation in Scotland.

1.6 Interception models

In literature several models have been developed to simulate forest interception. Almost all of these models concentrate on canopy interception, sometimes including stem interception (Table 1.3). In principle these models can be expanded to include forest floor or any surface interception as well.

The most often used interception models are the conceptual model of Rutter et al. [1971] (Section 1.6.1) and the analytical model of Gash [1979] (Section 1.6.2) or revisions of these models. Furthermore, there exist some stochastic models, which will be described in Section 1.6.3. In Table 1.3 an overview and summary of the models is given. A more detailed overview and comparison can be found in Muzylo et al. [2009].

1.6.1 Conceptual Rutter model

The conceptual framework of the original Rutter-model is depicted in Figure 1.2. As can be seen the rainfall is divided into three parts:

1. Free throughfall, i.e. throughfall, which did not touch the canopy at all (pP_g)
2. Trunk input (p_tP_g)
3. Canopy input ($(1 - p - p_t)P_g$)

The rain that falls on the canopy can either drain to the ground (i.e. canopy drainage, D), or evaporate ($E_{i,c}^l$) or it can be stored on the canopy (S_c^l):

$$(1 - p - p_t) \int P_g dt = \int D dt + \int E_{i,c}^l dt + \int dS_c^l \quad (1.4)$$

The rain that falls on the trunk can either evaporate from the trunk ($E_{i,c}^t$) or drain in the form of stemflow (T_s) or it can be stored on the trunk (S_c^t):

$$p_t \int P_g dt = \int T_s dt + \int E_{i,c}^t dt + \int dS_c^t \quad (1.5)$$

with $E_{i,c} = E_{i,c}^l + E_{i,c}^t$ and $S_c = S_c^l + S_c^t$ for the total canopy interception.

The evaporation from the wet canopy is calculated with the Penman equation (Penman [1948]). Because the canopy is not always completely wet ($S_c^l < S_{c,max}^l$), the actual evaporation rate can be calculated by the fraction of the potential evaporation: $E_p \cdot S_c^l / S_{c,max}^l$. The same concept is applied for the trunks. However, for the determination of the potential evaporation of the trunks, the potential evaporation of the canopy is multiplied with an extra constant ϵ .

Stemflow is modelled as a threshold process, whereby no stemflow is generated when $S_c^t < S_{c,max}^t$, and when the threshold is exceeded stemflow equals the difference between S_c^t and $S_{c,max}^t$.

Canopy drainage is modelled in a similar way; however, when the threshold $S_{c,max}^l$ is exceeded drainage is defined as:

$$D = D_s \exp[b(S_c^l - S_{c,max}^l)] \quad (1.6)$$

with D_s the rate of drainage when the canopy is saturated and b [L^{-1}] as an empirical coefficient.

In 1997 Valente et al. revised the original Rutter model, to model interception in a more realistic way for sparse canopies. The main drawbacks of the original model were the partitioning of free throughfall and ‘canopy input’, and the conceptual error that evaporation from interception can theoretically be higher than potential evaporation (Valente et al. [1997]). Therefore they divided the conceptual model into two areas: a covered area (c) and an uncovered area ($1 - c$). Second, in the revised Rutter model water can only reach the trunk after it has flowed through the canopy as a part of the canopy drainage. Water which is not drained by the trunk is directly dripping to the ground. The final change was made that evaporation from the saturated canopy is not equal to the potential evaporation, but is reduced by a factor $1 - \epsilon$ ($0 < \epsilon < 1$). The remaining energy (ϵE_p) is then available for evaporating water from the saturated trunk.

Although the Rutter-models work well to estimate interception, they require quite some parameters, which are often (semi-)empirical and thus difficult to estimate. Liu [2001] developed a new model that is physically based and only needs three parameters. The main difference between the Rutter model and the Liu model is that trunk interception is combined with interception by the canopy and the way it deals with canopy wetting.

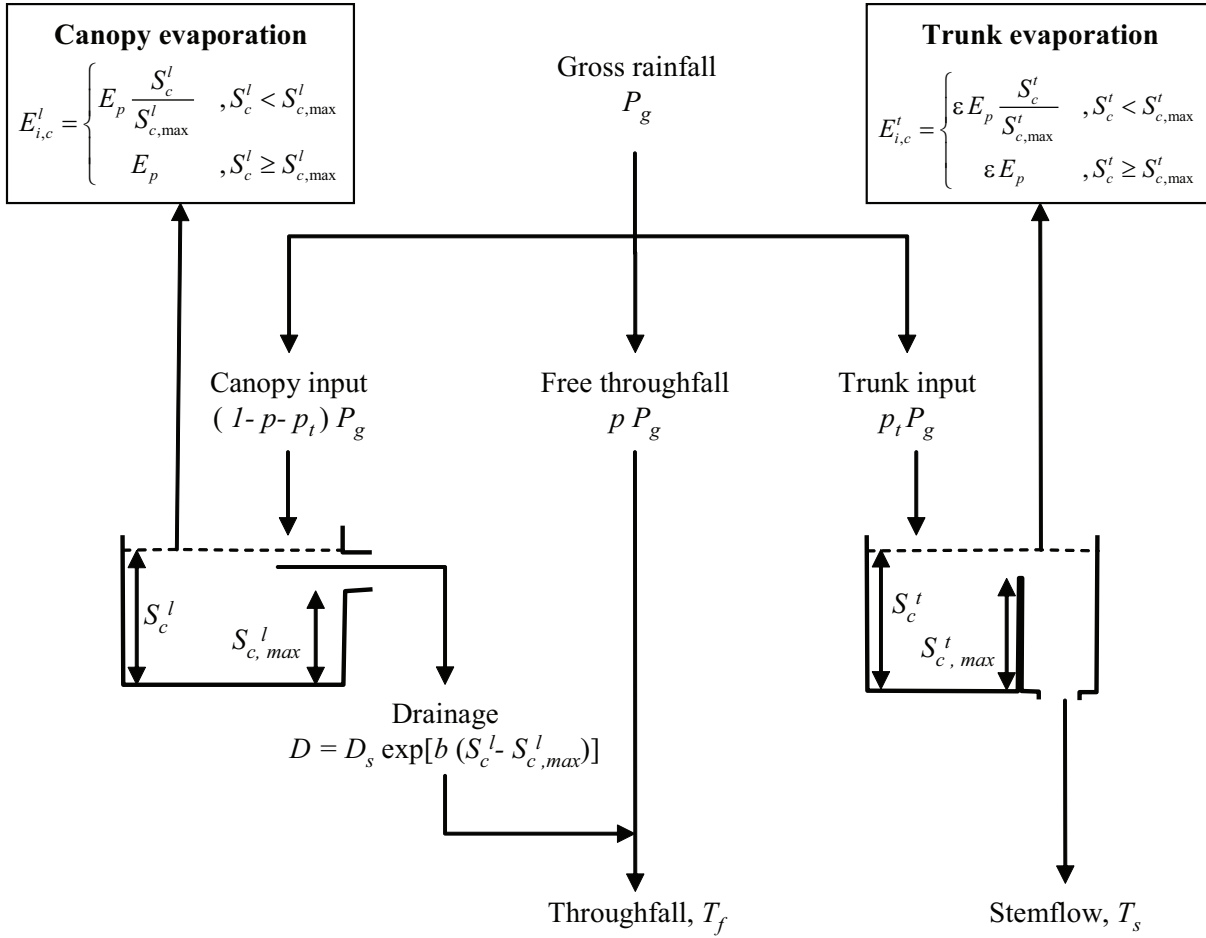


Figure 1.2: Conceptual framework of the Rutter model (after Valente et al. [1997]).

1.6.2 Analytical Gash model

The original Gash-model is conceptually the similar as the Rutter-model (see Section 1.6.1); however, it does not require meteorological data of high temporal resolution (hourly) and requires less computation time. The main assumption of the Gash-model is that it is possible to represent the real rainfall pattern by different discrete rainfall events, each consisting of three phases:

1. wetting phase
2. saturation phase
3. drying phase (long enough to dry the entire canopy)

Similar to the Rutter model, rainfall is divided into canopy input $(1-p-p_t)$, free throughfall (p) , and trunk input (p_t) .

The Gash-model makes a distinction between storms which are not large enough to saturate the canopy ($P_g < P'_g$: m storms) and storms which are large enough to saturate the canopy ($P_g \geq P'_g$: n storms). The amount of gross rainfall necessary to saturate the canopy is P'_g (see Table 1.4). Interception evaporation is then calculated for the canopy and the trunk.

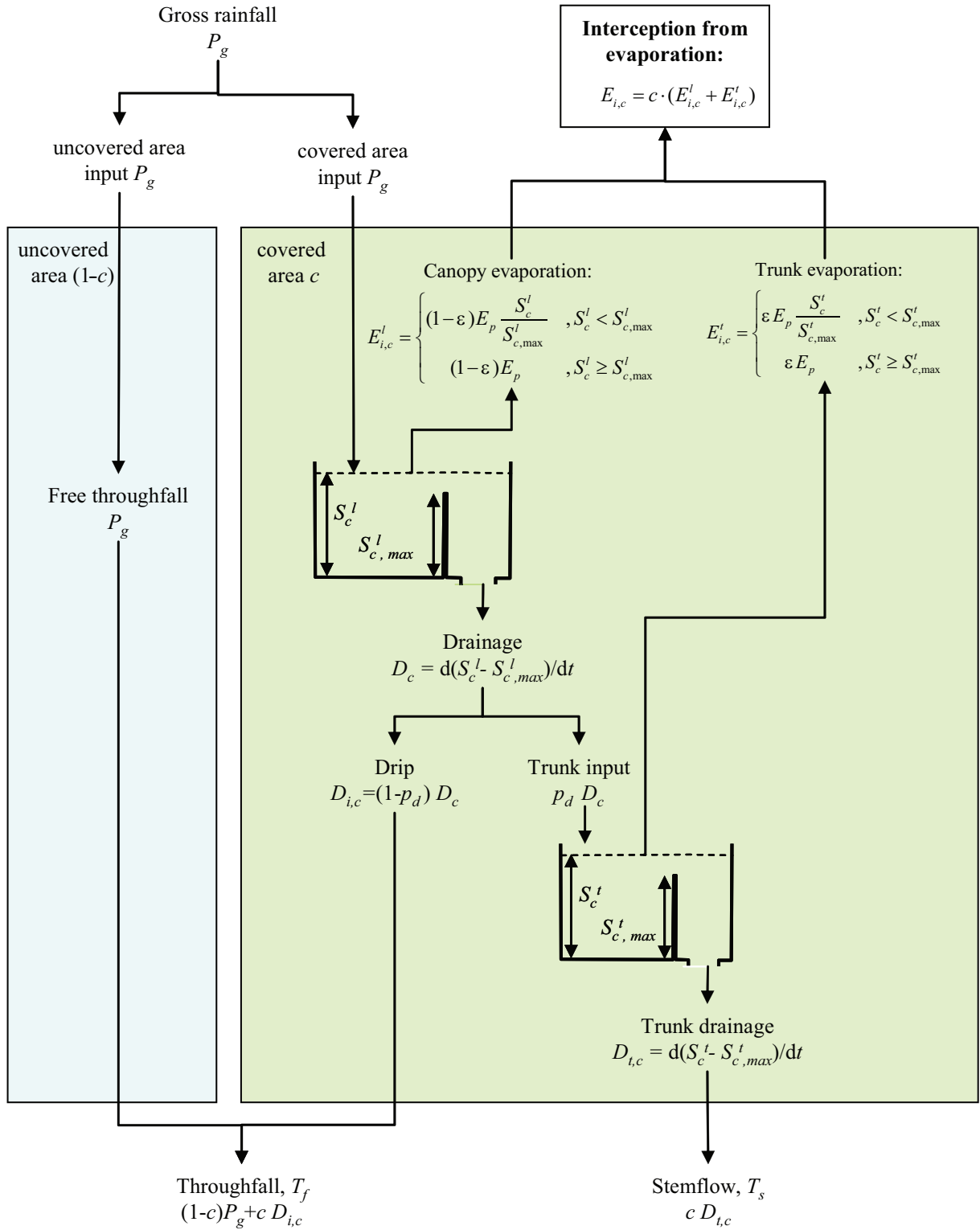


Figure 1.3: Conceptual framework of the revised Rutter model (after Valente et al. [1997]).

Although the original Gash-model appears to work well for several types of forest, it contains some weaknesses for modelling sparse forests, similar to the Rutter-model. Hence, Gash et al. [1995] revised their existing model accordingly to the revised Rutter model (Rutter et al. [1975]). An overview of the formulas of the revised Gash-model can be found in Table 1.4.

A limitation of the revised sparse canopy model is the simplification of constant canopy parameters, while many vegetation types have seasonal canopy density variations. Van Dijk and Bruijnzeel [2001] improved the revised model of Gash et al. [1995] by using time-variant model parameters.

A model that has similarities with the Gash-model is the DOCIORI-model by Murakami [2006]. The model is based on the theory that evaporation is related to rain intensity due to the evaporation of splash drops. The higher the rain intensity, the higher the kinetic energy to generate small droplets and thus more evaporation is possible. Murakami [2007] stated that according to this theory a physical explanation can be given for the relation between interception evaporation and rainfall.

1.6.3 Stochastic interception models

Poisson distribution

Calder [1986] developed a stochastic interception model, where he assumes that a tree consists of several elemental areas which all have the same probability to be struck by raindrops. The Poisson probability of an element to be struck by r drops equals:

$$P_r = \frac{m^r}{r!} \exp(-m) \quad (1.7)$$

with m the mean number of raindrops striking an element per storm.

If an element can hold q raindrops, the mean number of drops per element (n) can be expressed as:

$$n = \sum_{r=0}^q r \cdot P_r + q \cdot P(r > q) \quad (1.8)$$

$$= q + \sum_{r=0}^q P_r \cdot (r - q) \quad (1.9)$$

with $P(r > q)$ the probability of elements being struck by more than q drops and is equal to $1 - \sum_{r=0}^q P_r$.

To upscale from elemental area to canopy area the number of elemental surface areas per unit ground (L) is required and the mean volume of raindrops (v):

$$S_c = nvL \quad (1.10)$$

	Original Gash [1979]	Revised (sparse canopy) Gash et al. [1995]
Amount of gross rainfall necessary to saturate the canopy (P'_g) and trunk (P''_g)	$P'_g = -\frac{\bar{P}_g S_{c,max}}{\bar{E}_p} \ln \left[1 - \frac{\bar{E}_p}{(1-p-p_t)\bar{P}_g} \right]$ $P''_g = S_{c,max}^t / p_t$	$P'_g = -\frac{\bar{P}_g}{(1-\epsilon)\bar{E}_p} \frac{S_{c,max}}{c} \ln \left[1 - \frac{(1-\epsilon)\bar{E}_p}{\bar{P}_g} \right]$ $P''_g = \frac{\bar{P}_g}{\bar{P}_g - (1-\epsilon)\bar{E}_p} \frac{S_{c,max}^t}{p_t c} + P'_g$
Evaporation from canopy interception ($E_{i,c}^l$): - for m storms ($P_g < P'_g$) - for n storms ($P_g \geq P'_g$)	$(1-p-p_t) \sum_{j=1}^m P_{g,j}$ $n(1-p-p_t)P'_g + \frac{\bar{E}_p}{\bar{P}_g} \sum_{j=1}^n (P_{g,j} - P'_g)$	$c \sum_{j=1}^m P_{g,j}$ $c \left[nP'_g + \frac{(1-\epsilon)\bar{E}_p}{\bar{P}_g} \sum_{j=1}^n (P_{g,j} - P'_g) \right]$
Evaporation from trunk interception ($E_{i,c}^t$): - for q storms ($P_g \geq P''_g$) - for $m+n-q$ storms ($P_g < P''_g$)	qS_c^t $p_t \sum_{j=1}^{m+n-q} P_{g,j}$	qS_c^t $p_t c \left[1 - \frac{(1-\epsilon)\bar{E}_p}{\bar{P}_g} \sum_{j=1}^n (P_{g,j} - P'_g) \right]$

Table 1.4: Components of interception of the original Gash [1979] model and the revised Gash et al. [1995] model for sparse canopies.

$$S_{c,max} = qvL \quad (1.11)$$

$$P = mvL \quad (1.12)$$

Evaporation is then obtained by (with $dS_c/dE_{i,c} = -1$):

$$\frac{dn}{dE_{i,c}} = \frac{dS_c}{dE_{i,c}} \times \frac{dn}{dS_c} = \frac{-1}{vL} \quad (1.13)$$

The Calder model is very simple and describes the threshold behaviour of interception very well; however, it is difficult to upscale from drop size scale to forest size scale. This hinders the applicability of the model.

Markov chains

De Groen and Savenije [2006] developed a monthly interception model based on a daily interception model and the daily rainfall characteristics. They assumed interception on a daily scale as (Savenije [1997], Savenije [2004]):

$$E_{i,d} = \min(D_{i,d}, P_d) \quad (1.14)$$

The probability distribution of rainfall on a rain day can be described as:

$$f_{i,d}(P_d) = \frac{1}{\beta} \exp\left(-\frac{P_d}{\beta}\right) \quad (1.15)$$

with β being the scaling factor, equal to the expected rainfall on a rain day, which can be expressed as:

$$\beta = \frac{P_m}{E(n_{r,d}|n_m)} \quad (1.16)$$

with P_m being the monthly rainfall and $n_{r,d}$ and n_m the number of rain days per month and amount of days per month, respectively. The number of rain days per month can be expressed by the use of Markov properties. Being p_{01} the Markov probability of the transition from a dry day to a rain day, and p_{11} the probability of a rain day after a rain day:

$$n_{r,d} = n_m \frac{p_{01}}{1 - p_{11} + p_{01}} \quad (1.17)$$

Multiplying Equation 1.14 and 1.15 and successively integrating results in monthly evaporation from interception:

$$E_{i,m} = E(n_{r,d}|n_m) \int_0^\infty E_{i,d} \cdot f_{i,d}(P_d) dP_d \quad (1.18)$$

$$= P_m \left(1 - \exp\left(-\frac{D_{i,d}}{\beta}\right)\right) \quad (1.19)$$

Hence, the model of De Groen and Savenije [2006] is a parsimonious model with only one measurable parameter, and Markov probabilities to model monthly interception based on daily information.

Gamma probability density function (PDF) and transfer functions

Keim et al. [2004] developed a stochastic model to obtain from 6-hourly rainfall 6-hourly throughfall for extreme events. They made use of the gamma probability density function (for 6 hourly rainfall). The gamma distribution is given by (with $0 < T_f/P < \infty$):

$$\frac{T_f}{P} \cdot 100\% = \frac{P^{\alpha-1} \exp(-\frac{P}{\theta})}{\Gamma(\alpha)\theta^{\alpha}} \quad (1.20)$$

The parameters α and θ can be estimated by dividing the 6-hourly rainfall in ranges and find the best fit sets.

After downscaling the rainfall and throughfall data, rainfall is transferred through the canopy by a linear system convolution to obtain high resolution throughfall data, which allows investigation of the effect of intensity smoothing:

$$T_f(t) = \int_0^t P(t)g(t - \tau)d\tau \quad (1.21)$$

with the transfer function $g(t - \tau)$. Keim et al. [2004] found that the transfer function can be best described with the exponential distribution:

$$g(t) = \alpha \exp(-\alpha t) \quad (1.22)$$

By coupling the stochastic model with the intensity smoothing transfer function, effects of forest canopies on extreme rainfall events can be investigated.

1.7 Consequences of underestimating interception for hydrological modelling and water resources assessment

Hydrologists often consider precipitation as the start of the hydrological cycle. After a rainfall event the first separation point in the cycle is on the earth surface. Part of the rain water is intercepted by the vegetation or ground surface and the remainder infiltrates into the unsaturated zone or runs off. The part of the rainfall that is intercepted successively evaporates from the temporary storage.

This first separation point in the hydrological cycle is not always considered a significant process. This is partly due to the technical difficulties that are inherent to interception measurements (Lundberg et al. [1997]; Llorens and Gallart [2000]), but it is also generally considered a minor flux, although, previous studies tell us that interception can amount to 10-50% of the precipitation depending on the vegetation type (Klaassen et al. [1998]). Even then, these studies mostly refer to canopy interception only. If forest floor interception is taken into account as well, the percentage is substantially higher.

Furthermore, it is often stated that interception is particularly not important for the generation of floods. This is not true. Interception strongly influences the antecedent soil moisture conditions, which are very important for the generation of floods (Roberts and Klingeman [1970]). Still interception is regularly (partly) disregarded in hydrological models, or taken as a fixed percentage of the precipitation. As a result, after model calibration, interception is generally compensated by other processes such as transpiration, soil evaporation or even recharge (Savenije [2004]).

Zhang and Savenije [2005] showed that the hydrograph at the outlet of the Geer basin in Belgium improved significantly when interception was included in a rainfall-runoff model using the Representative Elementary Watershed (REW) approach. Both the Nash-Sutcliffe efficiency and the percentage bias improved. They also showed that, in calibration, the soil moisture storage capacity compensated for the neglect of the interception process.

Keim et al. [2006b] investigated the effects of (canopy) interception. They looked at the influence on the subsurface stormflow generation and concluded that interception caused a delay in the onset of subsurface stormflow, lowered and delayed stormflow peaks, and decreased total flow and the runoff ratio. They also found that simply reducing the rainfall by a constant factor, did not result in a satisfactory peak flow response.

Fenicia et al. [2008b] looked at the change in the movement of the Pareto front when step-wise new processes were included in a variable model structure. They concluded that when interception was included and especially, when spatially distributed interception was included, the Pareto front moved significantly to the origin. Hence, their conclusion was that interception is an important process and should therefore be included in hydrological models.

1.8 Problem definition and study objectives

A lot of research has already been done on interception. A wide range of tree species have been investigated under a wide variety of climates resulting in extensive tables such as Table 1.1. However, often only one interception type is investigated, while the combination of the different interception storages is especially important. Not only the total storage is higher when more interception types are considered, but also the seasonality of each storage type causes different interception dynamics when compared to only one interception type. Hence it is important to investigate the combinations of different interception types.

Furthermore, many studies consider interception as a point process and completely neglect its spatial variability and the consequences of this variability on successive processes. Often the lack of data with the right temporal and spatial resolution hinder those studies. Besides, if such data is available these studies remain often site and case specific and are difficult to generalize for modelling purposes.

Another problem for modelling purposes is the time scale of interception. Most hydrological models have a daily to monthly time scale, while interception is a typical event process. Hence when one wishes to model interception one should include the temporal rainfall characteristics.

The main objective of this thesis is to investigate the role of interception in the hydrological cycle. The specific objectives are:

- Quantify the amount of canopy and forest floor interception for different vegetation species over time;
- Study spatial interception patterns and its persistence;
- Investigate the effect of interception on successive hydrological processes;
- Develop a model to upscale interception in time.

1.9 Thesis outline

In Chapter 2 the instrumentation of the study sites Huewelerbach, Westerbork, and Botanical Garden is described. Mainly the observations from these three study sites are used to investigate and test hypothesis on the interception process.

In Chapter 3 the spatial and temporal variations in canopy and forest floor interception are investigated. A clear distinction is made between temporal variations in evaporation flux and storage. The latter is used to analyse the effect of this variability on evaporation predictions with a Rutter model. For the spatial variability only throughfall and infiltration patterns are analysed on temporal characteristics and persistence.

The effect of spatial throughfall patterns on subsurface storm flow generation and soil moisture is described in Chapter 4. Since observations of all needed parameters were missing and because we did not want to be too case-specific, we applied the concept of a ‘virtual experiment’. We combined the throughfall pattern of the Huewelerbach on the Panola hillslope (USA) and modelled with HYDRUS-3D soil moisture patterns and trench outflow for different slopes and soil thicknesses.

In Chapter 5 a framework is presented to upscale a daily interception threshold model to the annual time scale by use of Markov properties. After combination with transpiration, an annual

evaporation model has been developed based on the daily rainfall characteristics. Furthermore, an analytical solution has been derived; however, this solution does not include Markov properties, but still captures the daily rainfall characteristics. Finally, the results of the analytical solution are compared to the Budyko curve.

The thesis ends with the conclusions in Chapter 6, where all findings are summarized and some recommendations are given for the future.

Chapter 2

Methods and materials

.....

Different kinds of instrumentation are used in three experimental plots to measure different components of the forest water balance. The most important ones are described in this chapter. First of all a device to measure forest floor interception. A special device has been developed, which consists of two aluminium basins which are mounted above each other. The upper basin is permeable and contains the forest floor. By continuously weighing both basins, evaporation from interception can be calculated. Secondly, canopy interception is measured by subtracting stemflow and throughfall from the gross precipitation. Stemflow is measured by a flexible tube wrapped around the stem of a tree. Throughfall is measured with collectors and gutters. Finally, the leaf area index is estimated by a fish-eye light sensor. In a beech forest in the Huewelerbach catchment in Luxembourg, all components have been measured, in Westerbork (the Netherlands) only forest floor interception of a moss/grass layer, and in the botanical garden in Delft (the Netherlands) both canopy and forest floor interception of a cedar.

.....

Based on: Gerrits, A. M. J., Savenije, H. H. G., Hoffmann, L., Pfister, L., 2007. New technique to measure forest floor interception - an application in a beech forest in Luxembourg. *Hydrology and Earth System Sciences* 11, 695–701; and Gerrits, A. M. J., Savenije, H. H. G., Pfister, L., 2009a. Canopy and forest floor interception and transpiration measurements in a mountainous beech forest in Luxembourg. *IAHS Redbook* 326, 18–24; and Gerrits, A. M. J., Savenije, H. H. G., Pfister, L., 2008. Forest floor interception measurements. *IHP-VI Technical Documents in Hydrology* 81, 81–86

2.1 Instrumentation

2.1.1 Throughfall

Throughfall measurements are difficult because the canopy is not homogeneous. To overcome this problem throughfall is measured in two ways: 1) with rain collectors to obtain information on the spatial distribution and 2) with gutters to obtain information on the temporal variation. A network of 3 gutters (16.5×215.5 cm) has been built (total collecting area of 1.07 m²). The gutters are connected to one tipping bucket [RM Young, 52203-L, 0.1 mm], so as to provide the temporal structure of throughfall below the canopy. Since the representativity of these gutters is difficult to assess, because of the high spatial variability of the canopy density, an additional network of rain collectors (SPIEA 1650-01; A = 400 cm²) has been installed inside the experimental stand. Eighty-one collectors have been put in a network at a spacing of 3 meters. This network of rain collectors gives both an indication of the spatial variability of throughfall, as well as a precise measurement of the amount of throughfall at a biweekly to monthly time-step. Every time the collectors and gutter were read out, they were cleaned to avoid congestion and evaporation by organic debris. The biweekly to monthly throughfall amounts ($\sum_{t=0}^{t=i} \bar{T}_{f,collector}$) are disaggregated via the measurements obtained by the tipping bucket gauges that are connected to the gutters ($T_{f,gutter}(t)$) below the canopy:

$$T_f(t) = T_{f,gutter}(t) \cdot \frac{\sum_{t=0}^{t=i} \bar{T}_{f,collector}}{\sum_{t=0}^{t=i} T_{f,gutter}(t)} \quad (2.1)$$

In Figure 2.1 the setup in the Huewelerbach is depicted.



Figure 2.1: Throughfall measurements in the Huewelerbach catchment.

2.1.2 Stemflow

Stemflow is measured by an open flexible tube (width 3 cm) wrapped around the trunk of two trees. The water collected from the trees is directed to a tipping bucket (RM Young, 52203-L,

0.1 mm & Isco 674, 0.1 mm). Stemflow is upscaled by calculating the average stemflow per tree and multiplying by the mean number of trees per m² in the stand (Gerrits et al. [2009a]). Although stemflow is often related to DBH (tree diameter at breast height) (e.g., Navar et al. [1999], Levia and Frost [2003]), we choose to apply this simple averaging method because 1) the average DBH of the sampled trees is close to the overall average DBH; 2) we measured two out of nine trees in the Huewelerbach, which is in our opinion quite a good representation of the plot (see also Figure 2.4). In Figure 2.2 the setup in the Huewelerbach is depicted.



Figure 2.2: Stemflow measurements in the Huewelerbach catchment.

2.1.3 Leaf Area Index (LAI)

The Leaf Area Index (LAI) is measured with a device developed by UNESCO-IHE, Delft. It consists of a fish eye lens connected to a light sensitive resistance. With a regular voltage meter the resistance is measured. In the laboratory the device was calibrated to know the relation between resistance and light intensity. Successively, the LAI is calculated with the Beer-Lambert law:

$$LAI = -\frac{1}{k} \ln \left(\frac{I}{I_0} \right) \quad (2.2)$$

with I the irradiance under the canopy and I_0 the irradiance in the open field. k is the extinction coefficient and estimated at 0.43 for the beech forest (Bréda [2003]).

The ratio I/I_0 was only measured at irregular basis when the experimental site was visited and therefore this data is only used as ‘soft data’. Under the canopy ten measurements were taken

in a radius of 15 m surrounding the forest floor device and in the open area three measurements were taken.

2.1.4 Forest floor interception device

To measure evaporation from intercepted rainfall on the forest floor (L & F layer (Hoover and Lunt [1952])), a special device has been developed. The device consists of two aluminium basins, which are mounted above each other and are weighed accurately with 2 sets of 3 strain gauge sensors (see Figure 2.3). The strain gauges are mounted in the Wheatstone configuration. The upper basin is filled with forest floor and has a permeable bottom of geotextile, so water can percolate into the lower basin. A valve is installed in this lower basin, which empties in general every day for 10 minutes to avoid evaporation from the lower basin as much as possible. In case of temperatures around freezing point, the valve opens more often to avoid freezing of the water in the lower basin. The space between the supporting structure and the aluminium basins is also minimized, in order to avoid evaporation by turbulent wind fluxes. In addition to the weight, the temperature is also measured in one of the lower and upper strain gauge casings and saved on a data logger every five minutes.

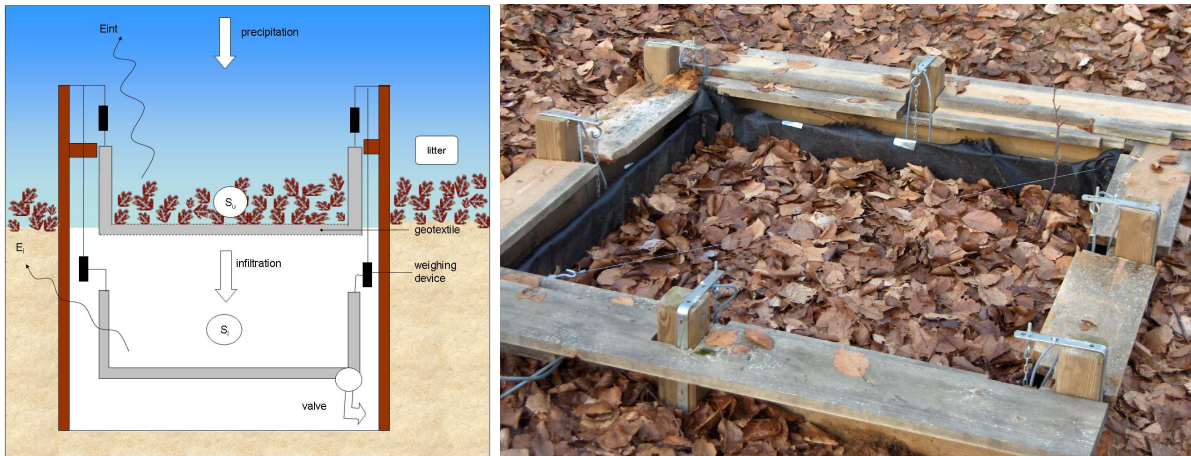


Figure 2.3: Schematisation of the forest floor interception device and the set-up as in the Huewelerbach.

To calculate the amount of evaporation from interception, a water balance is made of the system. When evaporation from the lower basin (E_l [$L T^{-1}$]) is neglected and the weight of the lower basin is corrected for the drainage from the valve (S_l [L]), evaporation of intercepted rainfall ($E_{i,f}$ [$L T^{-1}$]) can be calculated as:

$$E_{i,f}(t) = T_f(t) - \left(\frac{dS_u}{dt} + \frac{dS_l}{dt} \right) \quad (2.3)$$

where S_u and S_l are respectively the storage of the upper and the lower basins [L], which are obtained by dividing the weight of the basins [M] by the density of water [$M L^{-3}$] and the surface area [L^2] of the basin.

If Equation 2.3 is rewritten the interception process (I) for the forest floor equals:

$$I(t) = E_{i,f}(t) + \frac{dS_u}{dt} = T_f - F \quad (2.4)$$

where F is the infiltration [$L T^{-1}$] and equals dS_l/dt .

Temperature influence

Electronic instruments often have problems with temperature differences, and so does the logger and the sensors of the forest floor interception device. First of all, the resistance of the wires is sensitive to temperature changes. This is mainly important for the logger. To overcome this problem, we do not measure the actual resistance difference, but the relative. Hence we compare the change in resistance over the sensor (due to weight changes) with the change in resistance in the logger (due to internal temperature differences). In this way, the effect of resistance change of the electronics is largely reduced.

Secondly, the sensors are temperature dependent. Since the weighing sensors are made of a piece of metal with strain gauges, temperature changes have an effect on the sensor output due to the expansion and compression of the metal. From 2004 to 2006 the device was compensated with the relation between temperature and weight change observed in a dry period by linear regression (see Gerrits et al. [2007] for further details).

Since 2006 an additional sensor (so-called ‘dummy sensor’) has been installed to compensate for the temperature influence. The dummy sensor is a free hanging sensor with no weight on it and thus only reacts on temperature changes. The relation between the dummy sensor and the other sensors has been determined in the laboratory, which is then used to correct the observed data. For example, when the dummy shows an increase of 30 mV (ΔS_{dum}), we subtract 30 mV times factor α_i from the output of sensor i (ΔS_{obs}) to obtain the output due to weight change (ΔS_w):

$$\begin{aligned} \Delta S_{obs,i} &= \Delta S_{w,i} + \Delta S_{temp,i} \\ \Delta S_{temp,i} &= \alpha_i \cdot \Delta S_{dum} \end{aligned} \quad (2.5)$$

Disturbances

Inherent to an experimental field setup is the disturbance of the system causing possible errors in the observations. It is a challenge to minimize these effects as much as possible; however, some remain unavoidable. In our setup the rim of the upper basin, which sticks out about 5 cm, can alter the wind flow, causing maybe higher evaporation rates than in the undisturbed case. However, wind speed under the canopy is observed to be low. With a meteorological tower (HOBO Onset) under the canopy, we measured at 10 meter above the surface average wind speed varying from 0.02-0.4 m/s in 2008-2009. Near the surface wind speed is assumed to be even lower, resulting in a low rim effect.

Also the wooden shelves surrounding the device can be a disturbance. The shelves have been installed to avoid evaporation from the lower basin and to avoid direct rainfall into the lower basin. Although, the shelves solved these problems, they might influence the micro-climatic conditions by having a different reflection coefficient and/or heat conducting capacity. However, in the initial setup the shelves were not installed yet and did not observe significant differences in the observations. Hence we assume the effect of the shelves to be negligible.

Another disturbance of the setup can be the use of geotextile as a permeable interface between the forest floor and the lower basin. As stated by Helvey and Patric [1965] the geotextile (or any other artificial barrier) will cause water accumulation on the interface before drainage starts. After the event this water is then readily available for evaporation, resulting in an overestimation of forest floor evaporation. In our setup we never observed this effect during field visits. Only during a spraying experiment with extreme high rainfall intensities we observed that the geotextile acted as a barrier. However, it remains possible that the geotextile influences our observations.

Forest floor thickness

At our site in Luxembourg we only measured forest floor interception with one single device and therefore we did not take the spatial variability of the forest floor thickness into account. However, in the experimental plot no significant differences in forest floor thicknesses were observed. Maybe also because the experimental site is on a relative flat area, while along a hillslope differences in litter thickness are likely to occur. However no clear relation can be found in literature. As concluded by Burghouts et al. [1998] the litter layer increases in downslope direction, while Nooren et al. [1995] found the opposite.

Besides the variability in space, the layer thickness also changes in time. During the fall the canopy sheds its leaves, causing an increase in forest floor thickness. Due to snow, through compaction, it is observed that the layer thickness is decreased. Over time, the forest floor decomposes into a soil horizon. As a result over time we would gradually move from measuring forest floor interception to combined forest floor interception and soil evaporation. Therefore, we emptied every year the upper basin and refilled it with new material from the surroundings.

Concerning the spatial and temporal variability there may be a considerable uncertainty and variability in the forest floor interception storage. However, as we demonstrated in Chapter 3 and 5 the sensitivity to the interception storage is modest, whereas the temporal distribution of the rainfall is far more important.

2.2 Study areas

2.2.1 Huewelerbach

The Huewelerbach catchment (49°42'N 5°53'E) is a hill slope area in Luxembourg, which consists mainly of sandstone (see Figure 2.4). The catchment area is about 2.7 km², altitudes ranging from 290 m to 400 m and is almost completely covered with forest (91.5%) and some grassland (7%). The climate in Luxembourg is modified oceanic with mild winters and temperate summers. The average annual temperature is circa 8°C and the total rainfall is about 845 mm/a (Pfister et al. [2005]). In the Huewelerbach catchment, an experimental plot of 0.0596 ha has been set up in a 120 year old beech (*Fagus sylvatica*) forest with a density of 168 trees/ha and a mean DBH of 62±9 cm. The plot is on a relatively flat area and the average tree height is about 15 meter. In Figure 2.4b the distribution of the trees is depicted.

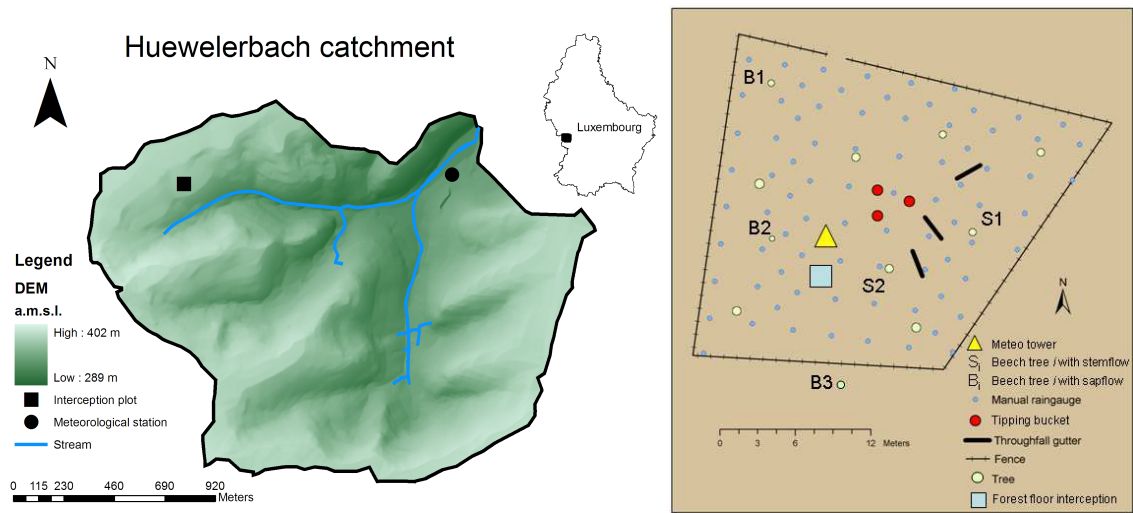


Figure 2.4: Overview of the Huewelerbach catchment (left) and interception plot (right).

In this plot throughfall, stemflow and forest floor interception are measured. Throughfall is measured with three gutters connected to a tipping bucket and 81 manual rain gauges in order to capture the spatial variability. Stemflow is measured on two trees, marked with S1 (DBH = 60 cm) and S2 (DBH = 67 cm) respectively. In the valley near the outlet of the catchment a weather station (Campbell Scientific) is located in the open to measure gross precipitation. We assumed that the measured rainfall in the valley equals above canopy rainfall. To verify the correct functioning of the tipping bucket, an additional rain collector collects gross precipitation and is read at weekly intervals.

A forest floor interception device is installed in the plot and filled with a circa 8 cm thick beech leaves (L & F layer) (Figure 2.5), which is similar as the surrounding forest floor thickness. The device has a surface area of 1 m² and measures every 5 minutes. For the water balance calculation of the device, the mean of the four surrounding throughfall rain gauges is used combined with

the temporal tipping bucket data. For verification an additional barrel is installed that collects the infiltrated water.



Figure 2.5: Forest floor device in the Huewelerbach with a beech layer.

In Table 2.1 an overview of the measuring periods used in this thesis are given:

Equipment	Measuring period
Throughfall (41 collectors)	October 2003 - April 2004
Throughfall (81 collectors)	May 2004 - July 2009
Stemflow	January 2004 - July 2009
Forest floor interception	November 2004 - March 2009
Leaf Area Index	May 2007 - December 2009
Weather station	April 2003 - July 2009

Table 2.1: Overview of the measuring periods used in this thesis (Huewelerbach).

2.2.2 Westerbork

The experimental plot in Westerbork (52°54'N, 6°36'E) is located in the area of the radio observatory ASTRON. On the plot a concrete bunker under a small sandy hill lock has been built. In this bunker gravity is measured very accurately, to investigate, among others, the relation between gravity and water storage. On top of the bunker the interception device is installed. The device is in an open area, about 25 m near a forest edge. The device is filled with a 10-15 cm thick layer of mosses and grass (see Figure 2.6). We observed that in winter moss dominated over grass, while in summer more grass was developing. The surface area of the device is 0.60 m² and thus smaller than the other setups and therefore more sensitive to the boundary conditions as described in Section 2.1.4. Next to the device, rainfall is measured with a tipping bucket (HOBO RG2-M; 0.2 mm). Precipitation equals the net precipitation, since the device is installed in the open field. The climate in Westerbork is temperate, marine with cool summers and mild winters. Westerbork has an average yearly rainfall sum of 774 mm/year and an average temperature of circa 9°C (Heijboer and Nellestijn [2002]).



Figure 2.6: Forest floor device in Westerbork with a moss/grass layer.

In Table 2.2 an overview of the measuring periods used in this thesis are given:

Equipment	Measuring period
Forest floor interception	September 2005 - December 2009
Precipitation	September 2005 - December 2009

Table 2.2: Overview of the measuring periods used in this thesis (Westerbork).

2.2.3 Botanical Garden

The experimental plot is located in the Botanical Garden in Delft in the west of the Netherlands (52°00, 47'N 4°22, 25'E). The garden is located in an urban area and has a temperate maritime climate, with mild summers and cool winters. The average annual precipitation is 840 mm/year and the average temperature is 10° Celsius (Heijboer and Nellestijn [2002]).

The forest floor interception device is located in a pine plot. In the surrounding of the device the dominant tree species is Blue Cedar (*Cedrus atlantica*). The device is directly under one single Blue Cedar. The device has a surface area of 1 m² and is filled with a 5 cm thick layer of Blue Cedar needles (Figure 2.7). Next to the forest floor interception device two tipping buckets (HOBO RG2-M) have been installed to measure throughfall. Canopy interception is not determined for this site, since the botanical garden is not a natural environment. Hence only the relation between throughfall and infiltration is investigated.

In Table 2.3 an overview of the measuring periods used in this thesis are given:

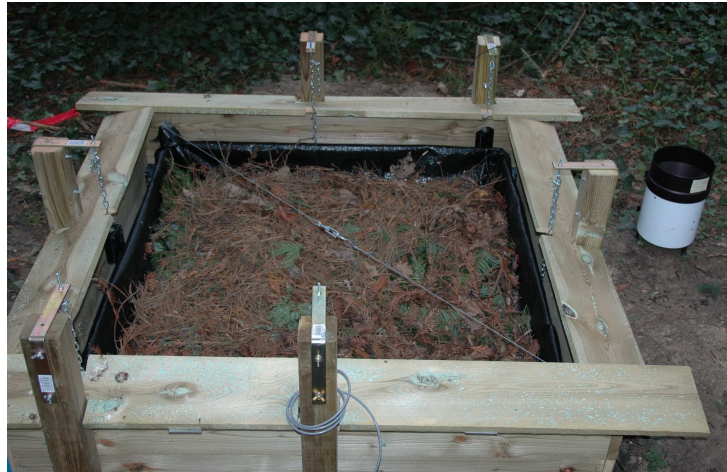


Figure 2.7: Forest floor device in the Botanical Garden Delft with a needle layer.

Equipment	Measuring period
Forest floor interception	January 2007 - March 2009
Throughfall	November 2006 - March 2009

Table 2.3: Overview of the measuring periods used in this thesis (Botanical Garden).

Chapter 3

Spatial and temporal variability of canopy and forest floor interception

.....

Depending on season, rainfall characteristics, and tree species, interception amounts to 15-50% of total precipitation in a forest under temperate climates. Many studies have investigated the importance of interception of different tree species in a range of different climates. Often authors merely determine interception storage capacity of that specific species and the considered event, and only sometimes a distinction is made between foliated and non-foliated trees. However, interception is highly variable in time and space. Firstly, since potential evaporation is higher in summer, but secondly because the storage capacity has a seasonal pattern. Besides weather characteristics like wind and rain intensity, snow causes large variations in the maximum storage capacity. Interception has been measured continuously on three different forests: beech leaves (Luxembourg), moss/grass (Westerbork), and cedar needles (Botanical garden). In the experimental beech plot in Luxembourg we found storage capacity of canopy interception to show a clear seasonal pattern varying from 0.4 mm in winter to 0.9 mm in summer. The capacity of the forest floor appears to be rather constant over time at 1.8 mm. Both have a standard deviation as high as $\pm 100\%$. However, the process is not sensitive to this variability resulting only in 11% variation of evaporation estimates. Hence the number of raindays and the potential evaporation are stronger driving factors on interception. Furthermore, the spatial correlation of the throughfall and infiltration has been investigated with semi-variograms and time stability plots. Within 6-7 m distance throughfall and infiltration are correlated and the general persistence is rather weak.

.....

Based on: Gerrits, A. M. J., Pfister, L., Savenije, H. H. G., 2010 (in press). Spatial and temporal variability of canopy and forest floor interception in a beech forest. Hydrological Processes doi: 10.1002/hyp.7712, –

3.1 Introduction

In a forest, part of the precipitation is intercepted by vegetation. Rain drops first hit the leaves and branches before they fall on the forest floor, where again a part is intercepted by litter on the forest floor. Progressively, the canopy and the litter dry-out by evaporation. Both processes are here considered to be part of the same interception process, I , which equals the sum of the change in interception storage (S_i) and the evaporation from this stock (E_i):

$$I = E_i + \frac{dS_i}{dt} \quad (3.1)$$

Interception is considered to be about 15 to 50% of the total incoming precipitation on forests in temperate humid latitudes (e.g., Rutter et al. [1975], Viville et al. [1993], Hörmann et al. [1996], and Savenije [2004]). Since the intercepted and evaporated water is not recharging the forest soils, the interception process is important to the forest soil moisture balance of forests. The intercepted water does not contribute to the soil reservoir and hence is not available to vegetation. In addition, the interception process plays an important role as a re-distributor of rainfall in space. In general, throughfall is less than gross precipitation, but often drip points are observed where the canopy and branches funnel the rainfall causing locally higher intensity throughfall (e.g., Germer et al. [2006] and Gerrits et al. [2009a]). This results in concentrated infiltration, which again may be the trigger for sub-surface flow. These throughfall patterns appear to have an important influence on the soil moisture patterns (Bouten et al. [1992]).

In literature, many studies on interception can be found (see Kittredge [1948], Zinke [1967], and Breuer et al. [2003] and references herein). Most of these studies consider interception of events or short duration periods (in the order of months). However, interception is highly seasonal. First of all the potential evaporation changes throughout the year and so does the storage capacity for deciduous trees. At best a distinction is made between leaf-on and leaf-off periods (e.g., Rutter et al. [1975], Rowe [1983], Hörmann et al. [1996], Zhang et al. [2006], Fenicia et al. [2008a], and Herbst et al. [2008]), but the transition between these states is rarely described. The spatial variability of the canopy coverage also causes large variations in the storage capacity and differs per season (Staelens et al. [2006]). Furthermore, the storage capacity depends on precipitation conditions that vary over time (e.g., snow/no snow, heavy rain/drizzle, low wind/strong wind). Hence, it is not possible to define one single storage capacity for a certain tree species in contrast to what many authors claim. This is especially important when these storage capacities are used for interception modelling.

The aim of this chapter is to investigate how the interception process changes over the seasons and how this affects evaporation predictions of an interception model. This model is used to investigate the spatial distribution and the persistence of spatial throughfall and infiltration patterns.

3.2 Methodology

To investigate the effect of forest interception both canopy and forest floor interception have been measured. Canopy interception is defined as precipitation (P_g) minus the sum of throughfall (T_f) and stemflow (T_s) (Equation 3.2):

$$E_{i,c} + \frac{dS_c}{dt} = P_g - T_f - T_s \quad (3.2)$$

where $E_{i,c}$ is evaporation from the canopy and S_c the storage on the canopy. Forest floor interception is defined as:

$$E_{i,f} + \frac{dS_f}{dt} = T_f - F \quad (3.3)$$

where $E_{i,f}$ is evaporation from the forest floor, S_f the storage on the forest floor and F the infiltration. For both interception types we have investigated the temporal variation of evaporation from interception.

The maximum storage capacity, S_c , is determined by the ‘mean-method’ of Klaassen et al. [1998], where the storage capacity is the negative intercept with the y-axis of the linear regression line of accumulated gross rainfall versus accumulated throughfall of an event. In this way the effect of evaporation during the event is taken into account (when the slope of the regression line is less than 1:1). For the storage capacity of the forest floor, S_f , the same procedure is used on accumulated throughfall versus accumulated infiltration.

Only those events that meet the following criteria have been selected:

- The event is large enough to saturate the storage capacity, causing throughfall to occur from the canopy or infiltration from the forest floor.
- The time between the events is long enough for the intercepted water to completely evaporate and that no water is stored before the start of the next event.

The storage capacities are determined for all events under different weather conditions to study the seasonality (average variation over time) and variability (variation within a certain season or period). Also the relation between storage capacity and rain intensity and wind speed is investigated.

To investigate the effect of the observed uncertainties on interception predictions we applied a modified Rutter model (Rutter et al. [1971]), which was extended with a forest floor interception reservoir. In Figure 3.1 an overview of the model structure is given. Drainage is modelled as an exponential function with D_0 taken from Rutter et al. [1971]. Drainage is also possible when $S_c^l < S_{c,max}^l$, taking care of the shake off of rain drops by wind.

The partitioning of the gross rainfall into canopy input, free throughfall and trunk input is based on site measurements. The factor p is determined by light interception measurements. A fish-eye lens is connected to a light sensible resistance and the ratio of light intensity under (I) and

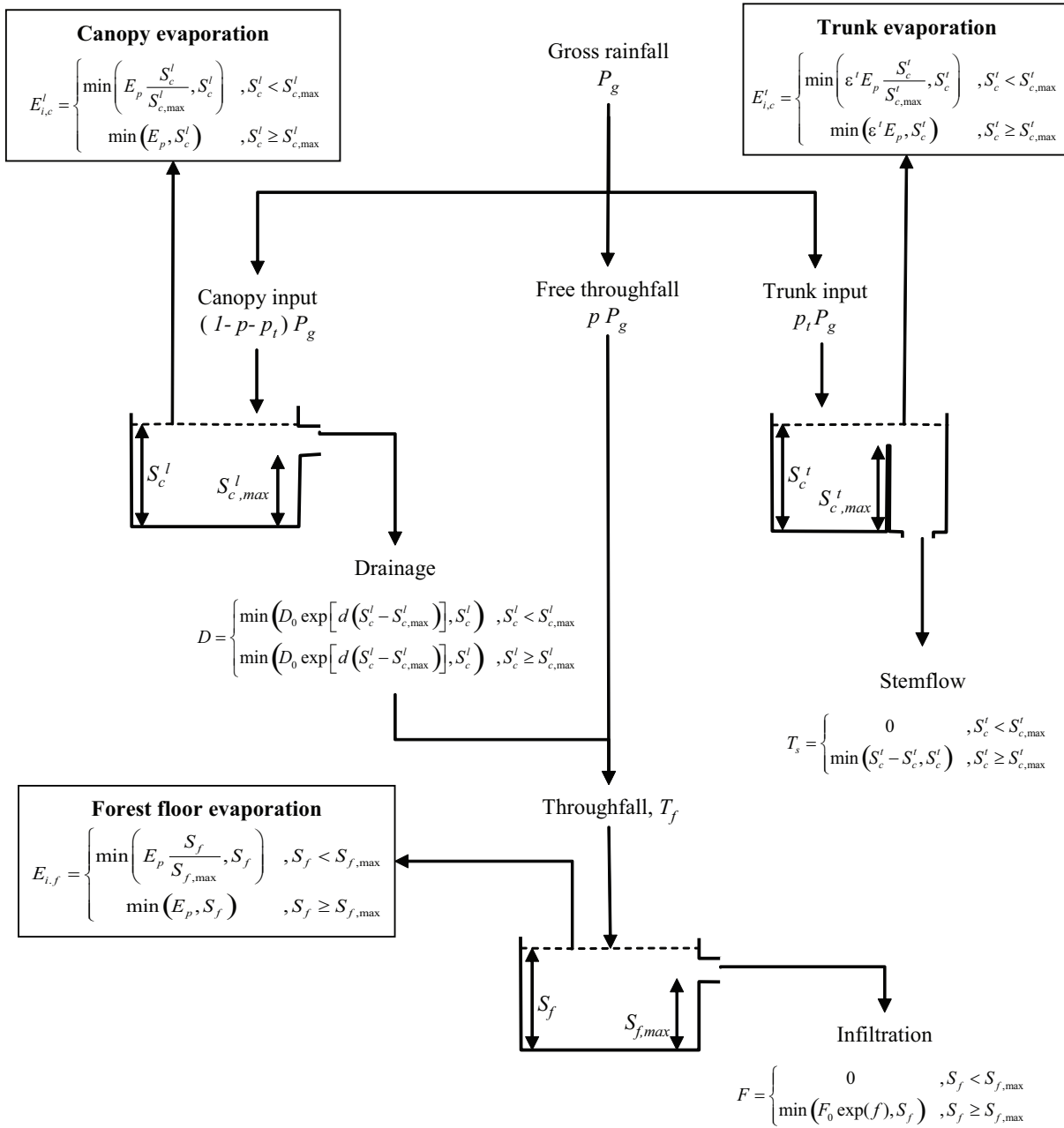


Figure 3.1: Overview of the adapted Rutter model, which is an extension on the model by Rutter et al. [1971] (Figure 1.2).

above (I_0) the canopy equals p .

The fraction p_t is determined as in Gash and Morton [1978] and Kittredge [1948]. We found a p_t fraction equal to 0.07. Since p_t is not changing over time, we consider p_t to be constant. The negative intercept with the y-axis determines the storage capacity of the trunk. We assume the trunk storage capacity to be a constant equal to 0.11 mm.

The maximum storage capacity of the canopy ($S_{c,max}^l$) and the forest floor ($S_{f,max}$) are derived from the measurements as described above and are dependent on the season. For calibration of the adjusted Rutter model we used the mean storage capacity per month.

The forest floor reservoir is modelled in the same way as the canopy reservoir: a threshold (S_f) and an exponential infiltration rate, F ; however, infiltration equals zero if $S_f < S_{f,max}$, because wind will not shake off rain drops at forest floor level.

Potential evaporation (E_p) is calculated with the Penman equation (Allen et al. [1998]). The potential evaporation for the forest floor is only slightly lowered by increasing the relative humidity by 2%. We acknowledge that this might be wrong because the incoming radiation under the canopy is much lower than above canopy and this reduces the potential evaporation for the forest floor; however, there is also a ground heat flux and less outgoing radiation under the canopy. Especially the ground heat flux can be an important energy provider for forest floor evaporation. Therefore, we assumed the potential evaporation for the canopy almost equal to the potential evaporation for the forest floor. We agree that the available energy requires more detailed study, but since this research focused on the water balance we did not include this in the set-up.

Finally, the spatial variability has been investigated through semi-variograms and time stability plots. We used the method as described by Keim et al. [2005] to calculate the semi-variogram:

$$\gamma(h) = \frac{\sum_{n(h)} \left(\tilde{N}_{x,y} - \tilde{N}_{x,y+h} \right)^2}{2n(h)} \quad (3.4)$$

Where h is the lag, $n(h)$ is the number of measurements pairs in the data set that are distance h apart and $\tilde{N}_{x,y}$ the normalized throughfall or infiltration at measuring point (x, y) :

$$\tilde{N}_{x,y} = \frac{N_{x,y} - \bar{N}}{\sigma(N)} \quad (3.5)$$

with σ the standard deviation. We used normalized data to be able to compare throughfall and infiltration with each other.

3.3 Temporal variation in interception measurements

3.3.1 Canopy interception

The observed gross precipitation, average throughfall, and stemflow of the beech forest in the Huewelerbach are depicted in Figure 3.2. We observe a clear seasonal pattern in the evaporation from canopy interception as a percentage of gross rainfall (Figure 3.2b). When there are leaves on the trees from April until September (indicated by the green bar) evaporation from interception is on average 15% of the precipitation compared to 7% in winter (Table 3.1).

Season	\bar{P} [mm/d]	\bar{T}_f [mm/d]	\bar{T}_s [mm/d]	$\bar{E}_{i,c}$ [mm/d]
Leaf-on (April-September)	2.10	1.71 (81%)	0.07 (3%)	0.32 (15%)
Leaf-off (October-March)	2.24	1.94 (87%)	0.14 (6%)	0.16 (7%)

Table 3.1: Mean waterbalance components for canopy interception in the Huewelerbach.

Furthermore, some positive and negative outliers can be seen in the percentage of canopy interception (Figure 3.2b). These events often coincide with small rainfall amounts (triangles), causing relatively large errors in the readings, or coincide with snow or ice events (asterisks). Snow and ice can prevent precipitation to be caught by the tipping bucket or the collector, or the recording to be delayed.

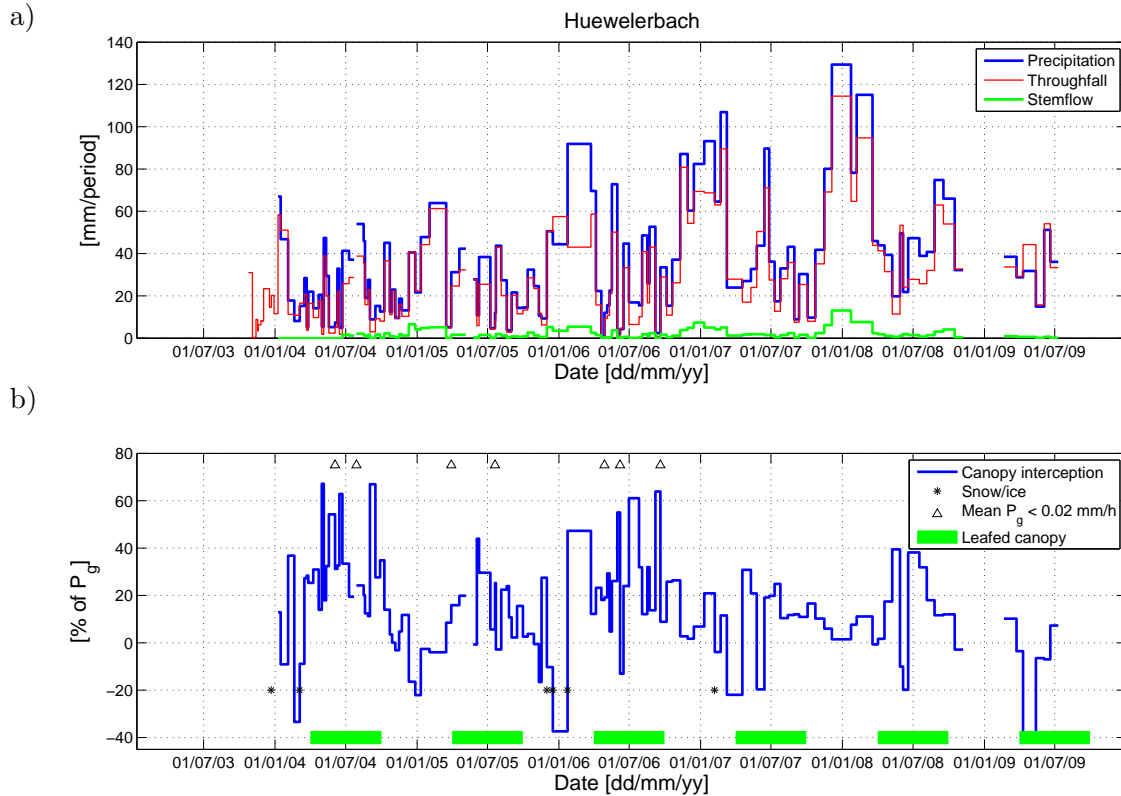


Figure 3.2: Precipitation, collector readings of throughfall (average over 81 collectors), and stemflow (a) and b) canopy interception percentage (of precipitation) over time in the Huewelerbach.

3.3.2 Forest floor interception

Beech leaves - Huewelerbach

In Figure 3.3 the results obtained from the forest floor interception device of beech leaves (Huewelerbach) are shown. The large data gaps are caused by several problems with the newly developed device. Lots of data was lost due to problems with the data logger, damage by branches that fell on the device, battery failures, etc. Even a completely new device was built, that caused in total a data gap of more than one year in 2005-2006.

Unlike with canopy interception, there is no clear seasonal trend. Although the amount of data is limited, we can see that evaporation from the forest floor is rather constant over the year, with a slight increase in summer. On average, evaporation is 22% (0.4 mm/day) of the throughfall when extreme values, related to snow events, are not included. Snow causes high water equivalents to be first stored in the upper basin of the device, which will drain towards the lower basin only when the temperature is again above 0°C. Similar to canopy interception, it appears that small rainfall events (and thus throughfall events) cause relatively high forest floor interception values.

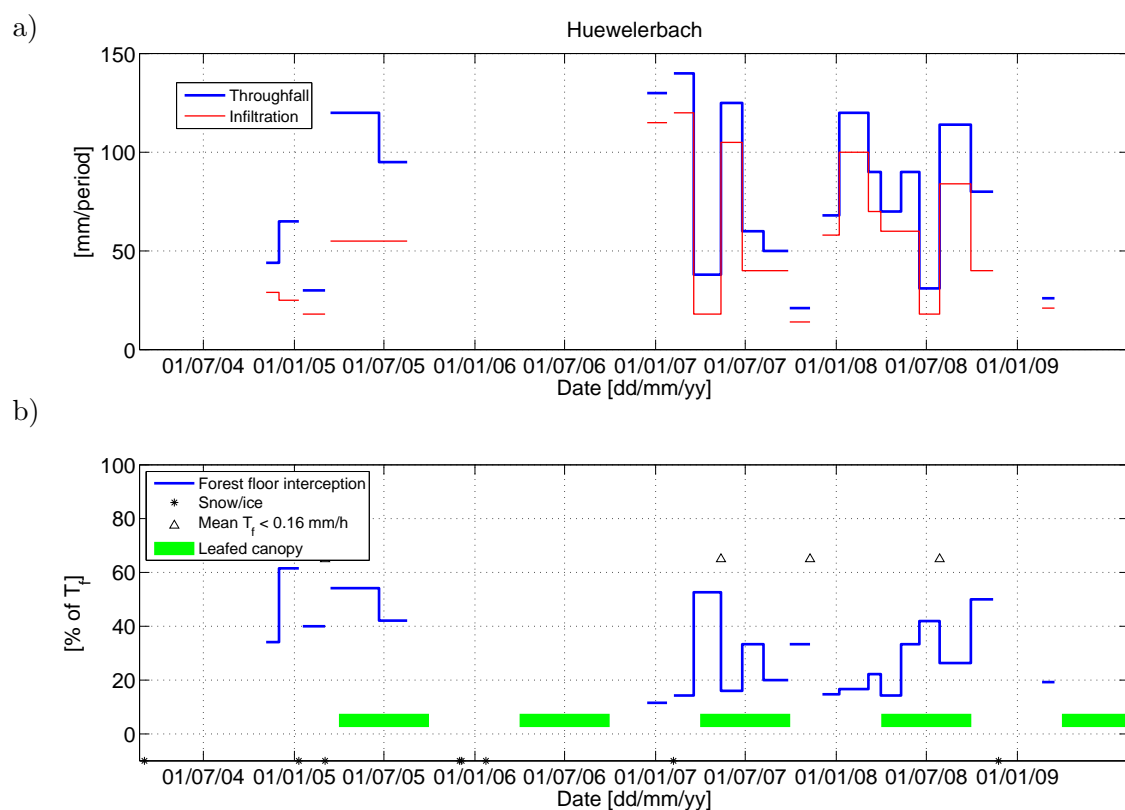


Figure 3.3: Beech leaves (Huewelerbach): a) Throughfall and infiltration and b) Temporal variation of forest floor interception as percentage of throughfall (four throughfall collectors nearest to forest floor interception device).

Combining results from canopy evaporation and forest floor evaporation, we can conclude that in winter 27% of the precipitation is intercepted from the beech forest and in summer as much

as 34%. Hence the seasonal effect of interception, if forest floor interception is included, is less strong when only based on canopy interception. The annual interception amounts to 27-34% of gross rainfall and amounts to 34-43% of the actual evaporation in the Huewelerbach catchment, based on water balance data from 2004 until 2006 (Atlas2004 [2004], 2005, and 2006). This is a considerable part of the total evaporation, taking into account the modest dimensions of the interception reservoir compared to the soil moisture storage capacity. The reason for this relatively high interception flux lies in the high number of rainfall events as compared to infiltration events.

Moss/Grass - Westerbork

The calculation of interception for moss and grass is different from beech leaves and cedar needles, because transpiration also occurs. The forest floor interception measurements are compensated by subtracting an approximation of transpiration for each time series. In a dry period after the intercepted water is assumed to be evaporated (> 1 week), it is assumed that depletion of the upper basin is only caused by transpiration. Successively, the calculated depletion rate is subtracted over the entire time series (of about one month). In this way seasonal variation in transpiration rate are taken into account. In Figure 3.4 the results are shown.

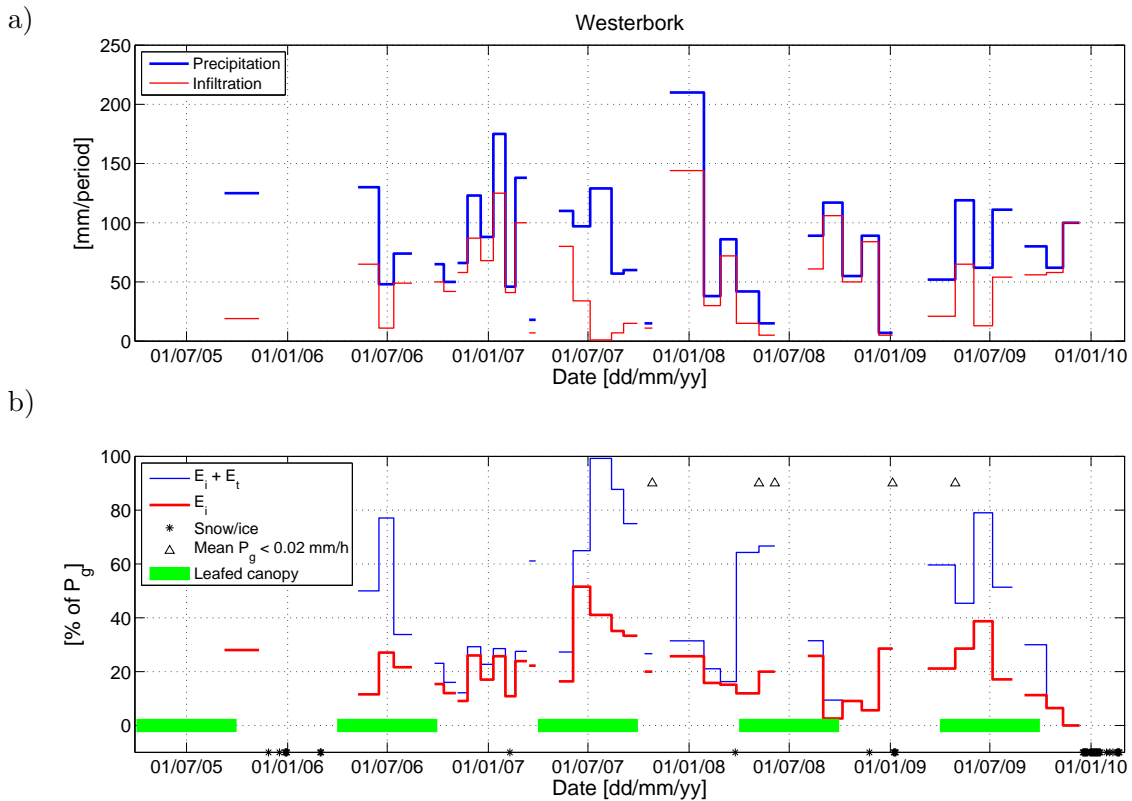


Figure 3.4: Moss/Grass (Westerbork): a) Precipitation and infiltration and b) Temporal variation of forest floor interception as percentage of rainfall.

Different from the beech floor, it appears that there is a seasonal trend in interception by moss/grass. In summer 25% of rainfall (0.7 mm/day) evaporates and in winter 15% (0.5 mm/day).

This is likely due to two reasons. First, the setup in Westerbork is installed in the open field, hence there is no canopy that attenuates the potential evaporation. Second, the vegetation changes over the year. From field observations we know that in winter moss dominates, while in summer more grass is developing. With the vegetation change the storage capacity changes, resulting in different interception values.

Cedar Needles - Botanical Garden

In Figure 3.5 the results for the Cedar floor of the Botanical Garden are presented. On average 18% of throughfall has been evaporated from the forest floor, which is comparable to the beech floor of the Huewelerbach. However, the average evaporation equals 0.2 mm/day (20% of T_f) in summer and 0.1 mm/day (16% of T_f) in winter, which is lower than the beech floor (0.4 mm/day). This is mainly due to the higher LAI of cedar trees, which results in less radiation to be able to penetrate through the canopy.

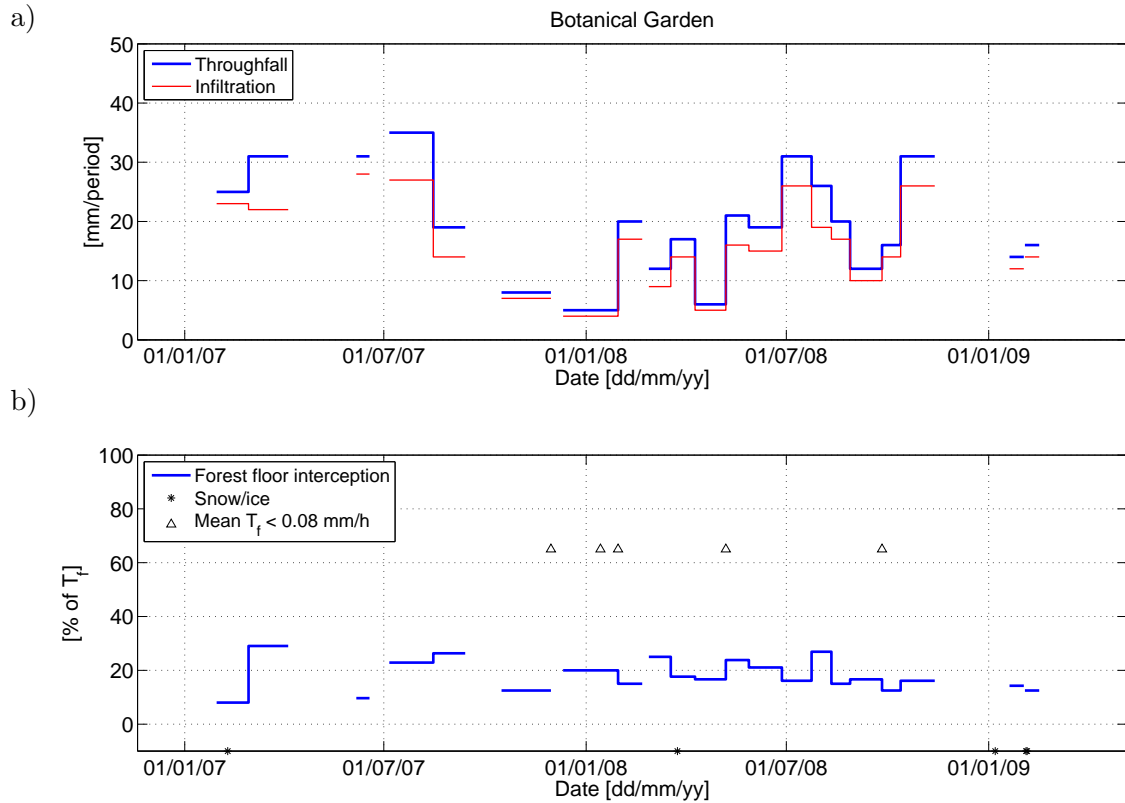


Figure 3.5: Cedar needles (Botanical Garden): a) Throughfall and infiltration and b) temporal variation of forest floor interception as percentage of throughfall.

3.4 Temporal variation in storage capacity

To determine the storage capacity of the canopy and forest floor, only those events have been selected that meet the criteria in the Methodology Section 3.2.

3.4.1 Canopy interception

For the analysis of storage capacity 52 recorded events meet the criteria for the beech forest. To ensure that the canopy is dry before an event, at least 2 days of no rain had to separate two events. As can be seen in Figure 3.6, there is a clear seasonal variability in the canopy storage capacity. In winter the capacity is on average low: 0.4 mm and in summer when the leaves are on the trees the capacity is on average 0.9 mm.

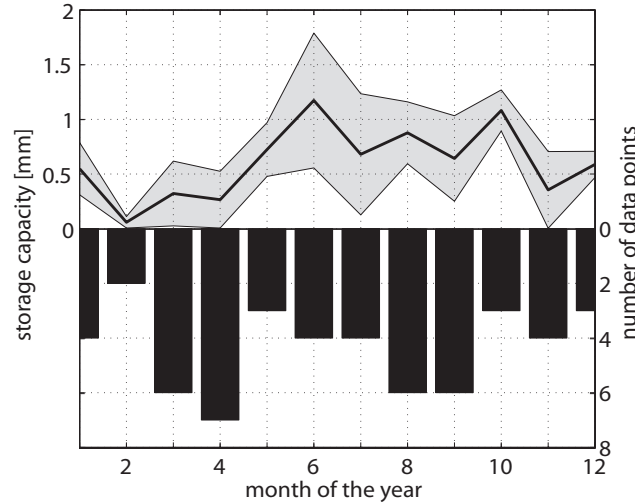


Figure 3.6: Variability of the canopy storage in the beech forest (Huewelerbach). The black line is the mean of all events in a certain month, and the grey area defines a bound of one standard deviation. The number of events is indicated by the black bars.

The grey area indicates a band of one standard deviation in the storage capacity of the different events. In winter the deviation is ± 0.2 mm ($c_v = 46\%$), compared to ± 0.5 mm ($c_v = 54\%$) in summer. Hence it is difficult to determine one single capacity value, especially when the canopy is developed. One of the reasons for the variability may be the applied regression method of Klaassen et al. [1998] to determine the storage capacity. As Rowe [1983] concluded, this approach is strongly influenced by wind speed and intensity. For example, Horton [1919], Klaassen et al. [1996] and Hörmann et al. [1996] found that with increasing wind speed the measured storage capacity is less, due to the fact that the wind shakes the rain water off the leaves. This effect is also visible in Figure 3.7a, although the relationship is weak. We also tested the relationship between maximum windspeed during the event and storage capacity, but the relationship is even worse.

There is no consensus in the literature on the effect of rainfall intensity on the storage capacity. On the one hand, Horton [1919] and Wang et al. [2007] concluded that the higher the rainfall intensity the lower the capacity, because high rainfall intensities cause splashing and shaking of leaves. On the other hand, Aston [1979] and Keim et al. [2006a] found the opposite: high rainfall intensities coincide with high storage capacities, due to dynamic storage. Based on our data we do not see a clear relationship, only a weak decline in storage capacity with increasing average

intensity (see Figure 3.7b). Also no relationship has been found with maximum rainfall or storm size.

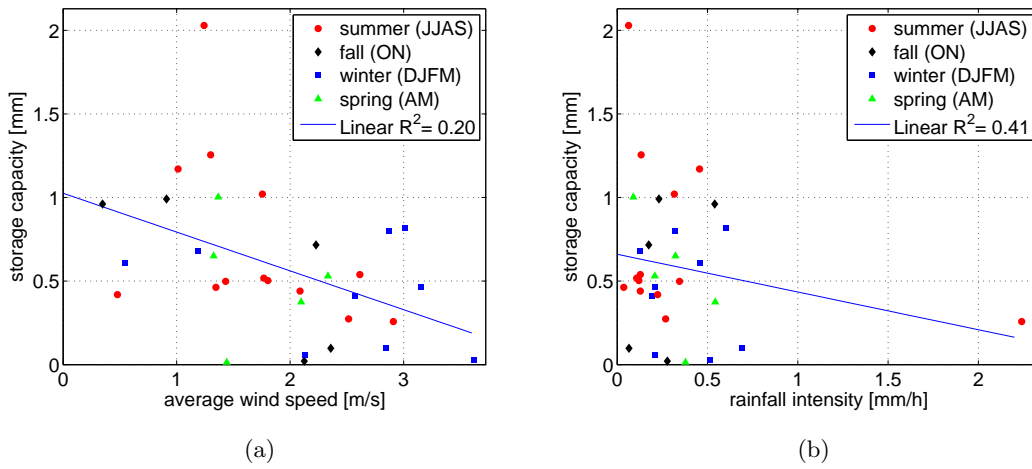


Figure 3.7: Effect of average 15-min wind speed per event (a) and average 15-min rainfall intensity per event (b) on canopy storage capacity during different seasons.

3.4.2 Forest floor interception

Beech leaves - Huewelerbach

For the forest floor 74 recorded events were available (we also used data from the gaps presented in Figure 3.3 in case the lower basin was working). The weight of upper basins was used to determine if the forest floor was dry before an event. In contrast to the canopy there is no apparent seasonal trend (see Figure 3.8a). The storage capacity is rather constant over the year (1.8 mm), with a temporal increase during early fall (2.8 mm). This can be explained by the fresh litter. The fresh leaves dry out quickly after they fall off the tree and obtain a curled shape, which has a high storage capacity. However, the curled shape can quickly disappear after rain or snow storms.

Furthermore, it can be seen that the variability is changing from winter to summer. In contrast to the canopy storage capacity, the variability in summer is lower ± 0.4 mm ($c_v = 19\%$) than in winter ± 0.8 mm ($c_v = 50\%$). This can be explained by the effect of snow, which has been repeatedly observed during field observations. If a snow event occurs, the leaves are completely flattened due to the snow weight, causing a small storage capacity. If no snow occurs, the leaves retain their original shape, with a large storage capacity. Hence, the capacity really depends on whether snow events occurred or not. This causes a large variability in winter values.

Additional variability may be caused by throughfall intensity. Putuhena and Cordery [1996], Sato et al. [2004] and Guevara-Escobar et al. [2007] found that with increasing intensity the dynamic, and also the static storage capacity increased. If we test this hypothesis on our data,

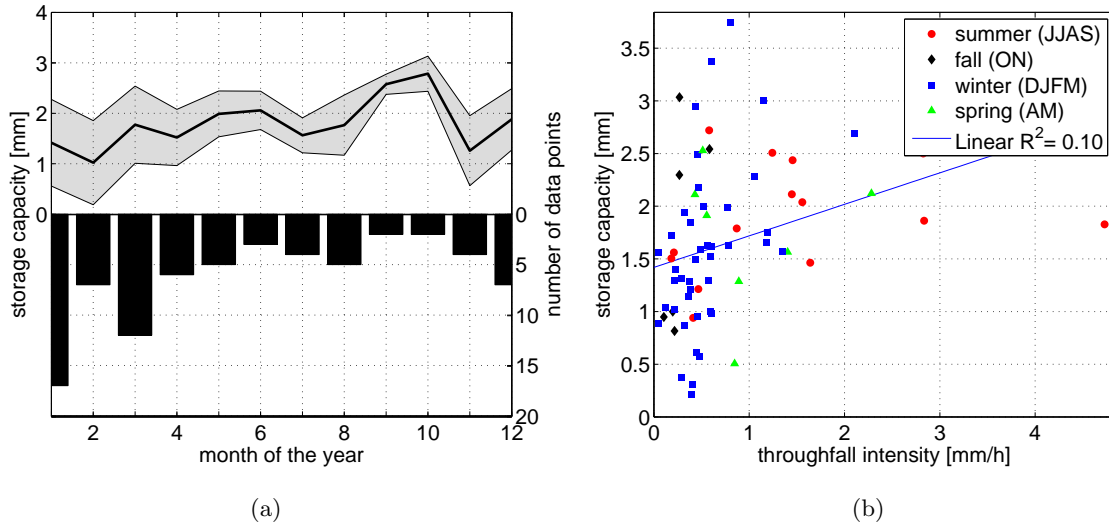


Figure 3.8: a) Variability of the storage capacity of the forest floor of beech leaves (Huewelerbach). The black line is the mean of all events in a given month, and the grey area defines the standard deviation. The number of events is indicated by the black bars. b) Effect of average throughfall intensity on storage capacity throughout the seasons.

we find a weak positive relationship (Figure 3.8b). The effect of wind is not investigated, since it is not likely that wind can shake off water at forest floor level.

Moss/grass - Westerbork

The determination of the storage capacity of a moss and grass floor is different from the two other setups, because after the interception storage is filled, the unsaturated soil layer is also recharged. The forest floor interception device is not able to distinguish between these two, and would overestimate the storage capacity if the storage in the soil layer is not taken into account.

To compensate for the soil storage we determined the saturation level of the soil if possible. This level is subtracted from the determined storage capacity to obtain the storage capacity of only the interception. If it was not possible to find the saturation level, we did not take these events into account. After the correction 53 events were available. In Figure 3.9a the result of the corrected storage capacity is shown.

As can be seen, there is a seasonal trend in the storage capacity. This was already observed during field visits. In winter moss dominated over grass, while in summer more grass was developing. On average the storage capacity is 3.1 mm with a variability of ± 0.9 mm ($c_v = 31\%$). This is comparable with the storage capacity of Guevara-Escobar et al. [2007], who investigated also grass, but with a laboratory sprinkling setup. In winter the storage capacity is lower: 2.0 mm ± 0.9 mm ($c_v = 45\%$) and in summer higher: 4.1 mm ± 1.0 mm ($c_v = 24\%$). There appears to be no significant relation between storage capacity and rain intensity.

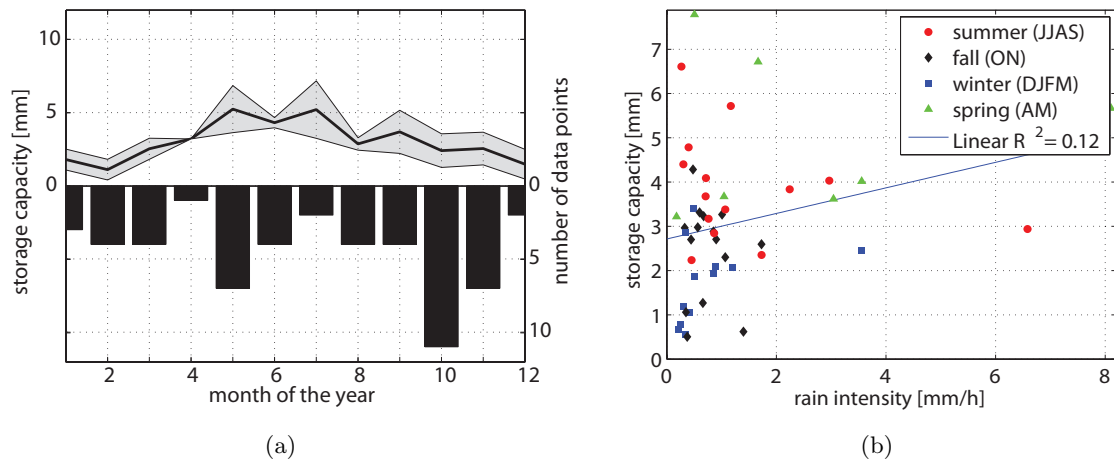


Figure 3.9: a) Variability of the storage capacity (corrected) of the forest floor of moss and grass (Westerborg). The black line is the mean of all events in a given month, and the grey area defines the standard deviation. The number of events is indicated by the black bars. b) Effect of average rain intensity on storage capacity throughout the seasons.

Cedar Needles - Botanical Garden

Forty nine events were available to determine the storage capacity of the cedar needles. In Figure 3.10a the calculated capacities are shown. The storage capacity is, as expected, constant over the year since coniferous trees do not drop their needles in one specific period of the year. The mean storage capacity is 1.0 mm and the variability is ± 0.3 mm ($c_v = 35\%$). This variability is not caused by snow events, because they rarely occurred. Also the effect of throughfall intensity did not appear to be significant (Figure 3.10b).

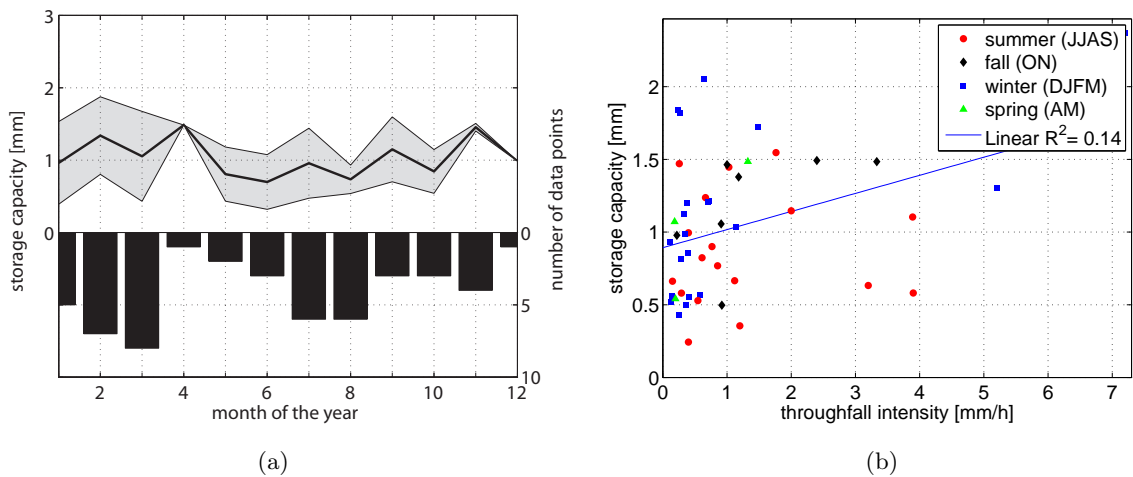


Figure 3.10: a) Variability of the storage capacity of the forest floor of Cedar needles (Botanical Garden). The black line is the mean of all events in a given month, and the grey area defines the standard deviation. The number of events is indicated by the black bars. b) Effect of average throughfall intensity on storage capacity throughout the seasons.

3.5 Effect of variability in storage capacity on Rutter model predictions

The consequences of the variability in storage capacity on prediction with a Rutter model (Rutter et al. [1971]) have been analyzed to assess the prediction error due to uncertainty in the storage capacity. We choose to use the observations from the beech forest in the Huewelerbach catchment.

In Table 3.2 the model parameters are given. The model is evaluated on throughfall, infiltration, forest floor evaporation, and forest floor wetness. SIM1 (winter) and SIM2 (summer) are used to calibrate the model. The other simulations are used for validation.

Parameter	Value	Parameter	Value
p	[-] I/I_0	ϵ^t	[-] 0.5 (calibrated)
p_t	[-] 0.07	D_0	[L T ⁻¹] 0.03 mm/15 min (Rutter et al. [1971])
$S_{c,max}^l$	[L] Figure 3.6	d	[L ⁻¹] 0.9 mm ⁻¹ (calibrated)
$S_{c,max}^t$	[L] 0.11 mm	F_0	[L T ⁻¹] 0.04 mm/15 min (calibrated)
$S_{f,max}$	[L] Figure 3.8	f	[L ⁻¹] 2.0 mm ⁻¹ (calibrated)

Table 3.2: Model parameters of adjusted Rutter model (beech forest).

In Table 3.3 the model results of the adjusted Rutter model are presented for 6 simulation periods. Given are the Root Mean Square Error (RMSE), the relative bias and the Nash-Sutcliffe efficiency (Nash and Sutcliffe [1970]). Overall the performance of the model is reasonable, although the goodness-of-fit measures are sometimes poor. RMSE is not very good due to fluctuations that may be caused by the temperature sensitivity of the forest floor interception device and phase lags in loggers. However, the bias is generally small. Throughfall is best modelled, especially in winter time. In summer time, due to the variability in the storage capacity, the performance is lower. However, it should also be mentioned that the results are not independent. If throughfall is wrongly modelled, this causes a wrong input to the forest floor reservoir.

Furthermore, the effect of the variability in the storage capacity is visible. The Rutter model is calibrated on the mean storage capacity per month. However, it can really vary between years when, for example, the leaf growth or fall starts. This timing has a large impact on the actual storage capacity and can thus deviate from the mean storage capacity for that specific month. This effect could be the reason for the lower performance of the simulations in fall and spring.

To investigate the effect of the variability of the storage capacity on the modelled evaporation we applied the model with a low, a mean, and a high storage capacity. For $S_{c,max}^l$ and $S_{f,max}$ we used the upper and lower limits of Figure 3.6 and 3.8. In Figure 3.11 the results for SIM1 are shown and in Table 3.4 the mean evaporation rates for all six simulations. In Figure 3.12 the results are shown graphically.

Run		RMSE	rel. bias [%]	NS [-]
SIM1	T_f	3.55 mm/d	4	0.59
02-11-04	F	2.61 mm/d	-5	0.62
to	$E_{i,f}$	0.74 mm/d	5	0.24
01-12-04	S_f	0.37 mm	11	0.53
SIM2	T_f	9.34 mm/d	9	0.30
21-06-05	F	11.07mm/d	30	0.02
to	$E_{i,f}$	2.06 mm/d	0	-1.02
17-08-05	S_f	0.64 mm	-40	0.22
SIM3	T_f	5.80 mm/d	8	0.71
14-12-06	F	4.26 mm/d	1	0.66
to	$E_{i,f}$	1.14 mm/d	40	0.16
11-01-07	S_f	0.60 mm	-21	0.66
SIM4	T_f	4.81 mm/d	3	0.83
07-02-07	F	4.21 mm/d	0	0.72
to	$E_{i,f}$	1.41 mm/d	-9	0.10
27-02-07	S_f	1.10 mm	-4	0.37
SIM5	T_f	3.52 mm/d	7	0.81
04-12-07	F	7.14 mm/d	4	-0.18
to	$E_{i,f}$	0.98 mm/d	98	0.14
07-01-08	S_f	0.93 mm	-34	0.37
SIM6	T_f	5.16 mm/d	11	0.70
07-01-08	F	4.43 mm/d	-3	0.65
to	$E_{i,f}$	0.81 mm/d	45	-0.44
23-01-08	S_f	0.37 mm	14	0.42

Table 3.3: Model results (Beech forest, Huewelerbach) of the adjusted Rutter model for throughfall (T_f), infiltration (F), forest floor evaporation ($E_{i,f}$), and forest floor wetness (S_f). Given are the root mean square error, relative bias, and Nash-Sutcliffe efficiency.

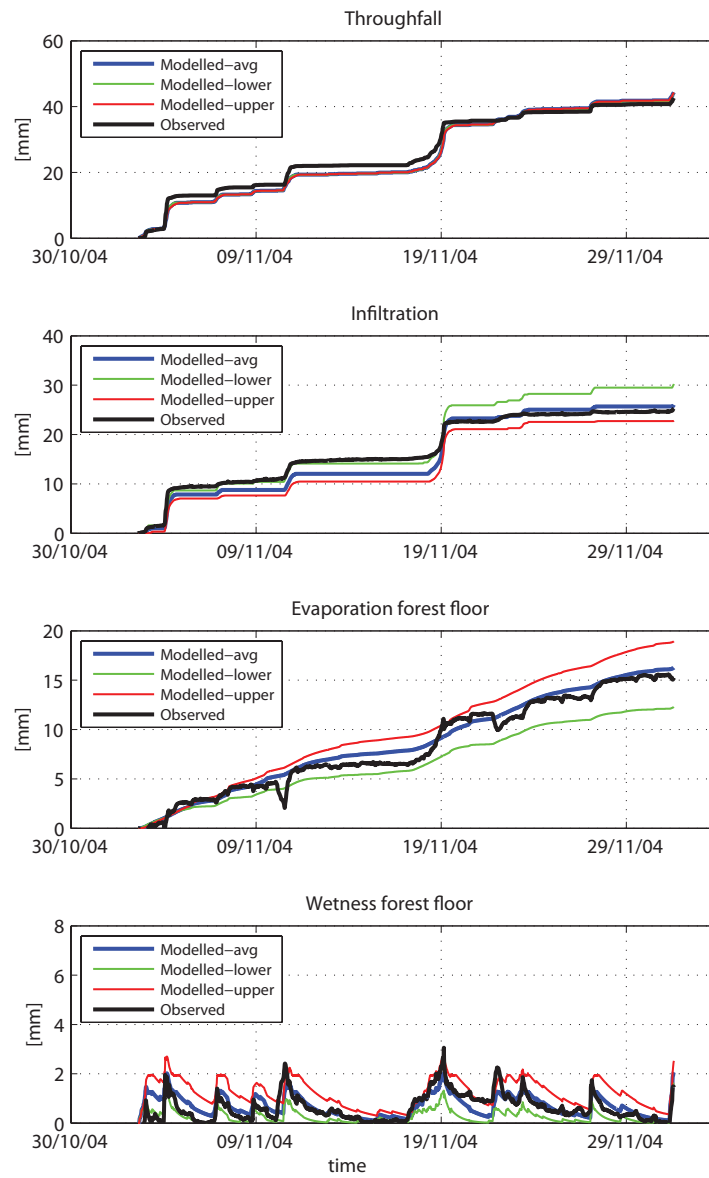


Figure 3.11: Model results for SIM1. The green line represents the results with the lower limit storage capacity, the blue the mean, and the red line the upper limit storage capacity.

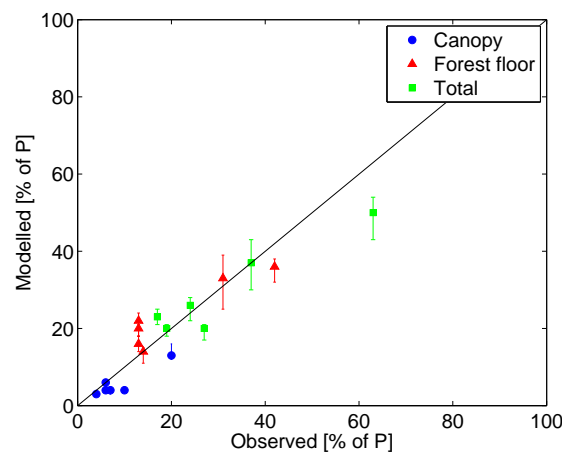


Figure 3.12: Graphical representation of Table 3.4, showing the performance of the Rutter model for canopy interception, forest floor interception, and total interception.

As can be seen in Figure 3.11 the observed data fits between the upper and lower estimates. However, sometimes the model prediction deviates from the observed data. This is mainly the case during the wetting, thus on the rising limb, and not on the falling limb during drainage and evaporation. During the falling limb the model performs well, showing that the Rutter model is capable of predicting evaporation. The rising limb gives more problems, which can be explained by variability of the storage capacity in the instrument. This may, for example, be due to unequal litter distribution in the instrument caused by wind or snow. Figure 3.2 and 3.3 illustrate the temporal variability of the storage capacity.

As can be seen from Table 3.4 the effect of the storage capacity on canopy interception evaporation is limited. On average the increase or decrease is about 5%, with an average coefficient of variation in the storage capacity of 56%. Hence a large variation in the storage capacity has a low impact on the evaporation predictions, and thus canopy interception is more driven by the number of raindays and the potential evaporation than by the storage capacity.

This is the opposite for the forest floor. Here the average coefficient of variation of the forest floor storage capacity is 48%, and the average increase or decrease is 12%. Hence the influence of the storage capacity on evaporation predictions is higher, indicating that forest floor interception is more driven by the storage capacity than by the number of raindays and the potential evaporation. This supports the findings of Baird and Wilby [1999] and Gerrits et al. [2007].

The impact of uncertainties in the storage capacity (which can be as high as $\pm 100\%$) on the total interception evaporation is about 11% and the difference in the lower or upper storage capacity is 15% and 8% respectively. This indicates that interception is more influenced by the rainfall pattern than by the storage capacity. Hence, in interception modelling, the value of the storage capacity is of minor concern.

Run	\bar{P} [mm/day]	S_{max}	$\bar{E}_{i,c}^l$ [mm/day]	$\bar{E}_{i,c}^t$ [mm/day]	$\bar{E}_{i,c} = \bar{E}_{i,c}^l + \bar{E}_{i,c}^t$ [mm/day]	$\bar{E}_{i,f}$ [mm/day]	obs.	\bar{E}_i [mm/day]	obs.
SIM1 (02-11-04 to 01-12-04)	1.69 (100%)	lower	0.03 (2%)	0.04 (3%)	0.08 (5%)	0.42 (25%)		0.50 (30%)	
		mean	0.02 (1%)	0.04 (3%)	0.07 (4%)	[6%]	0.56 (33%)	[31%]	0.63 (37%) [37%]
		upper	0.02 (1%)	0.04 (3%)	0.07 (4%)	0.65 (39%)		0.72 (43%)	
SIM2 (21-06-05 to 17-08-05)	2.22 (100%)	lower	0.19 (9%)	0.07 (3%)	0.26 (12%)	0.70 (32%)		0.90 (43%)	
		mean	0.23 (10%)	0.07 (3%)	0.29 (13%)	[20%]	0.81 (36%)	[42%]	1.10 (50%) [63%]
		upper	0.30 (13%)	0.07 (3%)	0.36 (16%)	0.85 (38%)		1.2 (54%)	
SIM3 (14-12-06 to 11-01-07)	3.11 (100%)	lower	0.06 (2%)	0.05 (2%)	0.11 (3%)	0.45 (14%)		0.55 (18%)	
		mean	0.06 (2%)	0.05 (2%)	0.11 (4%)	[7%]	0.51 (16%)	[13%]	0.62 (20%) [19%]
		upper	0.07 (2%)	0.05 (2%)	0.11 (4%)	0.55 (18%)		0.66 (21%)	
SIM4 (07-02-07 to 27-02-07)	4.78 (100%)	lower	0.19 (4%)	0.08 (2%)	0.27 (6%)	0.53 (11%)		0.80 (17%)	
		mean	0.19 (4%)	0.08 (2%)	0.27 (6%)	[6%]	0.67 (14%)	[14%]	0.94 (20%) [20%]
		upper	0.19 (4%)	0.08 (2%)	0.27 (6%)	0.74 (15%)		1.00 (21%)	
SIM5 (04-12-07 to 07-01-08)	2.29 (100%)	lower	0.04 (2%)	0.04 (2%)	0.07 (3%)	0.42 (18%)		0.49 (21%)	
		mean	0.04 (2%)	0.04 (2%)	0.08 (3%)	[4%]	0.46 (20%)	[13%]	0.54 (23%) [17%]
		upper	0.05 (2%)	0.04 (2%)	0.08 (4%)	0.48 (21%)		0.56 (25%)	
SIM6 (07-01-08 to 23-01-08)	3.28 (100%)	lower	0.07 (2%)	0.06 (2%)	0.13 (4%)	0.58 (18%)		0.72 (22%)	
		mean	0.08 (2%)	0.06 (2%)	0.13 (4%)	[10%]	0.71 (22%)	[13%]	0.85 (26%) [24%]
		upper	0.08 (2%)	0.06 (2%)	0.13 (4%)	0.79 (24%)		0.93 (28%)	

Table 3.4: Model results of average interception evaporation compared to average rainfall over the simulation periods (beech forest, Huewelerbach). In bold the observed percentages.

Furthermore, Table 3.4 shows the relative importance of canopy, trunk, and forest floor interception evaporation. The model results show that in fall (SIM1) 4% of precipitation evaporates from the canopy (6% observed) and 33% from the forest floor (31% observed). In winter (SIM 3-6) this is 4% (observed 7%) from the canopy and 18% (observed 13%) from the forest floor. There are no simulations in spring. In summer (SIM2) this is 13% (observed 20%) from the canopy and 36% (observed 42%) from the forest floor.

3.6 Daily threshold model

Although the Rutter model performs reasonably and enables to distinguish evaporation from the different components at small time steps, it requires quite some parameters, which makes the application for most model purposes difficult. Furthermore, this detail is often not necessary and a daily interception model provides enough information.

As shown by many studies interception on a daily time scale can be modelled as a threshold process (e.g., Deguchi et al. [2006], Helvey and Patric [1965], Rutter et al. [1971], Viville et al. [1993], Savenije [1997], and Savenije [2004]). All rain will be intercepted until the storage capacity is reached. Hereafter, all rainfall will infiltrate. Besides the limitation by the storage capacity, also the rainfall (P) and potential evaporation (E_p) can be a limitation in certain climates. In equation form we can write:

$$E_{i,d} = \min(D_{i,d}, P_d, E_{p,d}) \quad (3.6)$$

with $E_{i,d}$ (L T^{-1}) the interception evaporation and $D_{i,d}$ the interception threshold (L T^{-1}), all on the daily time scale. One should be careful to not confuse $D_{i,d}$ with S . Although they are related $D_{i,d}$ is a flux, while S is a stock. Multiplying S with the mean number of events per day approximates $D_{i,d}$.

For the six simulation periods we applied this simple daily threshold model and calibrated on $D_{i,d}$. In Table 3.5 the results are presented. Compared to the complex Rutter model the results are also reasonable, especially if we take into account that the Rutter model has ten parameters and the daily threshold model just one.

The calibrated threshold values are comparable with values from literature (e.g., Pitman [1973] and De Groen [2002]) and vary between 1.5 mm/d in winter to 6 mm/d in summer. The threshold consists of both the storage in the canopy and on the forest floor.

Run	Period	$D_{i,d}$ [mm/d]	\bar{E}_i [mm/d]		RMSE [mm/d]	rel. bias [%]	NS [-]
			simulated	observed			
SIM1	02-11-04 to 01-12-04	2.0	0.67 (40%)	0.60 (36%)	0.62	11	0.43
SIM2	21-06-05 to 17-08-05	6.0	1.45 (65%)	1.36 (62%)	1.24	5	0.59
SIM3	14-12-06 to 11-01-07	2.0	0.76 (24%)	0.62 (20%)	1.49	22	0.03
SIM4	07-02-07 to 27-02-07	1.5	0.78 (16%)	0.94 (19%)	1.10	-17	0.17
SIM5	04-12-07 to 07-01-08	1.5	0.43 (18%)	0.41 (17%)	0.95	6	0.29
SIM6	07-01-08 to 23-01-08	1.5	0.93 (27%)	0.74 (22%)	0.80	26	-0.11

Table 3.5: Model results of a simple daily threshold model for total interception in a beech forest.

3.7 Spatial variation in throughfall and infiltration

Besides the temporal variation, interception varies also in space, mainly due to the heterogeneity of the vegetation density. In Figure 3.13a an example of the spatial distribution of interpolated (triangle-based cubic) observed throughfall is given. It encompasses a period in spring 2006 with 70 mm of gross rainfall. It can be clearly seen that the forest canopy redistributes the rainfall. In general throughfall is lower around trees, due to interception. However, the trees can also funnel the rainfall, as can be seen near the tree at coordinates (15m, 15m). The structure of this tree really acts like a funnel, causing even higher throughfall than gross rainfall close to the tree, and lower throughfall values around the tree. This effect is also mentioned by Germer et al. [2006] and Gerrits et al. [2009a].

In Figure 3.13b the resulting canopy interception pattern is shown. Evaporation from canopy interception is calculated here as gross rainfall minus (observed) throughfall and hence stemflow is neglected. Because throughfall can exceed gross precipitation, this results in negative interception evaporation values. These values have been removed from the analysis in Figure 3.13b (but not in the adjusted Rutter model for calculating infiltration and forest floor evaporation).

Since we do not have spatial observations of forest floor interception, we used the adjusted Rutter model. To reduce the modelling error as much as possible we used observed throughfall data as input for the forest floor module instead of modelled throughfall. In Figure 3.13c and 3.13d the model results of the infiltration and forest floor evaporation are shown. In order to see if the spatial pattern of canopy interception is different from that of the forest floor, and to investigate if the pattern changes throughout the seasons we calculated the spatial correlation with semi-variograms.

In Figure 3.14 the semi-variograms of the throughfall and infiltration are shown per season as well as per year. The range r is defined as the lag h , whereby the variance (γ) is 95% of the sill c , and is a measure for the correlation between the points. High spatial correlation between the collectors causes the range to be high and vice versa. We fitted an exponential model (Chilès

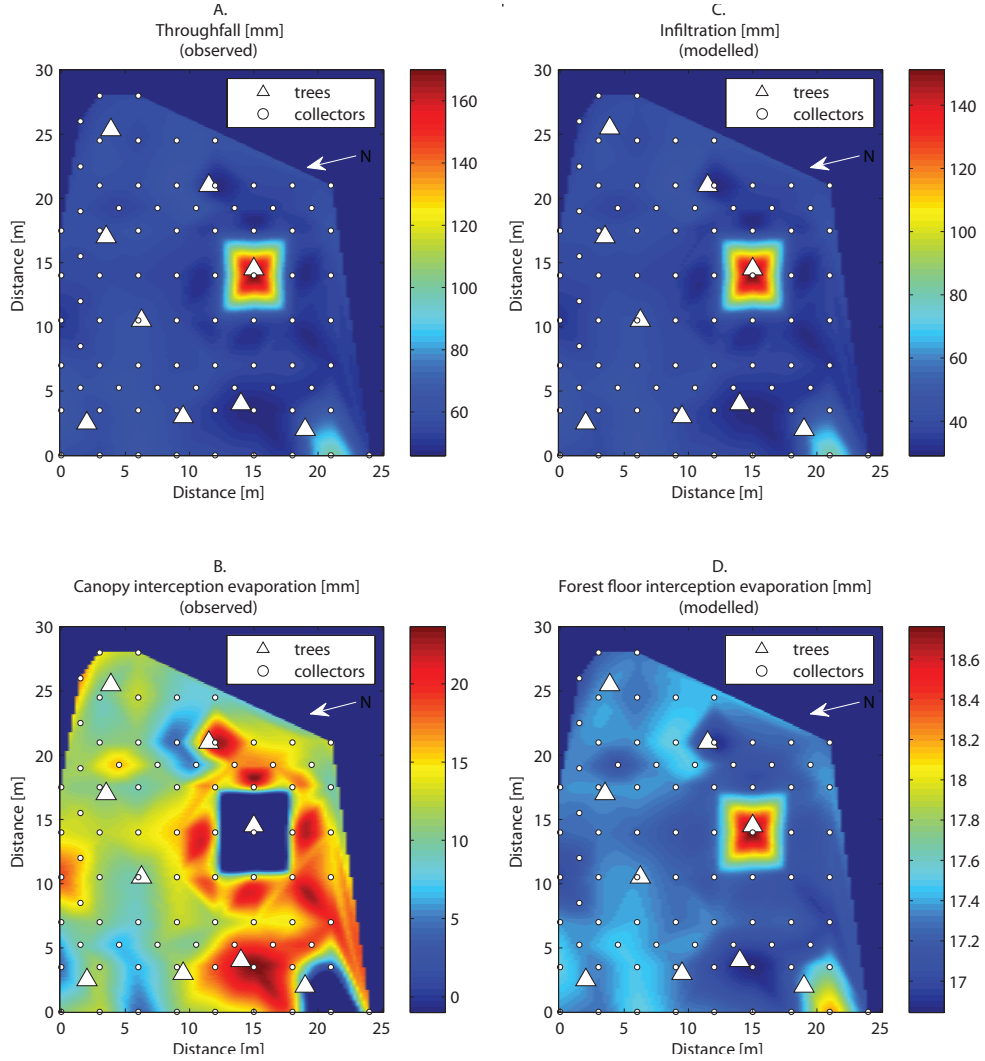


Figure 3.13: Spatial variability of canopy interception (observed) and forest floor interception (modelled with adjusted Rutter model) in mm over the period 24 March to 6 April 2006 with 70 mm of gross rainfall. Triangles indicate the position of the beech trees and the circles the positions of the collectors.

and Delfiner [1999]):

$$\gamma(h) = c \left(1 - \exp \left(\frac{-3h}{r} \right) \right) \quad (3.7)$$

As expected the range in winter is larger (higher spatial correlation) after leaf senescence (Western et al. [1998]); however, this not a clear relation. Furthermore, it seems that in summer and winter the range is relatively larger than during the transition seasons. This is both the case for throughfall and for infiltration.

To investigate if these patterns are persistent in time, time stability plots (TSP) can show if there exist persistent dry or wet collectors by ranking the normalized throughfall/infiltration $\tilde{N}_{x,y}$. From a time stability plot two types of persistence can be derived: extreme persistence and general persistence (Keim et al. [2005] and Zimmermann et al. [2008]). Extreme persistence occurs if steep tails exist, and general persistence refers to the overall slope of the middle range.

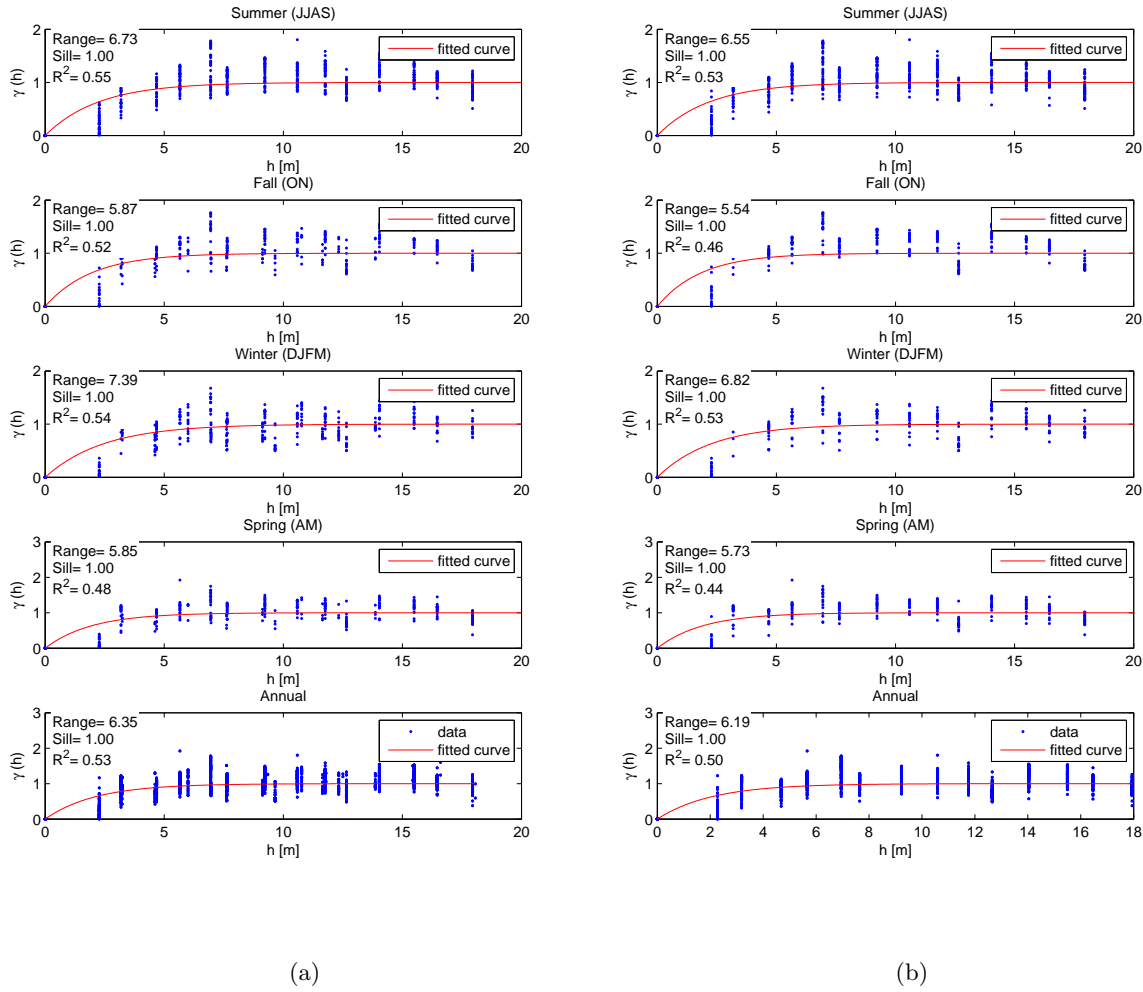


Figure 3.14: Semi-variogram of throughfall (a) and (modelled) infiltration (b) per season and per year.

In Figure 3.15 the time stability plots of throughfall (a) and (modelled) infiltration (b) are presented. As can be seen, the difference between the TSP of throughfall and infiltration is small and extreme persistence only occurs in the ‘wet’ tail. The general persistence is rather weak. Only 25%, 7%, 14%, 7% and 7% of the collectors are significantly (65%) drier than the mean for summer, fall, winter, spring, and annually respectively. This suggests that the variation in winter and summer is smaller than in the transition seasons.

In Figure 3.16 and 3.17 the mean time stability plots (red line in Figure 3.15) are plotted in space to investigate where the drier and wetter spots are located and how they vary throughout the seasons. As can be seen, the collector near the tree at coordinates (15m, 15m) is consistently wetter than the surrounding collectors. Furthermore, it can be seen that a second drip point develops at coordinates (20m, 0m) in fall which vanishes again in spring. Hence this drip point is really determined by the branch structure and less by the canopy structure. It is also possible to see from the dark blue rings around the drip points that the funneled rain is collected from the surrounding areas. Furthermore, the effect of the canopy development over time is visible.

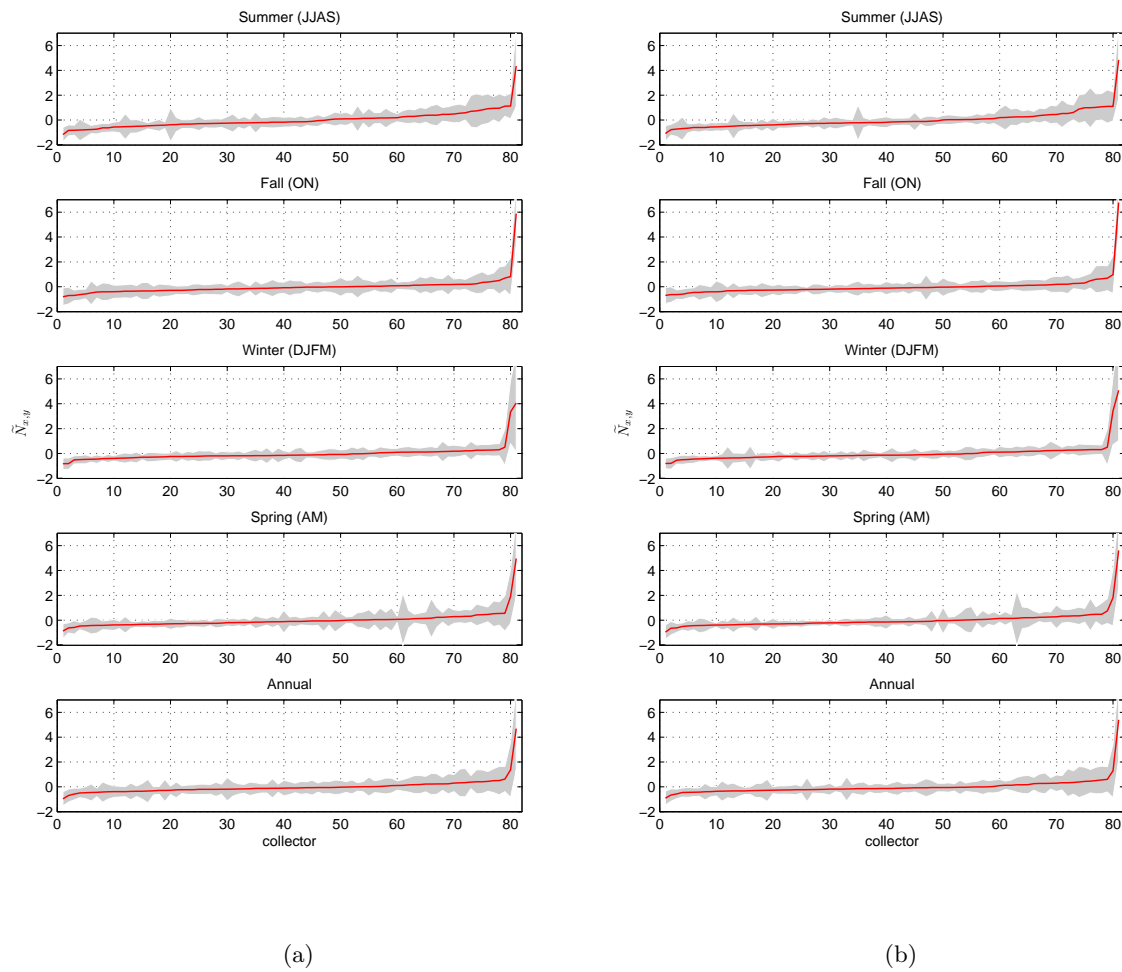


Figure 3.15: Time stability plot of normalized throughfall (a) and (modelled) infiltration (b) per season and per year. The grey areas indicates one time the standard deviation.

In summer the spatial pattern is much more heterogeneous. Also the forest gap in the upper left corner receives relatively more throughfall in summer than the covered parts.

3.8 Conclusions

Evaporation from the beech canopy has a clear seasonal trend. In the leaf on period evaporation from the canopy is on average 15% of the precipitation and in the leaf off period 7%. There is less seasonal variation in the forest floor evaporation: 22% of the throughfall. Both in the canopy and on the forest floor there are outliers which coincide with low rainfall amounts (causing high ratios) or snow events (causing low or even negative ratios). Combined, canopy and forest floor interception amount to 27% of the rainfall in winter and 34% in summer. Annually, this amounts to 34-43% of the total evaporation in the Huewelerbach catchment, which is a lot for a flux which

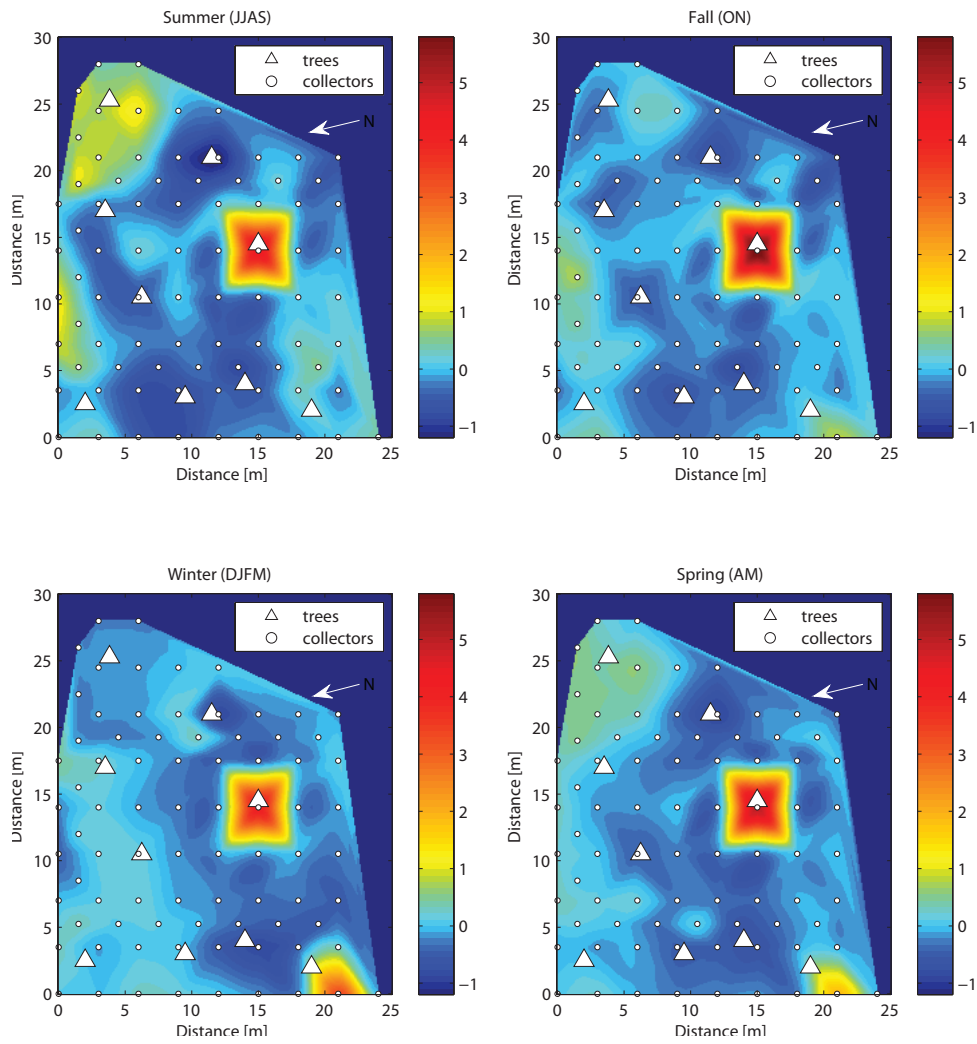


Figure 3.16: Spatial persistence of normalized throughfall. Triangles indicate the position of the beech trees and the circles the positions of the collectors.

is often disregarded or lumped with other evaporation fluxes.

The setup in Westerbork with moss and grass evaporation has a seasonal trend and ranges from 15% in winter to 25% in summer. This is likely due to the vegetation change from moss dominated in winter to grass in summer. The cedar needle floor in the Botanical garden has less seasonal variation and evaporated on average 18% of throughfall in summer 20% and in winter 16%.

A similar seasonal effect can be found in the storage capacities of the beech floor: for the canopy the average storage capacity ranges from 0.4 mm in winter to 0.9 mm in summer. The storage capacity of the forest floor is less variable over the year: around 1.8 mm on average with a maximum of 2.8 mm during the fall. The cedar needle floor has even less seasonal variation and has an average storage capacity of 1.0 mm. On the other hand, the moss/grass floor

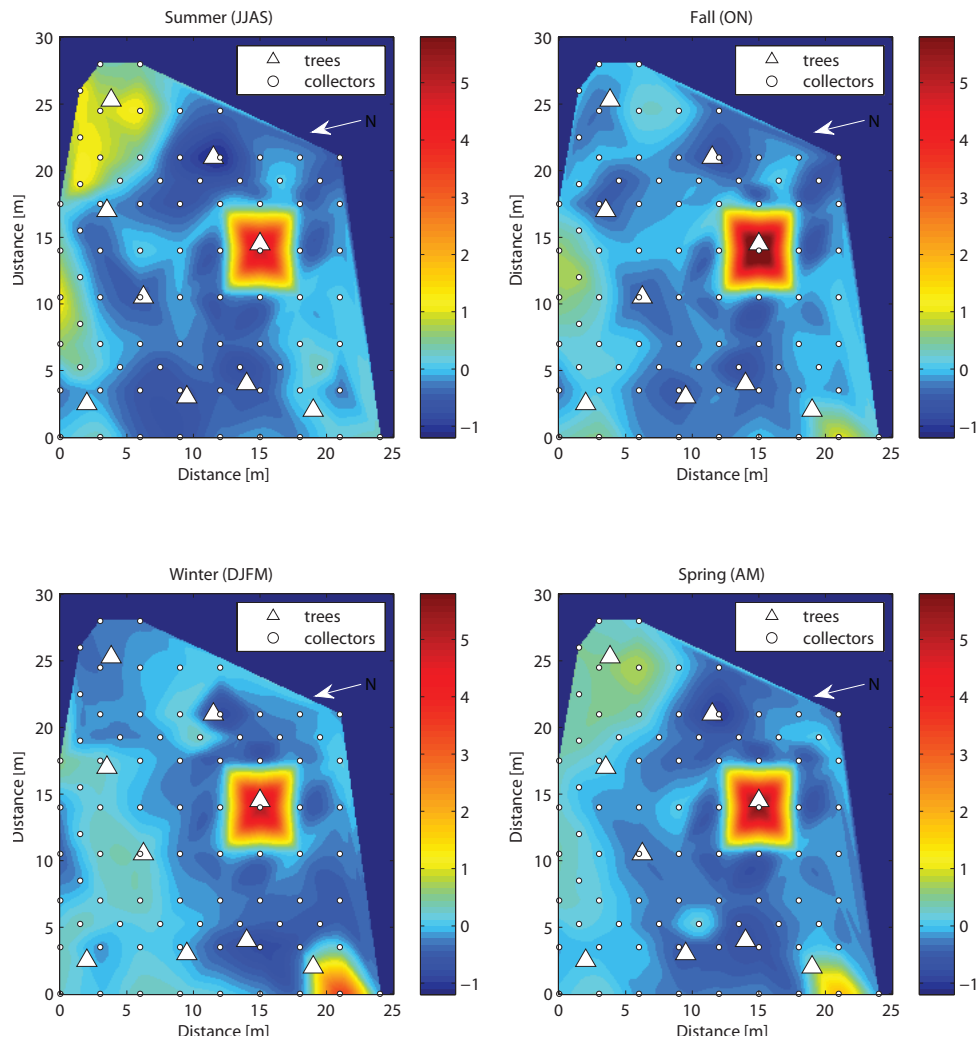


Figure 3.17: Spatial persistence of normalized (modelled) infiltration. Triangles indicate the position of the beech trees and the circles the positions of the collectors.

does have a clear and large variation over the year. In winter when moss dominates the storage capacity was 2.0 mm and in summer, when grass grows as well the capacity increased to 4.1 mm.

Besides this seasonal effect there is variability at a given point in time. The highest variability of the storage capacity of the beech forest floor is in winter (± 0.8 mm, $c_v = 50\%$) mainly due to the occurrence, or absence, of snow which decreases the storage by flattening the leaves. The variation in summer is ± 0.4 mm ($c_v = 19\%$). Similar results were found for the moss/grass floor, where the variation changes from 24% in summer to 45% in winter. The cedar floor has an average variation of 35%. The variability can also be related to wind or rainfall intensity. However, none of these factors revealed itself as a strong effect for all three measuring locations.

To investigate the sensitivity to different conditions, we applied a Rutter interception model with an additional forest floor reservoir for the beech forest. The model shows that a variation

in the canopy storage capacity of 56% results in only 5% difference in evaporation predictions from the canopy, while a variation of 48% in the storage capacity of the forest floor results in 12% difference in evaporation from the forest floor. Hence, we can conclude that canopy interception is not so much determined by the storage capacity, but rather by the number of raindays and the potential evaporation, and that for the forest floor the storage capacity is more important.

The Rutter model was also applied to investigate the spatial distribution of throughfall and infiltration. The spatial patterns show that also the canopy coverage can cause variation in the calculated storage capacity. For example, it makes a difference if the storage capacity is determined in a relatively open area or in a dense location in the forest. Furthermore, trees can create hot spots, where throughfall is higher than gross precipitation.

For the experimental beech plot in Luxembourg we found that the spatial correlation of throughfall is about 6-7 meters and that in summer and winter the spatial correlation is slightly higher than in fall and spring. Similar results are found for the infiltration pattern. Also the stability of the patterns was analyzed.

Overall, we can conclude that interception is a highly variable process, both in time and in space. Although the variation in storage capacity can be as high as $\pm 100\%$, the effect on evaporation estimates is relatively low (ca. 11%). This indicates that interception is more influenced by the rainfall pattern than by the storage capacity. As a consequence, in interception modelling, the value of the storage capacity appears to be of minor concern. The research shows that the combined effect of canopy and forest floor interception is a considerable flux in the rainfall runoff process (about 40% of the total evaporation), which cannot be denied in rainfall-runoff modelling.

Chapter 4

The effect of spatial throughfall patterns on soil moisture patterns and the generation of subsurface stormflow

.....

The generation and behaviour of subsurface stormflow at the hillslope scale is still poorly understood. Interactions between the permeable soil and the less permeable bedrock may cause non-linearity in subsurface flow depending on several hillslope attributes like soil depth, slope angle, and bedrock permeability. It is known that the size of storm events also controls subsurface flow generation. However, the effect of the spatial variability of throughfall on subsurface stormflow (SSF) generation and soil moisture patterns has not yet been studied in detail. The objectives of this study are three-fold: 1) to investigate if and how different configurations of a throughfall pattern change the SSF behaviour; 2) to investigate the interplay between the spatially variable input and the hillslope attributes (slope angle and soil depth) on the generation of SSF; and 3) to investigate a geo-statistical tool, that uses semi-variogram characteristics to analyse if soil moisture patterns during an event are dominated by throughfall patterns or by bedrock topography patterns. Virtual experiments are used to address these questions. A virtual experiment is a numerical experiment driven by collective field intelligence. It provides a learning tool to investigate the effect of separated processes in a complex system. In our virtual experiment we combined spatial throughfall data from the Huewelerbach catchment in Luxembourg with the topography characteristics of a well-studied hillslope within the Panola Mountain Research Watershed, Georgia, USA. We used HYDRUS-3D as a modeling platform. The effect of spatial throughfall pattern appears to be large on both SSF generation and the spatial variability of SSF along the hillslope, but only marginal on total SSF amounts. The spatial variability of SSF along the hillslope appears to be closely related to the drainage pattern of the bedrock. The geo-statistical analysis indicates that during the event soil moisture distribution reflects throughfall patterns whereas after the event, during the drainage of the hillslope, the bedrock topography increasingly dominates soil moisture patterns.

.....

Based on: Gerrits, A. M. J., Hopp, L., McDonnell, J. J., Savenije, H. H. G., Pfister, L., 2010 (work in progress). The effect of spatial throughfall patterns on soil moisture patterns and the generation of subsurface stormflow. Journal of Hydrology;

4.1 Introduction

Interception has been studied for a long time. Already in 1919 Horton described the interception process and studied interception characteristics of several tree species (Horton [1919]). After Horton many researchers continued investigating other trees species, under other different climates, under different circumstances (slope, tree density), and sometimes with new measuring techniques. In Kittredge [1948], Zinke [1967], and Breuer et al. [2003] some of these results were summarized, which show that 30-40% of the rainfall can evaporate through interception. Besides these average values, interception also plays an important role in redistributing the water. The canopy causes some parts of the ground surface to receive more water than others, while sometimes throughfall can exceed gross precipitation. On those ‘hotspots’ the tree acts like a funnel (e.g., Germer et al. [2006], Ziegler et al. [2009], and Gerrits et al. [2010 (in press)]). These throughfall patterns have an impact on the subsequent infiltration and percolation process (Bouten et al. [1992] and Staelens et al. [2006]).

In forested hillslopes, these heterogeneous throughfall patterns can become important in relation to subsurface storm flow (SSF) generation. Several studies have observed a threshold response in SSF after a storm event (Dunne [1978], Woods and Rowe [1996], Tromp-van Meerveld and McDonnell [2006a]). According to the fill and spill hypothesis of Tromp-van Meerveld and McDonnell [2006b] subsurface storm flow is triggered when the microtopographic depressions of the bedrock are fully filled and become connected. We hypothesize that spatially variable input influences the fill and spill of the depressions. Some depression may fill earlier when the bedrock depression is located under a throughfall hotspot, while other depressions may fill less due to low throughfall amounts.

Field data to test this hypothesis is scarce and if available it is difficult to generalize the outcome, since it is site and case specific. Besides, Buttle [2006] emphasized that it is important to consider the interactions of hillslope controls rather than investigate each control separately. A virtual experiment can overcome these limitations. Weiler and McDonnell [2004] defined a virtual experiment as ‘numerical experiment with a model driven by collective field intelligence’. A virtual experiment enables us to investigate the combined effect of different hillslope controls in relation with spatially variable input.

Subsurface storm flow is controlled by soil, vegetation, and topography (slope) characteristics of a hillslope (Whipkey and Kirkby [1978]). Mainly soil depth (Buttle and McDonald [2002]) and the soil hydraulic properties (Onda et al. [2001]) determine SSF behaviour, but also soil structure (e.g., macro pores, cracks) is important (Beven and Germann [1982]). Although one can argue that in turn soil structure can be influenced by throughfall hotspots, we did not include this in our analysis, since we wanted to compare our results with the virtual experiments of Hopp and McDonnell [2009].

Hopp and McDonnell [2009] investigated the process controls on SSF connectivity at the hillslope scale. They applied a spatially uniform rain storm on a Panola hillslope model (HYDRUS-3D) and varied the slope angle, bedrock permeability, and soil depth. This paper is a follow-up on this work, where the influence of spatially variable throughfall is investigated. Since bedrock permeability appeared not to be a major controlling factor in the earlier study we chose to exclude this variable. Additionally, we also investigated the effect of throughfall patterns on the soil moisture pattern, since soil moisture patterns are also influenced by throughfall, soil hydraulic properties and slope (Nyberg [1996] and Western et al. [2004]).

The questions addressed in this paper are:

- How do different throughfall pattern realizations influence SSF?
- How does the spatially variable input influence trench outflow compared to uniform input (see Hopp and McDonnell [2009]) when soil depth, storm size and slope angle are varied?
- Do soil moisture patterns reflect a balance between throughfall and bedrock patterns?

We emphasize that this paper only contains modelling results and therefore can not be seen as the real truth. In reality feedback mechanisms occur, which may influence our findings. For example trees may optimize their location on the hillslope by water availability, hence the throughfall pattern may not be completely random. However, our approach can be used to understand and identify hillslope interactions which are difficult to observe in reality.

4.2 Method and materials

4.2.1 Approach

To investigate the effect of spatially variable throughfall on subsurface stormflow, we selected a throughfall pattern from the Huewelerbach catchment and used this as input on a hillslope model. Hopp and McDonnell [2009] already developed a finite element model of the Panola hillslope. We decided to use the same model domain and combine it with the Huewelerbach throughfall pattern as a virtual experiment. Since the model domain of Panola is larger than the spatial throughfall pattern we needed to expand the throughfall pattern in a way that the spatial characterisation remained the same. Since we did not want to enlarge the pattern, we mapped the pattern in eight different ways on the Panola hillslope. We used two configurations and four initial patterns (see Figure 4.1). The four initial patterns are derived by mirroring the throughfall pattern along the vertical and horizontal dashed axes. These four patterns are subsequently mapped on the Panola model domain in two configurations: one where we mapped the initial pattern in the upper right corner of the Panola model domain and subsequently copied this pattern by mirroring along the dashed axes. In the second configuration we started in the upper left corner and then mirrored the pattern. We realize that this expansion method does not encompass all possible patterns that may result in significant different SSF; however, we prefer to retain the spatial characteristics of the original throughfall pattern.

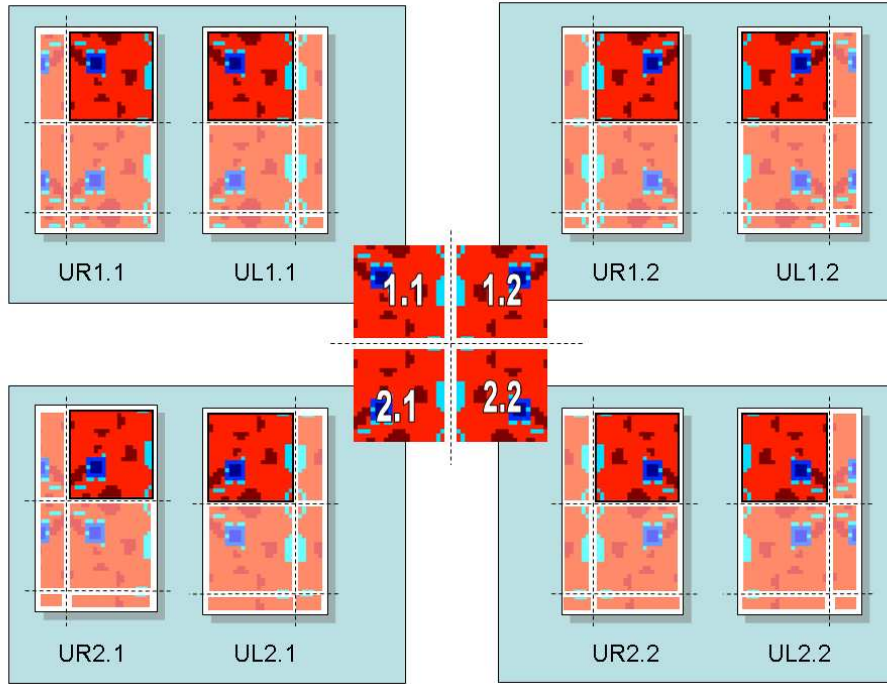


Figure 4.1: Method to map initial spatial throughfall pattern of Huewelerbach on the Panola hillslope. In the center the four initial patterns. Each initial pattern can be mapped on the hillslope in two ways: the ‘Upper Right’ configuration (UR) and the ‘Upper Left’ configuration (UL).

The first step is to investigate how the different patterns influence subsurface stormflow (SSF). Therefore, we compare the eight simulations with spatially variable input to the base-case scenario where uniform input was used. We assess the results based on the downslope outflow. The simulation with the highest deviation from the variance of segment SSF divided by total SSF is used for further analysis.

To understand the interplay of hillslope attributes and storm size on SSF, we applied different storm sizes (R) and changed the average slope angle (A) and average soil depth (S). In Table 4.1 the virtual cases are described. The asterisk indicates the base case scenario. By combining all input and hillslope attributes we obtain 36 simulations. The results are analysed on subsurface stormflow characteristics (like peak discharge, recession time, variance) and on the spatial patterns of soil moisture content.

The soil moisture patterns are analysed with semi-variograms (Cressie [1993], Chilès and Delfiner [1999]). A semi-variogram represents the variance of two points separated by a certain distance in a spatial field and is a measure for spatial continuity in that field (Keim et al. [2005]):

$$\gamma(h) = \frac{\sum_{n(h)} \left(\tilde{N}_{x,y} - \tilde{N}_{x,y+h} \right)^2}{2n(h)} \quad (4.1)$$

Where h is the lag distance, $n(h)$ is the number of measurement pairs in the data set that are

Input Storm size, R	Topography	
	Slope angle, A	Soil depth, S
32 mm	6.5°	0.62 m *
63 mm *	13° *	1.22 m
82 mm	26°	1.84 m
	40°	

Table 4.1: Variations of input and topography. Asterisks indicate the base case scenario.

a distance h apart, and $\tilde{N}_{x,y}$ are the normalized spatial data at measuring point (x, y) :

$$\tilde{N}_{x,y} = \frac{N_{x,y} - \bar{N}}{\sigma(N)} \quad (4.2)$$

with σ being the standard deviation. We used normalized data to be able to compare spatial patterns.

Important features of a semi-variogram are the nugget, sill, and range. The nugget is a measure for the randomness of observations at one and the same location. The sill is the limit of the semi-variogram, where no autocorrelation exist anymore. The range is the maximum distance over which this spatial correlation exists.

4.2.2 Study sites and selected rainstorm event and pattern

For this research study information from two sites has been used. The hillslope geometry and soil hydraulic properties have been derived from the well-studied Panola hillslope. Storm characteristics have also been obtained from Panola; however, the spatial throughfall pattern has been derived from the experimental interception plot in the Huewelerbach catchment in Luxembourg, since this information was not available for the Panola hillslope.

Panola hillslope

The Panola hillslope is located in the Panola Mountain Research Watershed (PMRW) in Georgia Piedmont, 25 km southeast of Atlanta. The climate is humid and subtropical with an average temperature of 16.3°C and average rainfall of 1240 mm/year. The hillslope faces southeast and has a slope of 13° . The surface topography is relatively planar, but the porous saprolite bedrock (soft disintegrated granite) is highly irregular (Figure 4.2a). This results in highly variable soil depths ranging from 0 to 1.86 m, and an average soil depth of 0.63 m. The soil consists of loamy sand with a 0.15 m deep organic-rich horizon. At the lower hillslope boundary a 20 m wide trench has been excavated, where subsurface flow is measured by ten two meter wide sections. Further details on the Panola hillslope were described by Freer et al. [2002], Tromp-van Meerveld and McDonnell [2006a], and Tromp-van Meerveld and McDonnell [2006b].

The subsurface flow regime of Panola hillslope is largely determined by the bedrock topography. Due to the large difference between the conductivity of the bedrock and the soil, subsurface water accumulates at the soil-bedrock interface and follows the bedrock topography. This topography also causes the SSF at Panola to behave like a real threshold process. First all the water has to accumulate in the underground depressions (filling) before it can drain (spilling). The amount of water that is needed for spilling is rather constant. Tromp-van Meerveld and McDonnell [2006b] and Tromp-van Meerveld and McDonnell [2006a] concluded that at Panola significant subsurface storm flow only occurred when rainfall exceeded the threshold of 55 mm.

For this study we selected the best studied rainstorm at the Panola dataset of 6-7 March 1996 (Burns et al. [2001] and Freer et al. [2002]). This storm had a return period of 3 years and a total storm depth of 87 mm in 31 hours divided over two peaks (see Figure 4.2b). It can be seen from Figure 4.2b that the first rainfall peak almost entirely went into storage, while the second peak generated the runoff peak. This clearly shows the threshold behaviour of Panola.

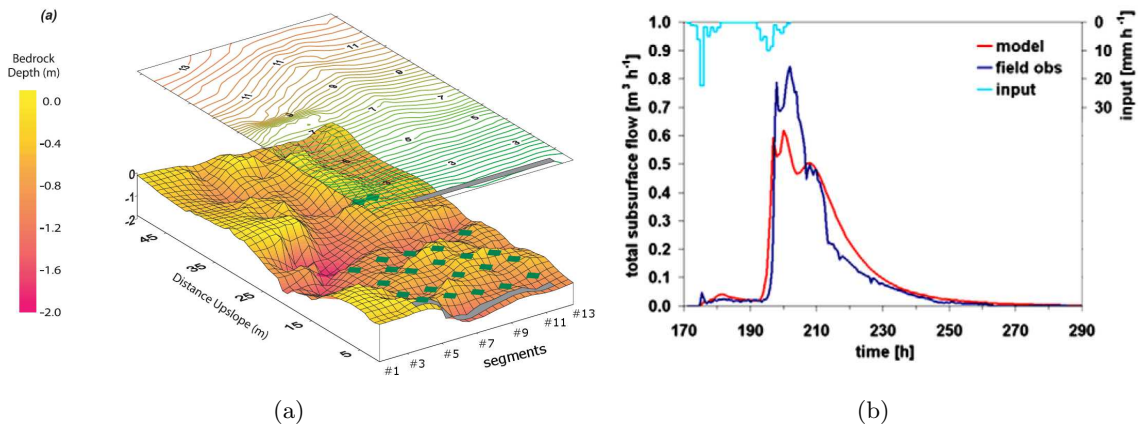


Figure 4.2: a) Panola hillslope: bedrock topography and surface topography. In grey the location of the 20 m wide trench for measuring subsurface flow (from Freer et al. [2002]). b) Storm of 6-7 March 1996 and trench observations (modelled and observed) (from Hopp and McDonnell [2009]).

Interception plot Huewelerbach

The interception plot is located in the Huewelerbach catchment in Luxembourg, 20 km north-west of Luxembourg city. The experimental plot has a total area of 596 m^2 and consist of beech trees (*Fagus sylvatica* L.) with an average stand density of 168 trees/ha. The climate is modified oceanic with mild winters and temperate summers. The average rainfall is 845 mm/a and the average temperature is 8°C (Pfister et al. [2005]). In the plot throughfall is measured with 81 manual rainfall collectors, installed in a grid with an average distance of about 3 m (Figure 4.3a). The collectors are read out at a bi-weekly interval. In an open valley close to the plot gross rainfall is measured by a tipping bucket raingauge. Further details on the interception plot can be found in Gerrits et al. [2007], Gerrits et al. [2009a], and Gerrits et al. [2010 (in press)].

From the throughfall data set we selected a random period with full canopy development, be-

	Class definition	ΣT_f [mm]	$\Sigma \bar{T}_f$ [mm]	$\Sigma \bar{T}_f / \Sigma P$ [%]	Class size [%]
1	0 - 25.0%	0 - 18.8	17.4	53	12
2	25.0 - 37.5%	18.8 - 28.1	22.6	69	76
3	37.5 - 50.0%	28.1 - 37.5	29.8	91	6
4	50.0 - 75.0%	37.5 - 56.3	43.3	132	4
5	75.0 - 100%	56.3 - 75	65.3	200	2

Table 4.2: Definition of the five classes and the main characteristics with T_f throughfall, P gross precipitation, and $\Sigma \bar{T}_f$ the mean throughfall sum in a class. The class size percentage is only calculated for the initial spatial throughfall pattern (see Figure 4.1).

cause we learned from a time stability analysis that the spatial pattern does not vary much in time (Gerrits et al. [2010 (in press)]). We selected the period starting from the 10th of May 2007 until the 25th of May 2007 (see Figure 4.3b). Total rainfall in this period was 33 mm.

An important funneling mechanism can be seen in Figure 4.3b at coordinates (15 m, 15 m) where throughfall exceeds precipitation. This location is around a tree that creates hotspots of high throughfall with lower throughfall values in a ring around the tree. This phenomenon is also observed in field experiments of for example Germer et al. [2006] and Ziegler et al. [2009].

For the analysis we use five classes of throughfall and defined them based on the percentage of maximum throughfall (Table 4.2).

Subsequently, the Panola storm of 6-7 March 1996 ($P_{panola}(t)$) is scaled for each class i as:

$$P_i(t) = P_{panola}(t) \times (\Sigma \bar{T}_f / \Sigma P)_i \quad (4.3)$$

4.2.3 Model description of base case scenario

To simulate SSF on the Panola hillslope, we used the finite element model HYDRUS-3D, version 1.10 (Simunek et al. [2006]). HYDRUS-3D solves the Richards equation for water flow in variably saturated porous media. We used the model as described in detail by Hopp and McDonnell [2009]. Here we only briefly describe the crucial information.

The model domain covers an area of 28 m by 48 m. The surface and bedrock topography have been derived from a survey with a spatial resolution of 2 meter. From this survey a Digital Elevation Model (DEM) has been generated with a spacing of one meter by linear interpolation; subsequently a mesh of triangular prisms was generated based on this DEM. The mesh consists of 10 layers, with each 1715 nodes. Layers 1 to 5 represent the bedrock sublayer, layers 6 to 10 the soil sublayer.

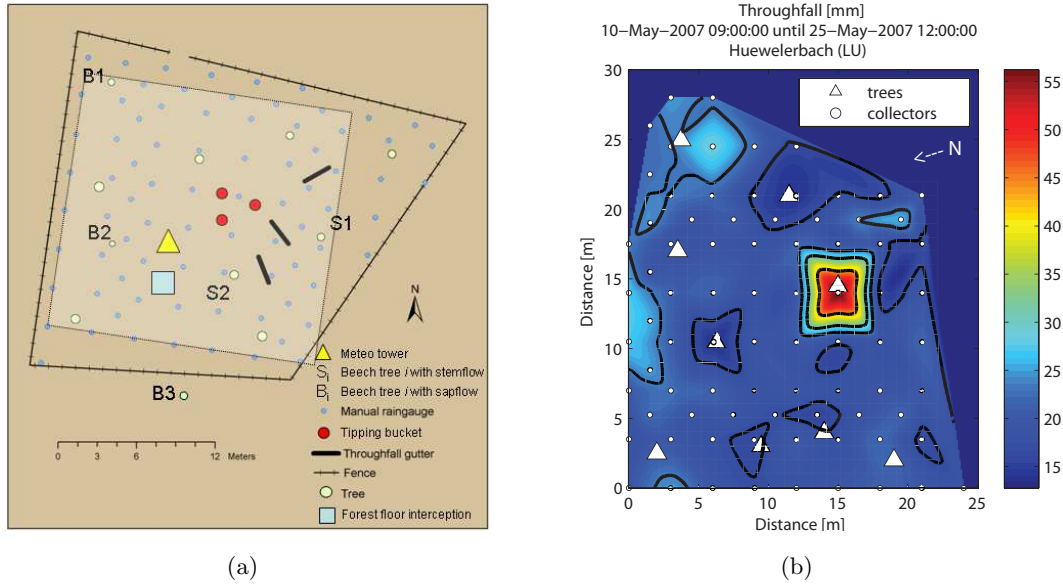


Figure 4.3: a) Interception plot Huewelerbach: location of the 81 raingauges to measure throughfall. b) Spatial throughfall pattern of May 2007. The black contour lines represent the five throughfall classes, and the white grid the selected area for the analysis.

The model has only been calibrated to the trench outflow on an event basis, and performed in a realistic way consistent with field observations of spatially distribute state variables (Figure 1 in Hopp and McDonnell [2009]). However, the model does not represent all complex processes of Panola like preferential flow, and has not been tested for long-term hydrological modelling.

Soil hydraulic properties are described by the van Genuchten-Mualem model (Van Genuchten [1980]). α and n are calibration parameters, θ_r (residual water content), θ_s (saturated water content), and K_s (saturated hydraulic conductivity) are determined based on long-term field observations (McIntosh et al. [1999] and Tromp-van Meerveld et al. [2007]). In Table 4.3 the soil hydraulic properties are given. For a more detailed explanation how soil parameters were specified see Hopp and McDonnell [2009].

The boundary conditions of the model domain for the upper and side boundaries are defined as ‘no flux’. The downslope boundary is different for the bedrock and for the soil layers. The downslope bedrock boundary is defined as ‘no flux’, thereby assuming negligible lateral flow in the bedrock. The downslope boundary of the soil layers is treated as a ‘seepage flux’, allowing water to leave the domain through saturated parts of the boundary. The bottom boundary is assigned as ‘free drainage’, meaning a unit total vertical gradient. For the surface boundary

Material	Layers			θ_r	θ_s	α	n	K_s
	S=0.62*	S=1.22	S=1.84	[m ³ m ⁻³]	[m ³ m ⁻³]	[m ⁻¹]	[-]	[m h ⁻¹]
1 (soil)	9-10	10-12	12-15	0.280	0.475	4.00	2.00	3.5
2 (soil)	7-8	7-9	9-11	0.280	0.460	4.00	2.00	1.5
3 (soil)	6	6	6-8	0.325	0.450	4.00	2.00	0.65
4 (bedrock)	5	5	5	0.300	0.450	3.25	1.75	6E-3
5 (bedrock)	1-4	1-4	1-4	0.280	0.400	3.00	1.50	6E-4

Table 4.3: Soil hydraulic properties of van Genuchten-Mualem model. Asterisks indicate the base-case scenario with mean soil depth $S = 0.62$ m.

we used the eight generated throughfall patterns as described above (Figure 4.1). Although the eight surface boundary patterns slightly differ, the total input into the model domain remains similar (63.3 ± 0.2 mm). As the initial conditions for the entire domain a pressure head of -0.7 m is used, followed by a 7 days drainage period where no rainwater enters the domain. This corresponds to the actual weather conditions that preceded the storm event of 6-7 March 1996.

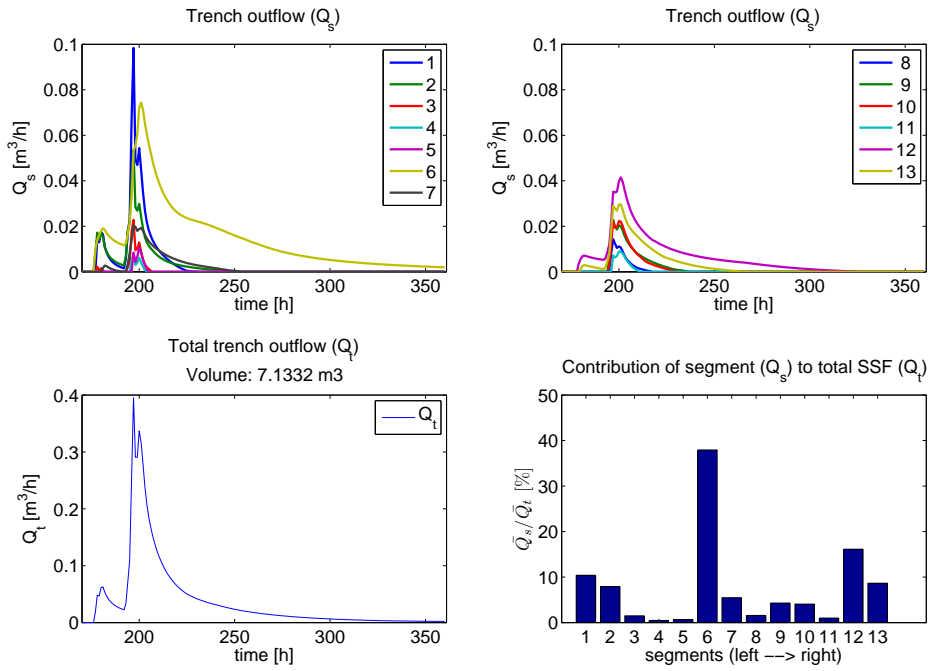
In this paper we consider the outflow over the entire hillslope width (28 m) and not only the outflow from the excavated trench (20 m) as described by Freer et al. [2002]. However we refer to ‘trench’ if we mean the entire downslope boundary for simplicity in writing. The trench is divided in 13 segments, where segment 1 equals the outflow from 1-3 m, segment 2 outflow from 3-5m, segment 3: 5-7, etc.

4.3 Results and discussion

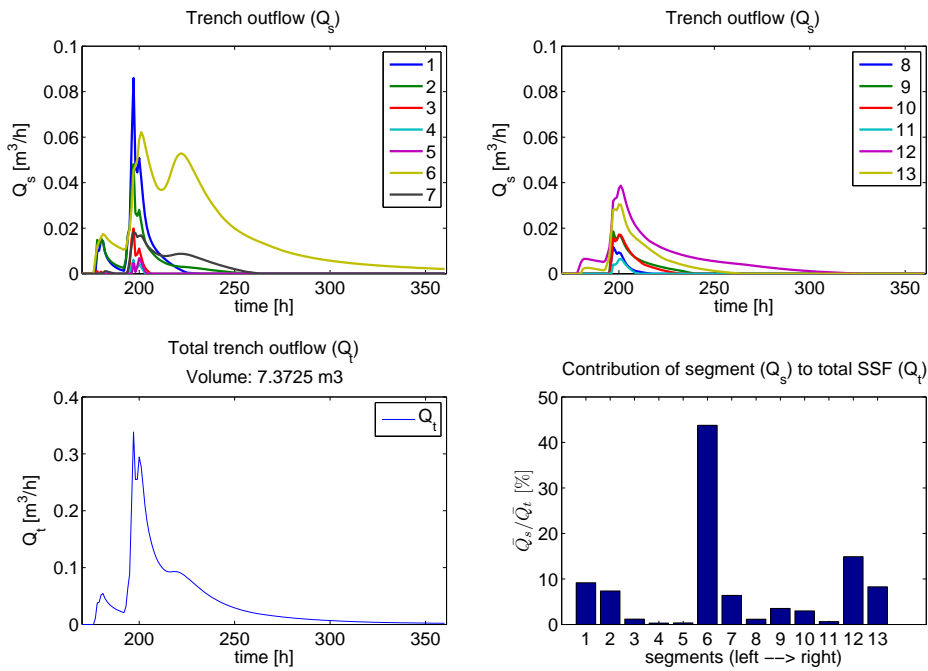
4.3.1 Pattern configuration

In Figure 4.4a subsurface stormflow along the downslope trench of the base case scenario ($R = 63$ mm, $A = 13^\circ$, $S = 0.62$ m) with uniform input is shown. The upper graphs show the subsurface flow per segment (Q_s), the lower left the total subsurface flow (Q_t), and the lower right the variation of subsurface flow along the trench. As can be seen, subsurface flow is variable distributed along the trench (variance $\bar{Q}_s/\bar{Q}_t = 10.4 \cdot 10^{-2}$), especially segment 6 drains the major part of the hillslope. This segment is on the transition of the very shallow soil to the thicker soil and discharges a relatively large upslope area.

The results of the eight different spatial input pattern configurations on the base case scenario are presented in Table 4.4. The variance of pattern ‘Upper Right-1.2’ deviates less from the uniform input, and ‘Upper Right-2.1’ deviates most from the uniform input. Not only is segment 6 discharging even more water, but also the hydrograph of this pattern is significantly different from the uniform pattern mainly caused by segment 6 and 7 (see Figure 4.4b). While the uniform pattern has a rather smooth recession curve, pattern ‘Upper Right-2.1’ has a double peak in



(a)



(b)

Figure 4.4: Subsurface storm flow for the entire width of the hillslope (28 m). The upper graphs show the hydrographs of the 13 segments along the trench, the lower left the total outflow and the lower right the variability along the trench. a) Subsurface storm flow of the base case scenario with uniform input; b) Subsurface storm flow of the base case scenario with spatially variable input 'Upper Right-2.1' (see Figure 4.1).

Configuration	Initial pattern	$\text{Var}(\bar{Q}_s/\bar{Q}_t)$ [-]	Q_p [m ³ h ⁻¹]	ΣQ_t [m ³]
Uniform	-	$10.4 \cdot 10^{-2}$	0.40	7.13
Upper left	1.1	$11.3 \cdot 10^{-2}$	0.39	7.39
	1.2	$8.9 \cdot 10^{-2}$	0.36	7.68
	2.1	$13.0 \cdot 10^{-2}$	0.35	7.24
	2.2	$11.7 \cdot 10^{-2}$	0.35	7.15
Upper right	1.1	$11.7 \cdot 10^{-2}$	0.37	7.56
	1.2	$9.6 \cdot 10^{-2}$	0.37	7.37
	2.1	$13.7 \cdot 10^{-2}$	0.34	7.35
	2.2	$11.5 \cdot 10^{-2}$	0.37	7.10

Table 4.4: Effect of different spatial input patterns on variance in segment subsurface storm flow, $\text{var}(\bar{Q}_s/\bar{Q}_t)$, peak discharge (Q_p), and total subsurface flow volume (ΣQ_t).

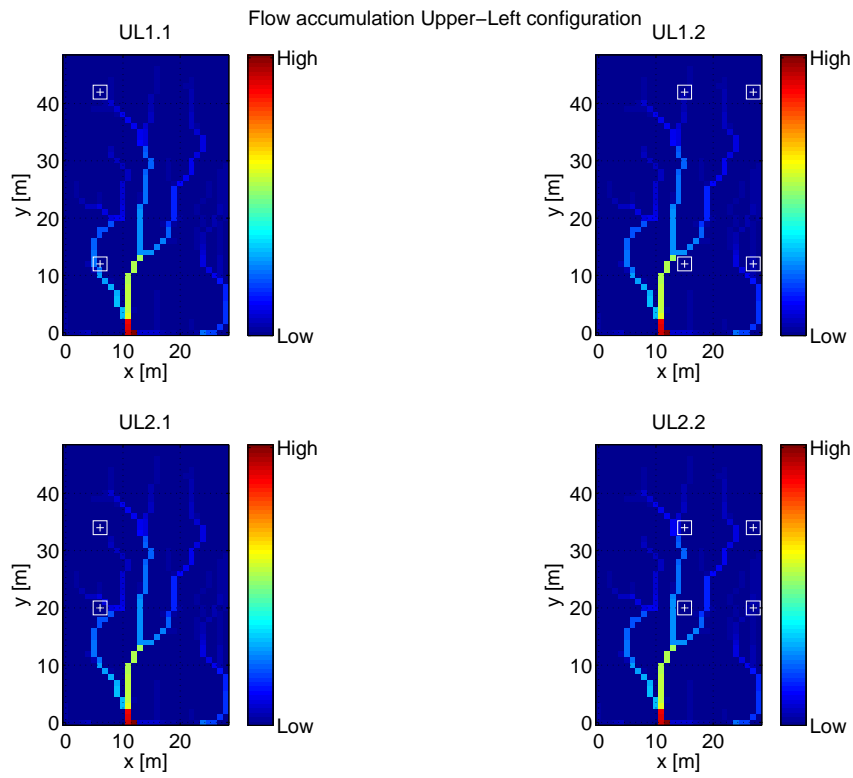
segment 6 and 7.

The double peak is probably caused by the location of the hotspot of high throughfall. If two hotspots are located above a ‘channel’ of high flow accumulation, this causes quick drainage of two flow peaks. In Figure 4.5 the flow accumulation map of the bedrock topography is presented with the location of the throughfall hotspots of the eight different input patterns. Segment 6, has the largest drainage area. The reason why pattern ‘Upper-Right 2.1’ is extremely responsive, is because four hotspots are located in the flow accumulation channel of segment 6 and two of them are at about the same travel distance from segment 6. Hence the spatial pattern does influence subsurface stormflow. It determines the variance in subsurface flow along the trench and, even more importantly the shape of the hydrograph.

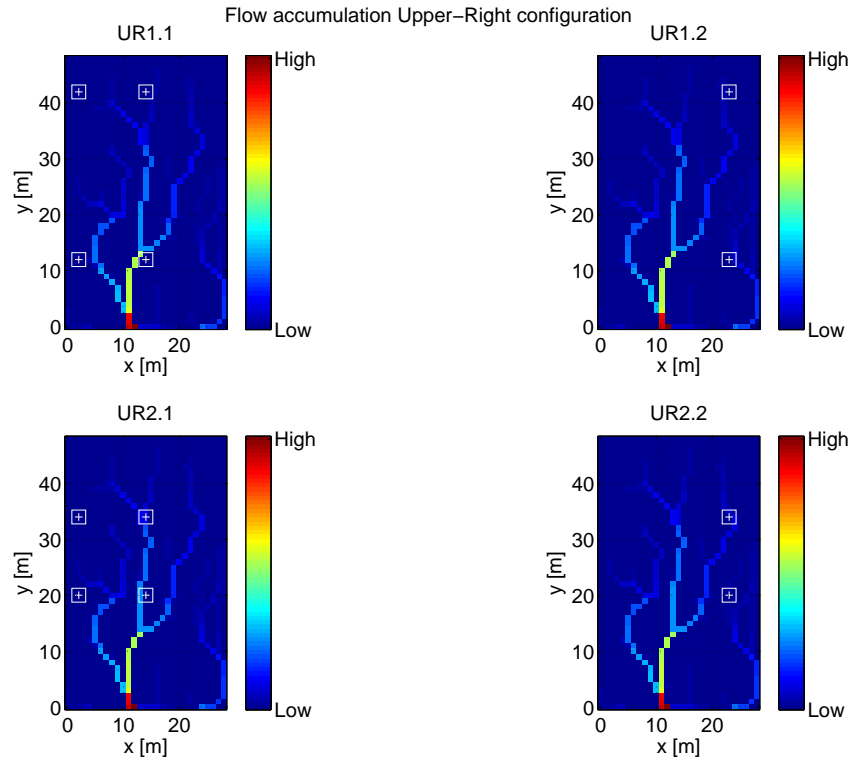
4.3.2 Interplay hillslope attributes on subsurface storm flow

The spatial pattern with the highest impact on the subsurface storm flow (SSF) has been used for further analysis. Based on the variance in segment SSF ‘Upper Right-2.1’ (UR2.1) deviates most from the uniform input (Figure 4.6). The storm depth, the average slope angle, and the average soil depth have been changed to investigate the interplay of input and hillslope attributes on six characteristics of the hydrograph of SSF. The six characteristics, which are used for this analysis are (Mosley [1979]):

- *Runoff coefficient* [%]: Total SSF at the trench divided by total rainfall.
- *Response time* [h]: Time between start of rain and start of SSF.
- *Time to peak* [h]: Time between start of rain and the peak discharge (second peak).
- *Peak discharge* [m³ h⁻¹]: Highest discharge of Q_t .
- *Recession time* [h]: Duration of recession curve starting after second peak.
- *Variance of segment outflow* [-]: Variance of \bar{Q}_s/\bar{Q}_t .



(a)



(b)

Figure 4.5: Flow accumulation map of bedrock topography and location of hotspots in Upper-Left configuration (a) and in the Upper-Right configuration (b).

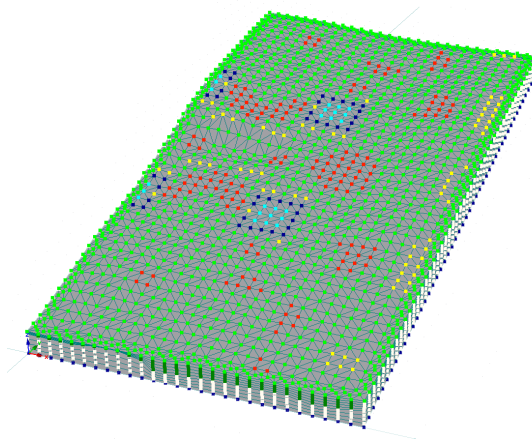


Figure 4.6: Input pattern ‘Upper Right-1.2’ on Panola hillslope with highest impact on subsurface outflow compared to uniform input.

In Figure 4.7 the interplay of the storm depth and the hillslope attributes are visualized using ‘response cubes’. Response cubes make it possible to visualize the interplay (or interactions) between variables in a three-dimensional space. The results of the 36 simulations are interpolated to obtain the response cubes. If the color gradient is parallel to one of the axes, this means that the variable along that axis is not influencing the hydrograph characteristic. For instance, the runoff coefficient is not influenced by the soil depth. In contrast, storm size and slope angle both affect the runoff coefficient similarly, resulting in a superposition of effects as indicated by the diagonal color gradient. To a lesser extent, this is also the case for the response time. However, here the soil depth slightly influences the response time by larger travel times for thick soil depths, and the influence of storm size and slope angle is much lower.

These results are similar to the results found by Hopp and McDonnell [2009] for uniform input. Hence, spatial variability does not influence the runoff coefficient or the response time.

The interplay on time to peak is not as regular as the runoff coefficient and the response time. For shallow soils the time to peak is relatively low and constant; however, for soils depths between 1.22 and 1.84 m it becomes a more complex system, likely caused by the connectivity of flow paths as explained by Hopp and McDonnell [2009]. The peak discharge is not as complex as the time to peak. As expected, peak discharge increases with storm depth, shallow soils, and hillslope steepness; however, the relation is not linear.

Since the results for time to peak and for peak discharge are different from the uniform input (Hopp and McDonnell [2009]), spatial variability in throughfall does matter. This can be explained by the connectivity theory as described by Hopp and McDonnell [2009]. If certain areas receive more water than others, connectivity can occur earlier, while other locations remain unconnected. This can result in differences in travel time and in peak discharge.

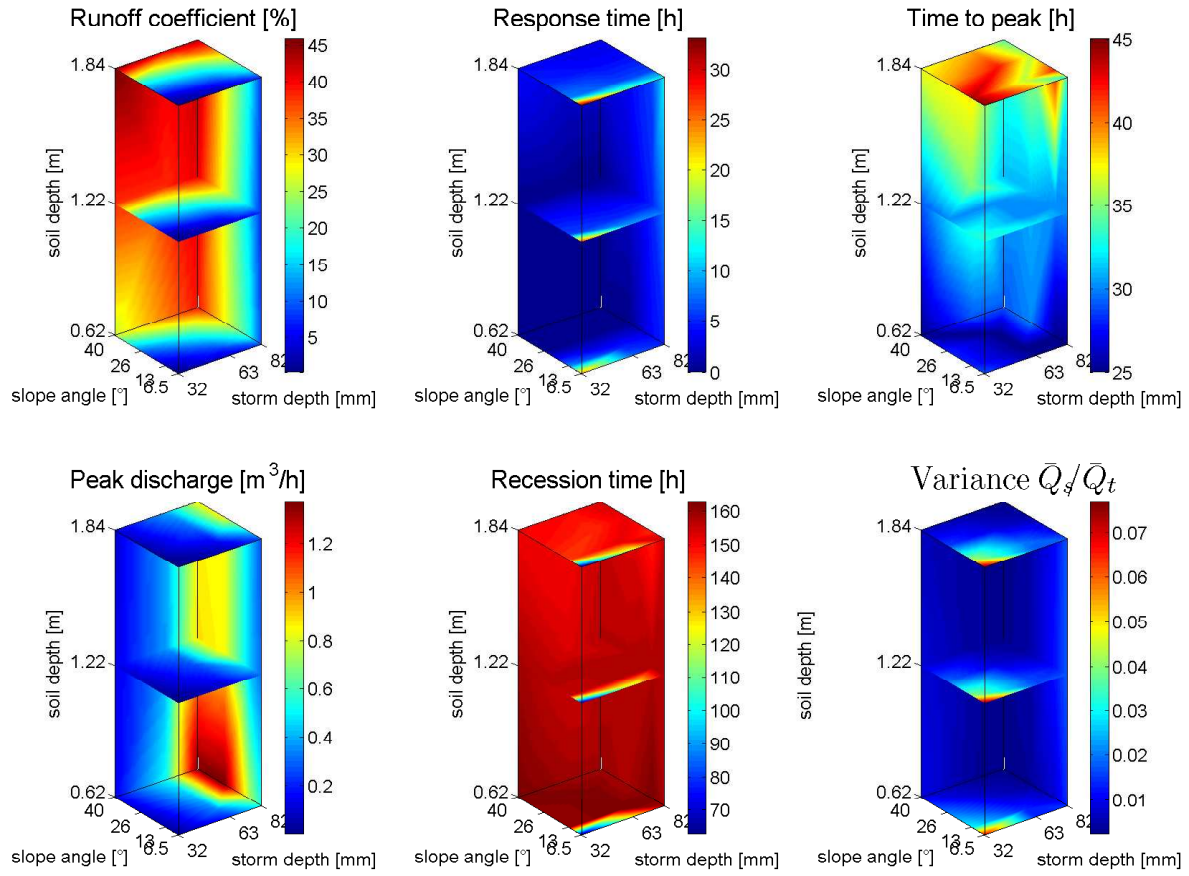


Figure 4.7: Response cubes showing interpolated results of the interplay of hillslope attributes and SSF.

The recession time behaves in a similar way as the response time: a quick response time results in a long recession time and vice-versa. The variance in the distribution of subsurface flow along the trench is not influenced by soil depth, but mainly by storm size and slope angle. Steep slopes with big storms have straight flow paths and distribute the water equally, while gentle slopes with small storms route the water along meandering flow paths as explained in detail by Hopp and McDonnell [2009].

4.3.3 Spatial pattern of soil moisture content

From the model results it appears that the soil moisture content (e.g., for the soil-bedrock interface) is highly correlated to the bedrock topography when it has been dry for a long time (Figure 4.8a) and that during a rainfall event, or shortly after, the soil moisture pattern represents the rainfall pattern (see Figure 4.8b).

Western et al. [1999] and Grayson et al. [1997] found similar results, although they considered the seasonal timescale and not the event scale. They found that during the wet state (winter period) the soil moisture pattern was dominated by lateral flow and thus was organized according

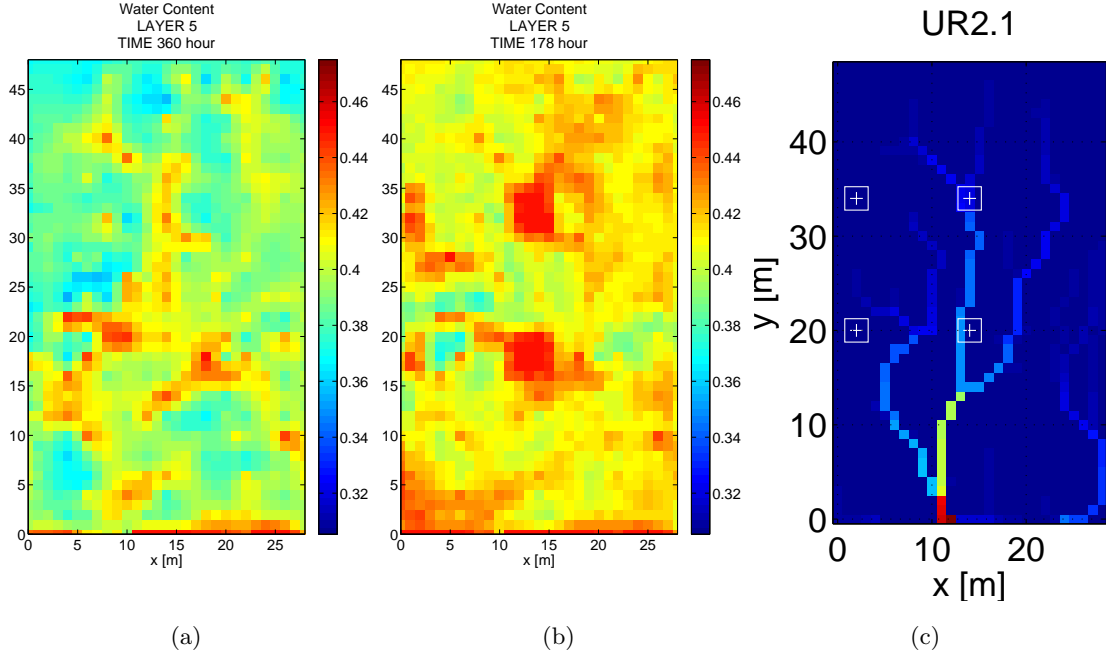


Figure 4.8: a) Soil moisture pattern (-) of the soil-bedrock interface after a long dry period ($t=360$ hour); b) shortly after a rain storm ($t=178$ hour) at layer 5 (i.e. bedrock interface layer); c) flow accumulation map and location of high intensity throughfall input.

the topography. During the dry state (summer period) vertical water flow was dominant and hence the soil moisture was less organized by the topography. Our study is comparable to a ‘wet season’.

Whether the soil moisture pattern resembles the pattern of the bedrock topography or follows the rainfall pattern is investigated with semi-variograms of normalized data (Keim et al. [2005]). We calculated the semi-variograms of the irregularity of the bedrock topography (i.e. DEM minus plane with slope A), the throughfall, and the soil moisture pattern (average of layers 5-10).

In Figure 4.9 the semi-variograms for the base case scenario are presented. We fitted an exponential model (Chilès and Delfiner [1999]) to find the range, r , of the semi-variogram, which is the correlation length:

$$\gamma(h) = c \left(1 - \exp \left(\frac{-3h}{r} \right) \right) \quad (4.4)$$

The range r is defined as the lag h , where the variance (γ) is 95% of the sill c , and is a measure for the correlation between the points. High spatial correlation between the throughfall collectors causes the range to be large and vice versa. In other words, it is the length over which the data points are still spatially correlated with each other.

As can be seen in the semi-variogram of normalized throughfall (Figure 4.9a) the sill is not constant. This is called a ‘hole-effect’ and reflects the tendency for high values to be systematically

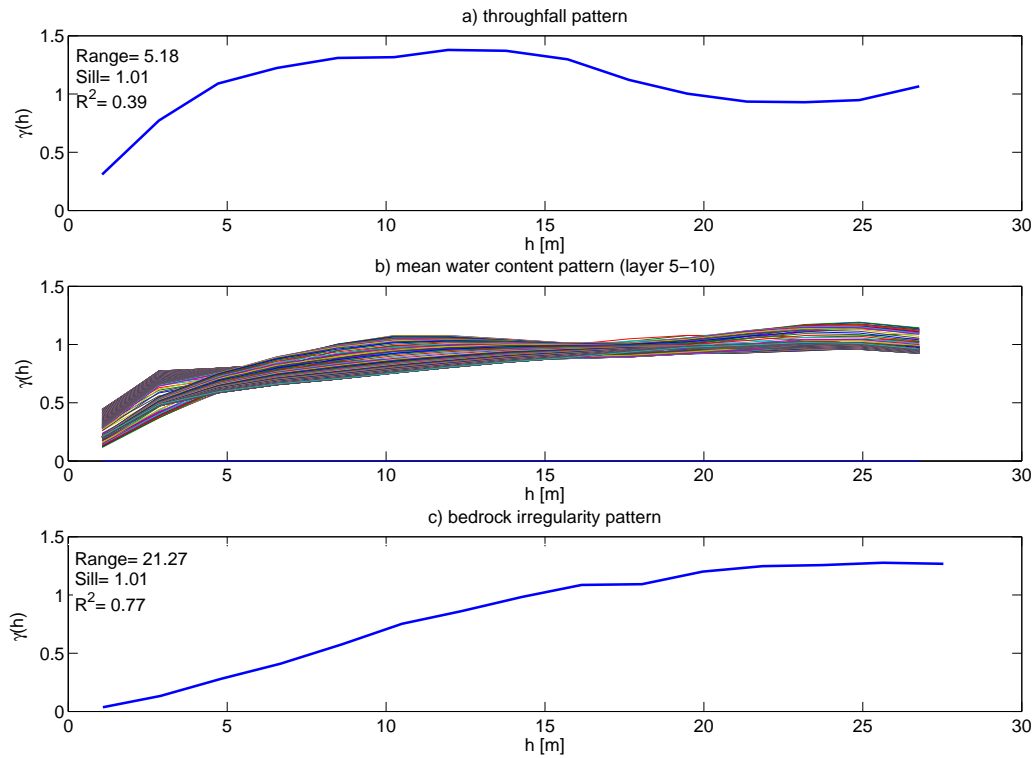


Figure 4.9: Semi-variograms for a) throughfall pattern, b) the mean soil moisture pattern for all time steps, and c) the bedrock irregularity pattern.

surrounded by low values and vice versa (Chilès and Delfiner [1999]). This probably represents the effect of canopy coverage, where certain areas are covered and others are not. This hole effect also causes the low R^2 for the fitted semi-variogram model (Equation 4.4).

Figure 4.9b shows the semi-variogram of the average soil moisture pattern for each time step and seems to change between the semi-variogram of the throughfall pattern and the bedrock topography (Figure 4.9c). To test this, we choose to look at the range as the main characteristic of the spatial pattern. For the throughfall we found a range of 5 meter and for the bedrock irregularity 21 meter. We hypothesize that between rainfall events the soil moisture pattern has similar spatial characteristics as the topography, but during a rainfall event this changes to the spatial characteristics of the throughfall pattern.

In Figure 4.10 this can be seen for the base case scenario. The range of the average soil moisture starts at 13 m and drops to 11 m during the first rainfall event. After rainfall ceases the range returns back in the direction of the range of the topography. When the second rainfall starts the range of the soil moisture pattern again drops towards the range of the throughfall pattern. And finally, after the rain stops, it again moves back in the direction of the range of the bedrock irregularity. Hence the change of the soil moisture range (blue line in Figure 4.10) acts like a hydrograph, and can be called a ‘geo-statistical hydrograph’.

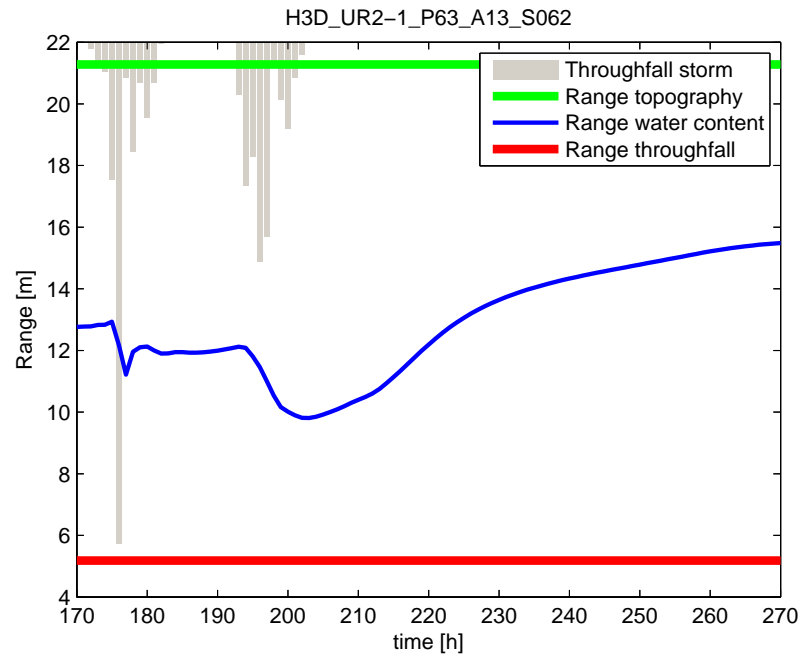


Figure 4.10: Change in range (average over soil layers) over time as a result of the storm event for the base case scenario.

The fact that the start and end range differ, is a consequence of the (non realistic) initial soil moisture pattern. At $t = 360$ the range approximates 16 meter (‘equilibrium state’). This analysis of the spatial patterns might help to understand and predict soil moisture patterns based on throughfall and bedrock patterns; however, one should be careful with using the range as the descriptor of the a spatial pattern. Two spatial patterns can have the same range, but can have a completely different pattern. Furthermore, this analysis is only possible when there is an impermeable bedrock layer.

If this plot is generated for all combinations of storm depth, angle, and soil depth, we can investigate if the hillslope attributes change the spatial pattern of the soil moisture. First, we looked at the performance of the fitted semi-variogram model (Equation 4.4). In Figure 4.11a the R^2 is presented. Although the overall performance is good with a mean R^2 of 0.8 ± 0.1 , it appears that the steep slopes perform relatively worse. For steep slopes, the soil moisture pattern has lateral flow paths just after the rainfall event, which can not described well with an exponential model, causing the relative bad performance.

Second, we looked at the equilibrium state. This is the final range of the soil moisture at $t = 360$ hours and is shown in Figure 4.11b for all cases. The interpolated cube shows that with increasing slope the final range becomes larger. Hence with increasing slope the topography becomes more important. Furthermore, there is a slight increase in final range with increasing storm size. This was also observed by Western et al. [2004] and is likely inherent to the method.

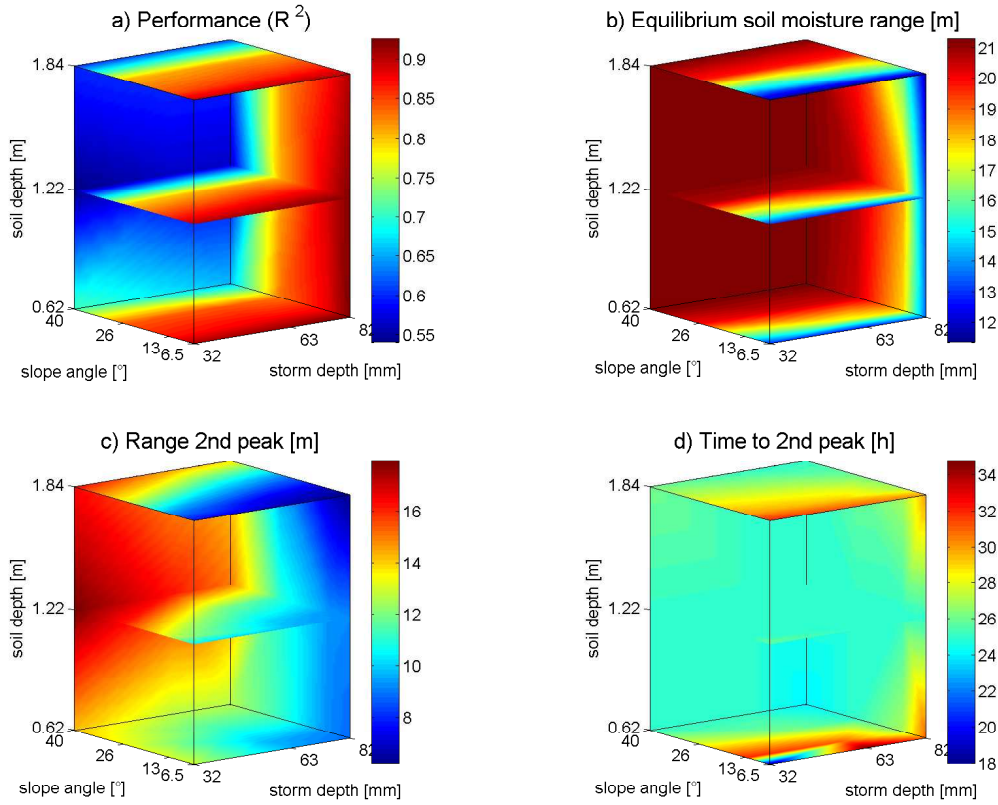


Figure 4.11: a) Interplay of hillslope attributes on model performance; b) Interplay of hillslope attributes on equilibrium range; c) Interplay of hillslope attributes on peak value of the mean range of the soil layers. Blue indicates that the range is very similar to the range of the throughfall pattern, and red indicates similarity to the range of the bedrock pattern; d) Interplay of hillslope attributes on the time to peak (i.e. time between start of rain and peak in range).

Third, we analysed the second peak value of the ‘geo-statistical hydrograph’ in Figure 4.11c. As can be seen the peak range is related to storm size and slope angle. The bigger the storm the more the storm pattern influences the soil moisture pattern and the steeper the slope, the more the bedrock topography influences the soil moisture pattern. This is because the high gradient drains the rainwater so quickly that the throughfall pattern only remains for a short period. The soil depth appears not to have any influence when the soil layer is thick enough. Only for very thin soil layers the throughfall pattern has a larger influence on the soil moisture pattern.

In Figure 4.11d the interplay of the hillslope attributes and the time to peak is shown. The time to peak is defined as the time between the start of the rain and the peak of the range in the soil moisture pattern. For deep soil depths the peak occurs faster with increasing storm size and slope angle; however, for a mean soil depth of 1.22 m it appears that slope angle and storm size do not have an influence. For the very thin soil layer the pattern is similar to the thick soil layer. However, for gentle slopes and small storms the time to peak is short.

4.4 Conclusions

The virtual experiment shows that spatial variable throughfall has a large impact on subsurface storm flow behaviour. It appears that the spatial pattern affects both the SSF generation and the spatial variability along the hillslope, but only marginally the total SSF amount. For the eight patterns tested it appears that the peak discharge is generally lower than in the uniform case, but for some patterns the SFF hydrograph has a double peak. This double peak is caused by the drainage pattern. If a location with high throughfall intensity (hotspot) is directly above a drainage line, a double peak occurs. Hence, we can conclude that throughfall has a large impact on SSF. A forest does not only reduce the amount of infiltration by interception, but also smooths (lower peak, longer recession) the SSF hydrograph by the interaction between infiltration and bedrock pattern.

The spatial pattern with the largest impact on SSF compared to the uniform case has been used to analyse the interplay between hillslope controls (slope and mean soil depth) and storm size. The results were comparable with the uniform case; however, the peak discharge and the time between the start of the rain and the peak discharge are different patterns. This is likely caused by a different connectivity pattern. Some depressions will be filled early, while others remain empty. This has a large impact on the SSF hydrograph.

The throughfall pattern also influences the soil moisture pattern, but only during and shortly after the storm event. By means of a geo-statistical analysis we investigated if the soil moisture pattern reflected a balance between the spatial variable throughfall pattern and that of the bedrock. As an indicator we used the range of the semi-variograms. We found that the soil moisture pattern has a similar range as the throughfall pattern during the storm and gradually returns to the range of the bedrock pattern after throughfall has ceased.

Finally, we looked at the impact of hillslope controls and storm size on the geo-statistical analysis. It appeared that the throughfall pattern is more important during large storms and that the bedrock topography becomes more important for steeper slopes. The mean soil depth appears to have no significant impact.

Overall, we can conclude that interception has a big influence on SSF generation and on the soil moisture patterns that occur during and shortly after rain events. Geo-statistical analysis can help to understand the relationship between soil moisture patterns, throughfall patterns and subsurface characteristics. However, more research is necessary to investigate other hillslope variables, such as antecedent wetness, macroporosity, rainfall intensity, soil evaporation, and transpiration. Also confronting our model results with real observed data from one site would be a next research step. This could validate our findings.

Chapter 5

Analytical derivation of the Budyko curve based on rainfall characteristics and a simple evaporation model

.....

The Budyko curve is often used to estimate the actual evaporation as a function of the aridity index in a catchment. Different empirical equations exist to describe this relationship; however, these equations have very limited physical background. The model concept presented in this paper is physically based and uses only measurable parameters. It makes use of two types of evaporation: interception and transpiration. It assumes that interception can be modeled as a threshold process on a daily time scale. If multiplied with the rainfall distribution function, integrated, and multiplied with the expected number of rain days per month, the monthly interception is obtained. In a similar way, the monthly interception can be upscaled to annual interception. Analogous to the interception process, transpiration can be modeled as a threshold process at a monthly time scale and can be upscaled by integration and multiplication with the expected number of rain months. The expected rain days per month are modeled in two ways: as a fixed proportion of the monthly rainfall and as a power function based on Markov properties of rainfall. The latter is solved numerically. It appears that on an annual basis the analytical model does not differ much from the numerical solution. Hence, the analytical model is used and applied on 10 locations in different climates. This paper shows that the empirical Budyko curve can be constructed on the basis of measurable parameters representing evaporation threshold values and the expected number of rain days and rain months and, in addition, a monthly moisture carryover amount for semi-arid zones.

.....

Based on: Gerrits, A. M. J., Savenije, H. H. G., Veling, E. J. M., Pfister, L., 2009b. Analytical derivation of the Budyko curve based on rainfall characteristics and a simple evaporation model. Water Resources Research 45, –

5.1 Introduction

In water resources modeling the Budyko curve is often used to simulate evaporation as a function of an aridity index in a simple supply-demand framework. In some locations of the world, annual evaporation may approach annual precipitation. This occurs if there is always sufficient energy available to evaporate the precipitation. Such locations are moisture constrained. In other locations, annual evaporation may approach potential evaporation. This happens if the available energy is less than the required energy to evaporate the annual precipitation. These locations are energy constrained. Depending on the dryness of the climate, either the available water or the available energy is the limiting factor.

The Budyko curve is based on two balance equations: the water balance and the energy balance (Arora [2002]).

$$\frac{dS}{dt} = P - E - Q \quad (5.1)$$

$$R_n = \rho\lambda E + H + G \quad (5.2)$$

where S is the water storage, P the precipitation, E actual evaporation, Q the catchment runoff, R_n the net radiation, λ the latent heat of vaporization, H the sensible heat flux, and G the ground heat flux. On an annual time scale we can assume that the water storage change is negligible ($dS/dt = 0$) and that the net ground heat flux approaches zero ($G = 0$). By dividing Equation 5.2 by 5.1 we obtain with $P_a = E_a + Q_a$ where the subscript a indicates annual values:

$$\frac{R_n}{P_a} = \frac{\rho\lambda E_a}{P_a} + \frac{H}{P_a} \quad (5.3)$$

If we successively define the annual potential evaporation as $\rho\lambda E_p = R_n$ (where Arora [2002] interprets potential evaporation as all energy being converted into evaporation and none in heating) and define the Bowen ratio as $B_r = H/\rho\lambda E_a$ we obtain:

$$\frac{E_p}{P_a} = \frac{E_a}{P_a} + \frac{B_r E_a}{P_a} = \phi = \frac{E_a}{P_a} (1 + B_r) \quad (5.4)$$

with ϕ the aridity index.

Since the Bowen ratio can also be expressed as a function of the aridity index (Arora [2002]), Equation 5.4 can be rewritten as:

$$\frac{E_a}{P_a} = \frac{\phi}{1 + f(\phi)} = F(\phi) \quad (5.5)$$

A lot of studies have been done on finding this relation. Classical studies were done by Schreiber [1904], Ol'dekop [1911], Budyko [1974], Turc [1954], and Pike [1964]. Their equations are summarized in Table 5.1 and plotted in Figure 5.1, with on the x-axis the aridity index, which expresses the ratio of annual potential evaporation and annual precipitation (E_p/P_a). Turc's curve is not shown in Figure 5.1, because it is similar to Pike's. The observations are from several water

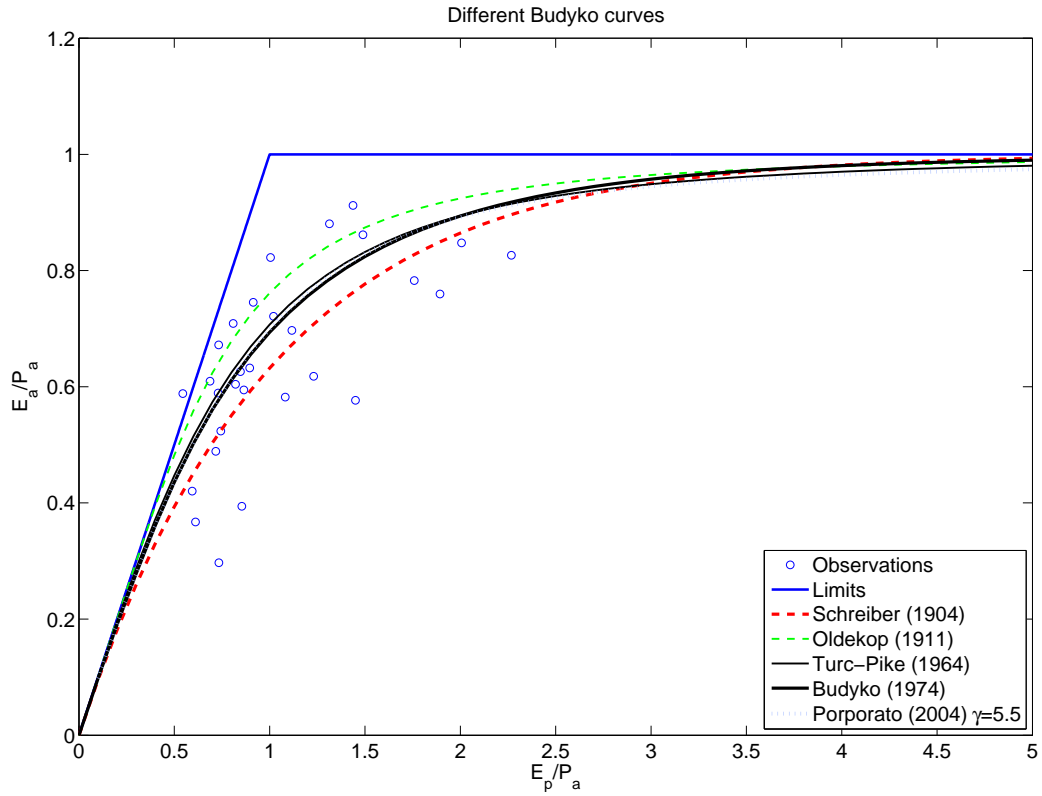


Figure 5.1: Different representations of the Budyko curves and some observations. The 1:1 limit expresses the limitation by available energy ($E_p < P_a$) and the horizontal limit expresses the limitation by available water ($E_p > P_a$)

Equation	Reference
$\frac{E_a}{P_a} = 1 - \exp(-\phi)$	Schreiber [1904]
$\frac{E_a}{P_a} = \phi \tanh(1/\phi)$	Ol'dekop [1911]
$\frac{E_a}{P_a} = \frac{1}{\sqrt{0.9 + (1/\phi)^2}}$	Turc [1954]
$\frac{E_a}{P_a} = \frac{1}{\sqrt{1 + (1/\phi)^2}}$	Pike [1964]
$\frac{E_a}{P_a} = [\phi \tanh(1/\phi) (1 - \exp(-\phi))]^{0.5}$	Budyko [1974]
$\frac{E_a}{P_a} = 1 - \frac{\phi \cdot \gamma^{\frac{\gamma}{\phi}-1} \exp(-\gamma)}{\Gamma(\frac{\gamma}{\phi}) - \Gamma(\frac{\gamma}{\phi}, \gamma)}$	Porporato et al. [2004]

Table 5.1: Different Budyko curves as a function of the aridity index (ϕ).

balance models with different catchment sizes (Perrin et al. [2007], Savenije [2003], Samuel et al. [2008], and Jothityangkoon and Sivapalan [2009]).

Building on these almost fully empirical relationships, other authors attempted to incorporate more physics in the equations. For example Choudhury [1999] added net radiation and a calibration factor α , Zhang et al. [2001, 2004] derived a model parameter, w , describing the integrated effects of catchment characteristics like vegetation cover, soil properties and catchment topography. Yang et al. [2006, 2008] added a catchment parameter, Donohue et al. [2007] tried to include vegetation dynamics, and Milly [1993], Porporato et al. [2004], and Rodríguez-Iturbe and Porporato [2004] developed a stochastic model, that incorporated the maximum storage capacity. However, these relationships were still not fully physically based. Even the equation of Yang et al. [2008], who found an analytical derivation for the Budyko curve which included a parameter n , representing catchment characteristics, contains a calibration factor. This extra parameter is a collection of all kinds of catchment characteristics and is therefore difficult to determine or to measure. The aim of this paper is to find an analytical derivation of the Budyko curve, based on a conceptual model and using only measurable parameters.

The derivation considers evaporation as the mechanism that feeds water back to the atmosphere and that includes all evaporative processes as defined by for example Shuttleworth [1993]:

$$E = E_i + E_t + E_o + E_s \quad (5.6)$$

Hence, evaporation includes evaporation from interception (E_i), transpiration (E_t), from open water (E_o), and from the soil (E_s). Interception is the evaporation from the entire wet surface, so not only the canopy, but also the understorey, the forest floor, and the top layer of the soil. Although the latter seems to have an overlap with soil evaporation, we distinguish them by the fact that soil evaporation refers to rainwater that is stored in the soil and is connected with the root zone (De Groen and Savenije [2006]). In this paper we assume that evaporation from the deeper soil is not significant or can be combined with evaporation from interception. Open water evaporation is mainly important in areas where for example great lakes exist and is therefore not considered in this paper. Hence, the following equation is used to calculate total evaporation:

$$E = E_i + E_t \quad (5.7)$$

An important distinction between the different types of evaporation is the time scale of the underlying processes. For example, interception is a process that has a short time scale in the order of one or a few days. Generally, canopy interception has a very short time scale (less than 1 day), which can be observed by the fact that after a rainfall event the canopy is dry within a couple of hours. Forest floor interception, on the other hand, has a somewhat larger time scale, since it may take more time (one to several days) to dry the forest floor (Gerrits et al. [2007]; Baird and Wilby [1999]). The time scale is estimated by dividing the stock by the flux. In the case of interception the stock amounts to a few millimeters and the evaporative flux is a few

millimeters per day, resulting in the conclusion that interception has a time scale in the order of one day. Transpiration on the other hand has a much longer time scale (e.g., Dolman and Gregory [1992], Savenije [2004] and Scott et al. [1995]). For transpiration the stock is in the order of tens to hundreds of millimeters, while the flux is a few millimeters per day (Gerrits et al. [2009a] and Baird and Wilby [1999]), resulting in a time scale in the order of month(s).

5.2 Methodology

When creating a model, it is important to model the different processes at the right time scale. If one wants to make a monthly interception model, it is imperative to use daily information on the precipitation. For the total amount of interception, it is important to know the rainfall intensity and the time between rainfall events. It makes a large difference if monthly rainfall consists of many small events, or a few very large events. A monthly interception model does not necessarily require the actual daily rainfall data, but it does need information on the daily rainfall distribution (e.g., Markov properties). This is the main idea behind the proposed model: we model the evaporation process at the time scale on which it occurs and upscale it by making use of the temporal characteristics of the rainfall.

In Figure 5.2 an overview of the model is shown. At a daily time scale interception can be modeled as a simple threshold process: all rain water is intercepted as long as the storage capacity is not exceeded. Hereafter water will infiltrate or run off (see experiments of e.g., Deguchi et al. [2006], Helvey and Patric [1965], Rutter et al. [1971], Viville et al. [1993]). When we have information on how the rainfall is distributed over the month it is possible to upscale daily interception to monthly interception. Analogously, we can upscale monthly interception to annual interception, if we have information on how monthly rainfall is distributed over the year and each month has similar rainfall characteristics.

Similar to interception, we can model transpiration as a threshold process at a monthly time scale as a function of net precipitation (rainfall minus interception). If the temporal characteristics of the net rainfall are known, we can upscale monthly transpiration to annual transpiration. Finally, summing annual interception and transpiration gives an expression for annual evaporation as a function of annual precipitation.

In the following sections, the model will be described in more detail. In Section 5.3 an analytical derivation of the model is presented. For the analytical solution we had to simplify the Markov properties of the daily rainfall. In Section 5.4 we derive a model that takes full account of the Markov properties. Both the analytical and numerical derivations are carried out with the mathematical software package MAPLE 9.5 (Waterloo Maple Inc.).

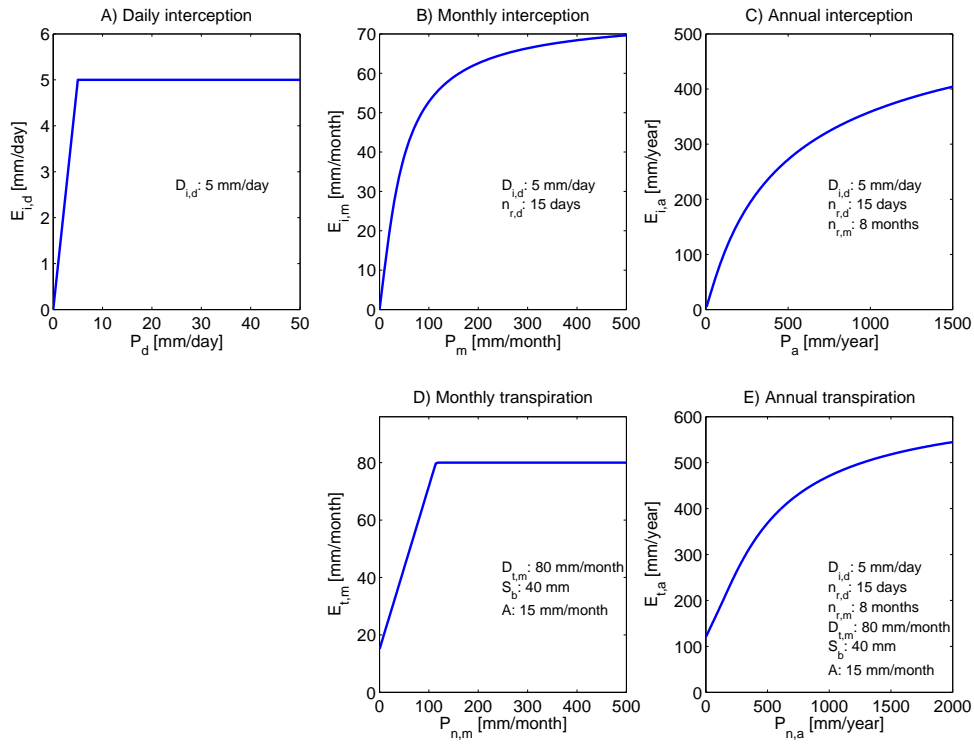


Figure 5.2: Stepwise integration from daily interception to annual interception and from monthly transpiration to annual transpiration.

5.2.1 Data

For this study ten locations in different parts of the world have been investigated. In Table 5.2 the characteristics of the locations are given. These ten locations have been chosen because both climate data and Markov coefficients were available. In the last column the available time series are shown together with the number of years used in the analysis. Only those years have been used that had complete monthly rainfall series.

The monthly rainfall data have been obtained from the Global Historical Climatology Network (GHCN) database, downloadable from <http://climexp.knmi.nl>. The annual potential evaporation data has been retrieved from the AHN, Remote Sensing and Image Research Center (Chiba University), downloadable from <http://www-cger.nies.go.jp/grid-e/>. The potential evaporation has been calculated with the Priestley-Taylor method (Priestley and Taylor [1972]).

5.3 Analytical derivation without Markov properties

5.3.1 Monthly interception equation (analytical)

On a daily basis, interception is a typical threshold process (e.g., Savenije [1997], Savenije [2004]). Rain water is intercepted by the canopy, the forest floor, or any other body as long as the

Place (country)	Location	Altitude [m]	P_a^1 [mm/y]	E_p^2 [mm/y]	Data availability P^3
Harare (Zimbabwe)	17.9S 31.1E	1500	793.8	1319	1950-1995 (44)
Masvingo (Zimbabwe)	20.0S 30.9E	1100	624.9	1344	1951-1996 (44)
Bulawayo (Zimbabwe)	20.2S 28.6E	1340	597.0	1378	1950-1996 (45)
Peters Gate (South Africa)	34.0S 18.6E	37	524.9	1051	1951-2006 (50)
Hyderabad (India)	17.5N 78.5E	545	785.6	1512	1871-2006 (121)
Indianapolis (IN, USA)	39.7N 86.3W	241	1024.5	816	1861-2007 (141)
Kansas City (MO, USA)	39.3N 94.7W	297	928.6	841	1871-2003 (121)
Sheridan (WY, USA)	44.8N 106.8W	1144	381.3	642	1894-2004 (98)
Tallahassee (FL, USA)	30.4N 84.4W	17	1503.7	1139	1886-2005 (114)
Lyamungu (Tanzania)	3.2S 37.3E	1337	1586.9	1567	1936-2003 (67)

a. Global Historical Climatology Network (GHCN) version 2 database.

b. AHN, Remote Sensing and Image Research Center.

c. Number of years is given in parentheses.

Table 5.2: Characteristics of investigated locations in this paper.

storage capacity is not exceeded. When the storage capacity is reached maximum interception is achieved. Hence daily evaporation from interception ($E_{i,d}$) can be modelled as:

$$E_{i,d} = \min(D_{i,d}, P_d) \quad (5.8)$$

where $D_{i,d}$ is the daily interception threshold [$L T^{-1}$], and P_d the daily rainfall on a rain day [$L T^{-1}$] (see Figure 5.2A).

Since we want to model interception on a monthly time scale, we have to make use of daily rainfall characteristics. As shown by many authors (Sivapalan and Blöschl [1998]; Todorovic and Woolhiser [1975]; Woolhiser et al. [1993]; De Groen and Savenije [2006]), the probability distribution of rainfall on a rain day can be described as:

$$f_{i,d}(P_d) = \frac{1}{\beta} \exp\left(\frac{-P_d}{\beta}\right) \quad (5.9)$$

β [$L T^{-1}$] being the scaling factor, equal to the expected rainfall on a rain day, which can be expressed as:

$$\beta = P_m / E(n_{r,d} | n_m) \quad (5.10)$$

with P_m [$L T^{-1}$] being the monthly rainfall and $n_{r,d}$ and n_m the number of rain days per month and amount of days per month, respectively.

Multiplying Equations 5.8 and 5.9 (De Groen [2002]) and integrating with respect to P_d from zero to $D_{i,d}$ (events which are too small to fill the storage capacity) and subsequently from $D_{i,d}$ to infinity (events which are larger than the storage capacity) leads to the average interception

per day. Successively, multiplying the average interception per day with the expected raindays per month leads to Equation 5.11. Equation 5.11 is plotted in Figure 5.2B.

$$\begin{aligned} E_{i,m} &= E(n_{r,d}|n_m) \int_0^\infty E_{i,d} \cdot f_{i,d}(P_d) dP_d \\ &= P_m \left(1 - \exp\left(\frac{-D_{i,d}}{\beta}\right) \right) \end{aligned} \quad (5.11)$$

If combined with Equation 5.10, $D_{i,d}/\beta$ is equal to the potential amount of monthly interception divided by the monthly rainfall, which is a sort of aridity index, $\phi_{i,m}$ [-]. Equation 5.11 can then be rewritten as:

$$E_{i,m} = P_m (1 - \exp(-\phi_{i,m})) \quad (5.12)$$

5.3.2 Annual interception equation (analytical)

To upscale monthly interception to annual interception, we make use of the probability distribution of rainfall in a rain month, which can also be described by an exponential function:

$$f_{i,m}(P_m) = \frac{1}{\kappa_m} \exp\left(\frac{-P_m}{\kappa_m}\right) \quad (5.13)$$

with κ_m [L T⁻¹] as the monthly scaling factor.

This relation is confirmed by the straight lines obtained when monthly rainfall is plotted against the logarithm of the probability of exceedance for all locations in Table 5.2. As an illustration the results for Zimbabwe and Tanzania are shown in Figure 5.3. Although at high rainfall amounts the line tends to deviate from the straight line, we may neglect this, because our interest is not on extreme rainfall amounts. In addition, the uncertainty of the extreme rainfall is large since they are based on a small number of events. However, we realize that in some climates these extreme events may be significant for the annual water balance.

Analogous to β , κ_m equals to the expected rainfall in a rain month expressed as:

$$\kappa_m = P_a / E(n_{r,m}|n_a) \quad (5.14)$$

where P_a [L T⁻¹] is the annual rainfall, $n_{r,m}$ the number of rain months in a year, and n_a the number of months per year. Since the number of rain months per year is constant for a given location, the scaling factor κ_m is directly proportional to P_a . This is confirmed by the high regression values in Figure 5.4 and Table 5.3 (only the results of Tanzania and Zimbabwe are shown). A rain month is defined as a month with more than 2 mm/month of rain.

The annual interception can be obtained by integration of the product of Equation 5.11 and 5.13 multiplied with the expected rain months in a year. If we assume $E(n_{r,d}|n_m)$ to be independent of P_m (which is not true) and assume it as a constant ($E(n_{r,d}|n_m) \approx n_{r,d} = \text{constant}$), then this can be integrated analytically. In Section 5.4 we shall compute the annual interception

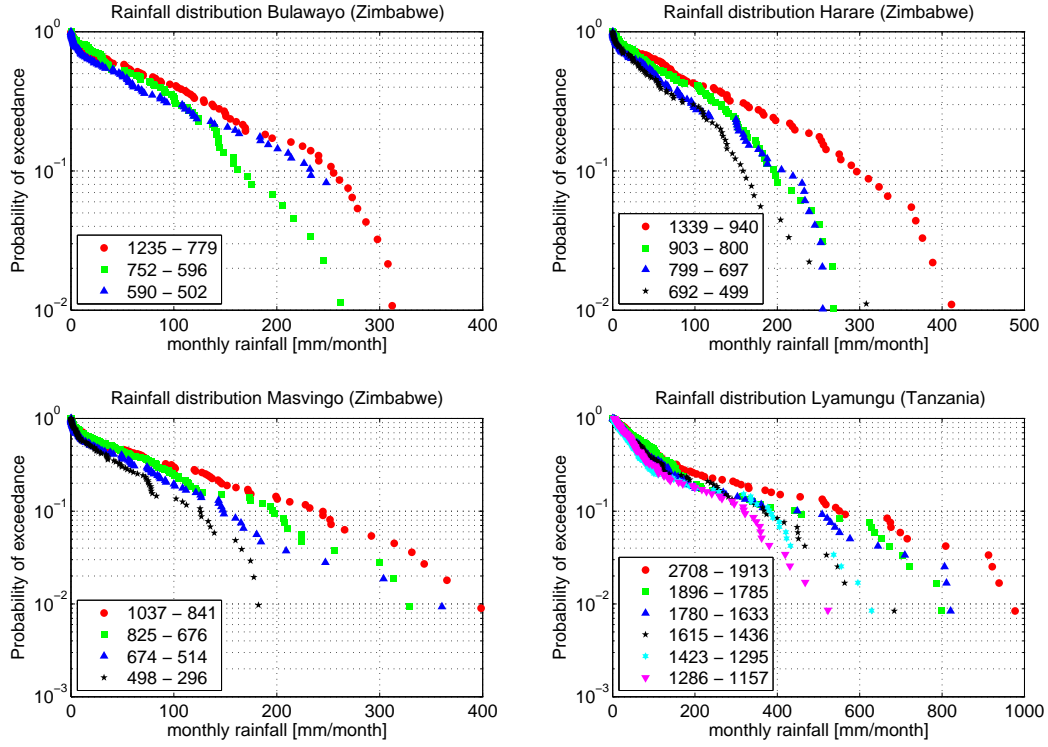


Figure 5.3: Probability of exceedance of rainfall amounts on rain months for different stations in Zimbabwe and Tanzania. The slope equals $-1/\kappa_m$.

numerically without this limiting assumption.

Analytical integration yields (Oberhettinger and Badii [1973], Part I, (5.34)) (see Figure 5.2C):

$$\begin{aligned}
 E_{i,a} &= E(n_{r,m}|n_a) \int_0^\infty E_{i,m} \cdot f_{i,m}(P_m) dP_m \\
 &= P_a \left(1 - 2 \frac{n_{r,d} D_{i,d}}{\kappa_m} K_0 \left(2 \sqrt{\frac{n_{r,d} D_{i,d}}{\kappa_m}} \right) \right) \\
 &\quad - P_a \left(2 \sqrt{\frac{n_{r,d} D_{i,d}}{\kappa_m}} K_1 \left(2 \sqrt{\frac{n_{r,d} D_{i,d}}{\kappa_m}} \right) \right)
 \end{aligned} \tag{5.15}$$

where K_0 and K_1 are Bessel functions of the first and second order, respectively. The fraction $n_{r,d} D_{i,d} / \kappa_m$ is the proportion of the potential amount of annual interception divided by the annual rainfall, which is a sort of aridity index for interception, $\phi_{i,a}$. Equation 5.15 can then be written as:

$$\begin{aligned}
 E_{i,a} &= P_a \left(1 - 2 \phi_{i,a} K_0 \left(2 \sqrt{\phi_{i,a}} \right) \right) \\
 &\quad - 2 \sqrt{\phi_{i,a}} K_1 \left(2 \sqrt{\phi_{i,a}} \right)
 \end{aligned} \tag{5.16}$$

Location	Analytical $n_{r,d}^1$	Numerical				Analytical/numerical		
		$p_{01} = q(P_m)^r$ q	$p_{11} = u(P_m)^v$ r	u	v	$n_{r,m}^2$	$n_{nr,m}^2$	A^3
Harare	15	0.020	0.55	0.200	0.24	8.3 (0.66)	7.4 (0.74)	15
Masvingo	11	0.030	0.43	0.200	0.24	8.9 (0.74)	6.9 (0.67)	15
Bulawayo	10	0.044	0.34	0.200	0.24	7.9 (0.47)	6.6 (0.60)	15
Peters Gate	11	0.094	0.33	0.034	0.40	11.2 (0.85)	8.1 (0.74)	5
Hyderabad	10	0.092	0.38	0.024	0.53	8.6 (0.72)	6.7 (0.68)	20
Indianapolis	11	0.129	0.30	0.045	0.42	12.0 (1.00)	11.7 (0.96)	0
Kansas City	11	0.129	0.27	0.061	0.30	11.8 (0.97)	10.6 (0.85)	0
Sheridan	10	0.216	0.22	0.084	0.30	11.7 (0.95)	6.2 (0.72)	0
Tallahassee	15	0.127	0.29	0.017	0.55	11.8 (0.99)	11.5 (0.95)	0
Lyamungu	17	0.053	0.39	0.170	0.20	11.8 (0.97)	10.1 (0.77)	0

a. CRU TS 2.1. Only wettest months are used.

b. Value in parentheses is r^2

c. Estimated values in [mm/month].

Table 5.3: Expected number of rain days for the analytical solution and for the numerical solution with power function coefficients describing Markov probabilities. The analytical solution is from Equations 5.16 and 5.23. Also given are the number of rain months per year (for gross, $n_{r,m}$, and net, $n_{nr,m}$, rainfall) and the carryover value A for different locations. Markov probabilities are taken from De Groen and Savenije [2006].

5.3.3 Annual transpiration equation (analytical)

Transpiration is a different process than interception. Firstly, transpiration depends on soil moisture storage and not directly on rainfall. Secondly, the time scale of transpiration is much longer (order of 10 days to several months depending on the soil moisture storage capacity). Often, actual transpiration (E_t) is modeled as potential transpiration ($E_{t,p}$) times a fraction depending on the wetness of the soil (e.g., Shuttleworth [1993]):

$$E_t = E_{t,p} \cdot \min\left(\frac{S}{S_b}, 1\right) \quad (5.17)$$

where S is the available soil moisture [L] and S_b the available soil moisture below which transpiration is soil moisture constrained [L].

Although transpiration is not directly dependent on (net) rainfall, De Groen [2002] showed that monthly transpiration, $E_{t,m}$ [L T⁻¹], can be described as (see Figure 5.2D):

$$E_{t,m} = \min(A + B \cdot (P_m - E_{i,m}), D_{t,m}) \quad (5.18)$$

with A the initial soil moisture [L T⁻¹] (‘carry-over value’) and B equal to:

$$B = 1 - \gamma + \gamma \exp\left(-\frac{1}{\gamma}\right) \quad (5.19)$$

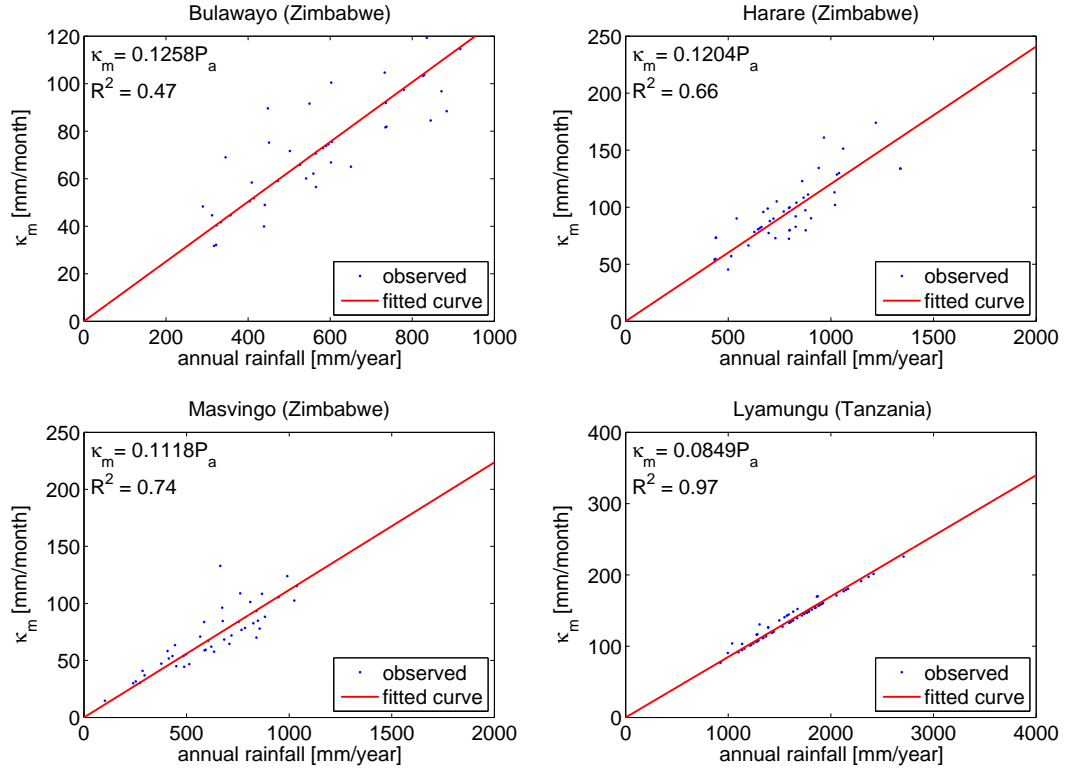


Figure 5.4: κ_m can be assumed directly proportional to the annual rainfall.

where $\gamma = S_b / (D_{t,m} \cdot \Delta_{t,m})$ and $\Delta_{t,m}$ equals unity.

While the distribution of monthly rainfall over time can be described with an exponential probability function (Equation 5.13), we found that this is also valid for the net monthly rainfall. To obtain net monthly rainfall ($P_{n,m}$), monthly interception has been subtracted from the monthly rainfall. Monthly interception is modeled by the expression found by De Groen and Savenije [2006] with the implementation of the Markov property of daily rainfall (Equation 5.26), explained in Section 5.4.1. We could also have used the model presented in Section 5.3.1 (Equation 5.12); however, De Groen [2002] showed that the monthly interception model with Markov properties performed better. Hence we choose the best available monthly interception model. The power functions used for the Markov probabilities are shown in Table 5.3. In Figure 5.5 the results are shown. Hence, the distribution function of the net rainfall can be described as:

$$f_{t,m}(P_{n,m}) = \frac{1}{\kappa_n} \exp\left(\frac{-P_{n,m}}{\kappa_n}\right) \quad (5.20)$$

where κ_n is a function of the monthly interception ($\kappa_n = \kappa_m - \kappa_i$) and κ_i is the scale factor for the monthly interception (see Figure 5.6).

The average monthly transpiration is then obtained by:

$$\overline{E_{t,m}} = \int_0^{D_{t,m}} (A + B \cdot P_{n,m}) f_{t,m} dP_{n,m} \quad (5.21)$$

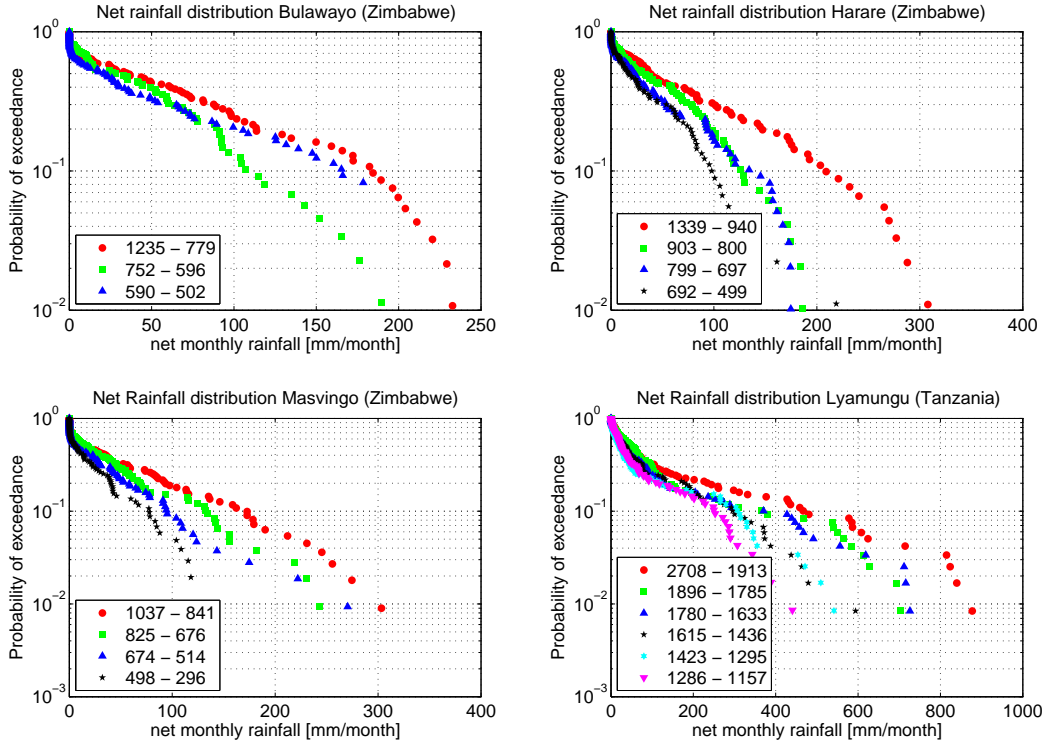


Figure 5.5: Probability of exceedance of net rainfall amounts on rain months for different stations in Zimbabwe and Tanzania with $D_{i,d} = 5$ mm/day. The slope equals $-1/\kappa_n$.

$$\begin{aligned}
 & + \int_{D_{t,m}}^{\infty} D_{t,m} f_{t,m} dP_{n,m} \\
 & = A + \kappa_n B - \kappa_n B \exp\left(\frac{-D_{t,m}}{\kappa_n}\right) \\
 & \quad \times \left(\frac{A}{\kappa_n B} + 1 + \frac{D_{t,m}}{\kappa_n} - \frac{D_{t,m}}{\kappa_n B}\right)
 \end{aligned}$$

When successively multiplied with $E(n_{nr,m}|n_a) = P_{n,a}/\kappa_n$ and substituting $P_{n,a} = P_a - E_{i,a}$ we obtain the annual transpiration as a function of annual precipitation. Similar to κ_m being linear to P_a , we can assume κ_n to be linear with net monthly rainfall, as can be seen in Figure 5.7 and Table 5.3. Of course, this expression is dependent on the daily interception threshold, $D_{i,d}$. Hence multiplying Equation 5.21 with $E(n_{nr,m}|n_a) = P_{n,a}/\kappa_n$ and $P_{n,a} = P_a - E_{i,a}$ results in:

$$\begin{aligned}
 E_{t,a} &= E(n_{nr,m}|n_a) \cdot \overline{E_{t,m}} \\
 &= (P_a - E_{i,a}) B \left(\frac{A}{\kappa_n B} + 1\right) \\
 &\quad - (P_a - E_{i,a}) B \exp\left(\frac{-D_{t,m}}{\kappa_n}\right) \\
 &\quad \times \left(\frac{A}{\kappa_n B} + 1 + \frac{D_{t,m}}{\kappa_n} - \frac{D_{t,m}}{\kappa_n B}\right) \\
 &= 2BP_a \left(\phi_{i,a} K_0\left(2\sqrt{\phi_{i,a}}\right) + \sqrt{\phi_{i,a}} K_1\left(2\sqrt{\phi_{i,a}}\right)\right) \\
 &\quad \times \left(\frac{A}{\kappa_n B} + 1 - \exp\left(\frac{-D_{t,m}}{\kappa_n}\right)\right)
 \end{aligned} \tag{5.22}$$

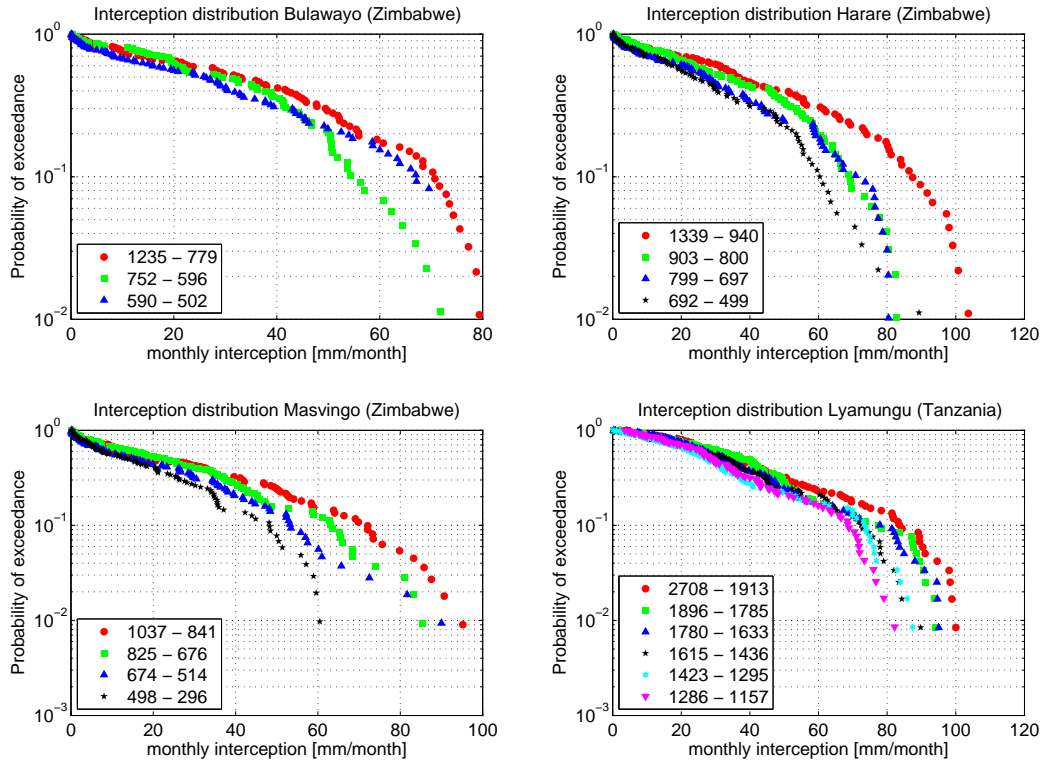


Figure 5.6: Probability of exceedance of interception amounts for different stations in Zimbabwe and Tanzania with $D_{i,d} = 5$ mm/day. The slope equals $-1/\kappa_i$.

$$\times \left(\frac{A}{\kappa_n B} + 1 + \frac{D_{t,m}}{\kappa_n} - \frac{D_{t,m}}{\kappa_n B} \right)$$

Introducing $\phi_{t,a} = D_{t,m}/\kappa_n$ as an ‘aridity’ index, this equation becomes (see Figure 5.2E):

$$\begin{aligned} E_{t,a} &= 2BP_a \left(\phi_{i,a} K_0 \left(2\sqrt{\phi_{i,a}} \right) + \sqrt{\phi_{i,a}} K_1 \left(2\sqrt{\phi_{i,a}} \right) \right) \\ &\times \left(\frac{A}{\kappa_n B} + 1 - \exp(-\phi_{t,a}) \right) \\ &\times \left(\frac{A}{\kappa_n B} + 1 + \phi_{t,a} - \frac{1}{B} \phi_{t,a} \right) \end{aligned} \quad (5.23)$$

5.3.4 Total evaporation (analytical)

In the previous subsections annual interception and transpiration have been derived analytically. The total evaporation ($E_{i,a}$) can be obtained by summing up Equations 5.16 and 5.23. In Table 5.4 the equations of the analytical solution are summarized.

In Figure 5.8 the sensitivity of the analytical model to thresholds and rainfall distribution is shown. All model parameters are varied within realistic ranges. The parameter sensitivity is more pronounced for high annual rainfall amounts. From these figures it can be seen that the annual evaporation is obviously sensitive to threshold values, but also to seasonality (the number

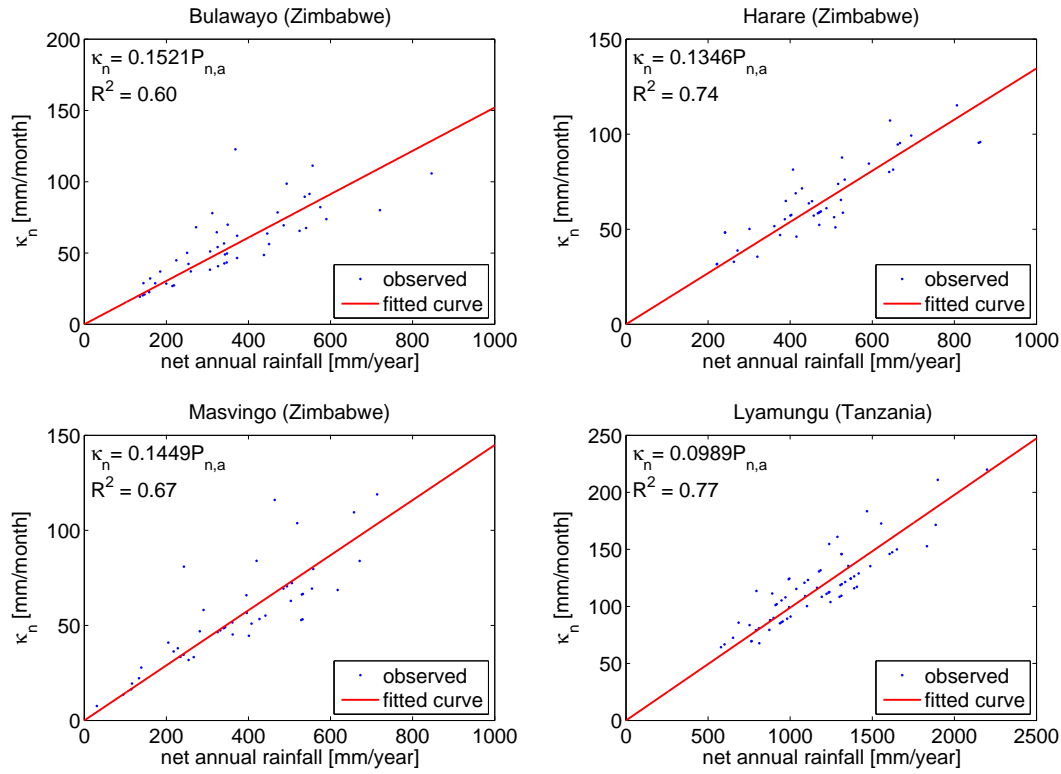


Figure 5.7: κ_n can be assumed directly proportional to the annual rainfall $P_{n,a}$ for given $D_{i,d} = 5$ mm/day.

of rain months ($n_{r,m}$). An increase of the number of rain months by a factor two, results in an evaporation increase by the same factor two for $P_a = 2000$ mm/year. Because the uncertainty in the determination of the number of rain months per year (the seasonality) is quite low, this effect is not important at a given location (see also Figure 5.4).

5.4 Numerical derivation with Markov properties

In the previous section we assumed $E(n_{r,d}|n_m)$ to be constant. However, the expected number of raindays per month is not constant but a function of the monthly rainfall. If the monthly rainfall increases, then the expected number of raindays per month increases as well.

5.4.1 Monthly interception equation (analytical/numerical)

De Groen [2002] showed that the expected number of raindays per month can be described as:

$$E(n_{r,d}|n_m) = n_m \frac{p_{01}}{1 - p_{11} + p_{01}} \quad (5.24)$$

By definition p_{11} is the transition probability which gives the probability of a future rain day if the present day is also a rain day. p_{01} is the transition probability, which gives the probability of

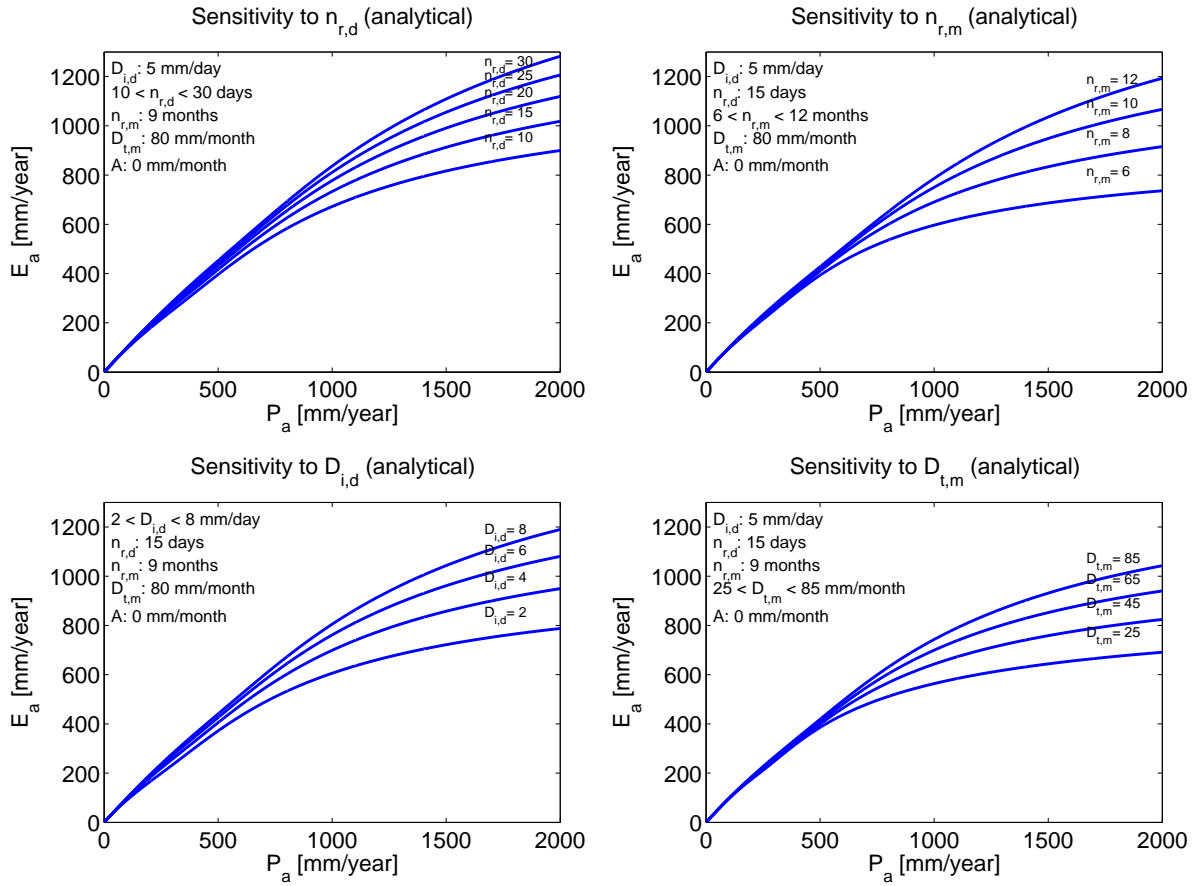


Figure 5.8: Sensitivity of the parameters of the analytical evaporation model to $n_{r,d}$, $n_{r,m}$, $D_{i,d}$ and $D_{t,m}$ with $\gamma = 0.5$.

a future rain day if the present day is a dry day. De Groen [2002] showed that these transition probabilities can be described by simple power functions:

$$p_{01} = q(P_m)^r \quad (5.25)$$

$$p_{11} = u(P_m)^v$$

With $p_{11} + p_{10} = 1$ and $p_{00} + p_{01} = 1$. The parameters q , r , u and v can be derived from historical daily rainfall data.

In upscaling equation (5.11) the expected number of raindays per month is now considered to depend on P_m , and thus $E(n_{r,d}|n_m)$ should be computed with Equations 5.24 and 5.25. The analytical solution is then (De Groen and Savenije [2006]):

$$E_{i,m} = P_m \left(1 - \exp \left(\frac{-D_{i,d} n_m q}{P_m^{1-r} - u P_m^{1-r+v} + q P_m} \right) \right) \quad (5.26)$$

In Figure 5.9 this equation is plotted and compared with the analytical solution of Equation 5.12. As can be seen, Equation 5.12 overestimates the low values and underestimates the higher values. This can be explained by the fact that for low rainfall β is higher when the Markov properties are applied. A higher β causes a lower monthly interception and so also a lower annual interception. For high rainfall the opposite is valid.

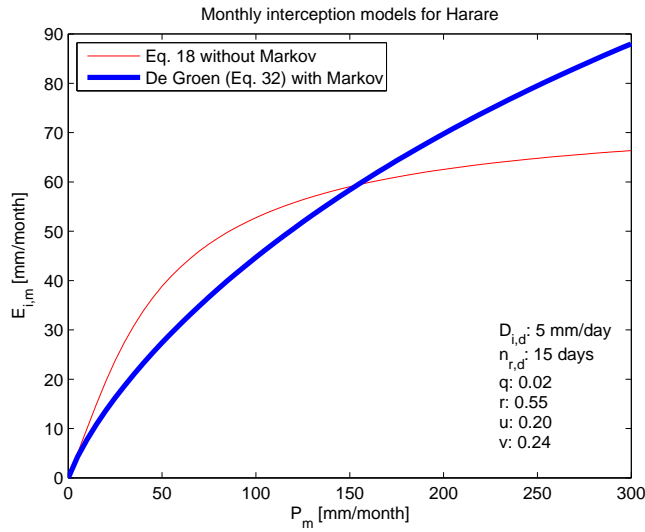


Figure 5.9: Analytical monthly interception model without Markov properties (Equation 5.12) and with Markov properties (Equation 5.26).

5.4.2 Annual interception equation (numerical)

In Figure 5.10 the numerical solution of the annual interception model is shown as circles. As can be seen, the analytical model overestimates interception for low rainfall amounts and underestimates it for high rainfall amounts. This is the result of the deviation in the monthly interception, which is now accumulated.

5.4.3 Annual transpiration equation (numerical)

The numerical solution for the annual transpiration is shown in Figure 5.11.

In contrast to the interception model, the analytical model underestimates transpiration for low rainfall and overestimates it for high rainfall amounts. This is due to the difference between the analytical and numerical solution of interception. Since $P_{n,a} = P_a - E_{i,a}$ this influences the transpiration results.

5.4.4 Total evaporation (numerical)

The differences between the analytical and numerical interception and transpiration appear to cancel out for the total evaporation at all locations where the rainfall is circa less than about 1500 mm/year. As an illustration the results for Harare are shown in Figure 5.12. From this graph we can see that the difference between the analytical and the numerical model are small as long as the annual rainfall is less than 1500 mm/year.

The crosses in Figure 5.12 show observations of the Mupfure catchment at Beatrice in Zimbabwe from 1970-1979 (Savenije [2004]). The Mupfure River lies southwest of Harare. At Beatrice the basin has an area of circa 1215 Mm². Although Harare is located just outside the Mupfure

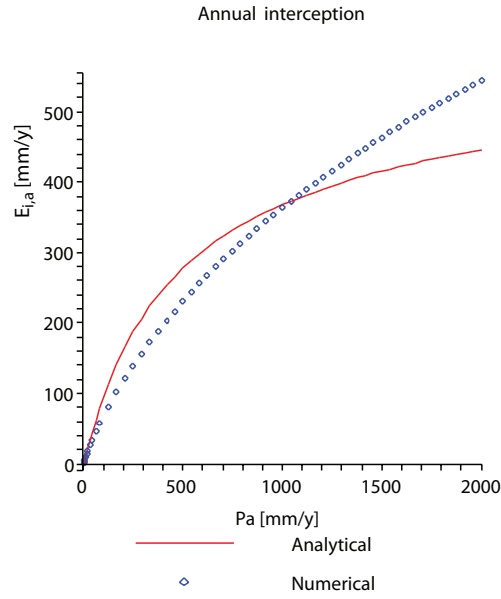


Figure 5.10: Comparison of the numerical (with Markov properties of Harare) and analytical (without Markov properties, $E(n_{r,d}|n_m) = 15$ days) annual interception model ($D_{i,d} = 5$ mm/day, $D_{t,m} = 82$ mm/month).

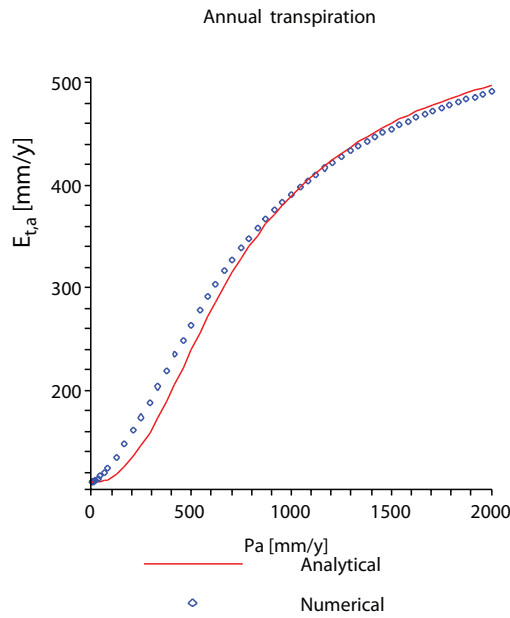


Figure 5.11: Comparison of the numerical (with Markov properties of Harare) and analytical (without Markov properties, $E(n_{r,d}|n_m) = 15$ days) annual transpiration model ($D_{i,d} = 5$ mm/day, $D_{t,m} = 82$ mm/month, $A = 15$ mm/month).

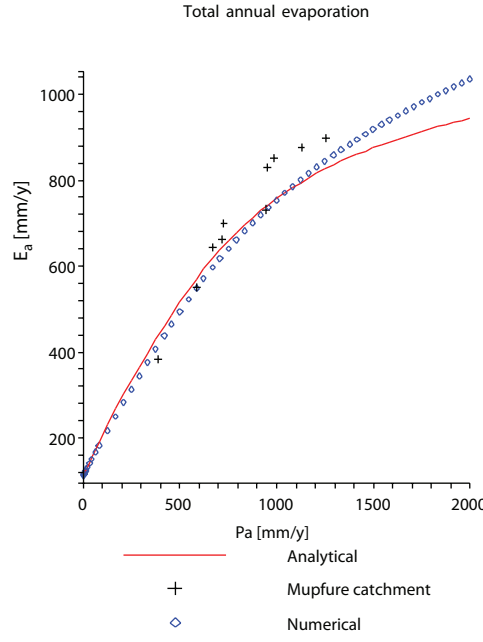


Figure 5.12: Comparison of the numerical (with Markov properties of Harare) and analytical (without Markov properties, $E(n_{r,d}|n_m) = 15$ days) annual evaporation model ($D_{i,d} = 5$ mm/day, $D_{t,m} = 82$ mm/month, $A = 15$ mm/month) and observed data from the Mupfure catchment (Zimbabwe).

catchment (circa 50 km northwest of Beatrice), the observations at Beatrice are assumed to be highly correlated with our findings for Harare. It appears that our formula underestimates the annual total evaporation. The most likely cause of this discrepancy is that in the Mupfure catchment intensive irrigation takes place, which causes higher actual evaporation than in an undisturbed catchment where evaporation is calculated as the difference between precipitation and runoff. Mazvimavi [1998] (in IWRMS [2001]) estimated that this water use amounts to about 40 mm/year. Another reason for the discrepancy is that in the Mupfure basin the number of rain days is slightly higher than in Harare.

5.5 From evaporation model to Budyko curve

In Figure 5.13 the results of our model are compared with the different types of Budyko curves. In our approach each location appears as a single dot for every year. In principle at a given location a dot can be produced if P_a , E_p and rainfall characteristics are known. Here we only had one long term average value for E_p which was combined with the average annual rainfall characteristics. The number of rain days (i.e., days with more rainfall than 0.1 mm/day) are obtained from the CRU TS 2.1 data set (Mitchell and Jones [2005]). Furthermore, for all locations a daily interception threshold ($D_{i,d}$) of 5 mm/day has been used. The monthly transpiration threshold, $D_{t,m}$ is calculated as $(E_p - E_{i,a})/n_a$, which means that the interception process is considered to absorb the available energy first, while only the remaining potential evaporation is available for transpiration.

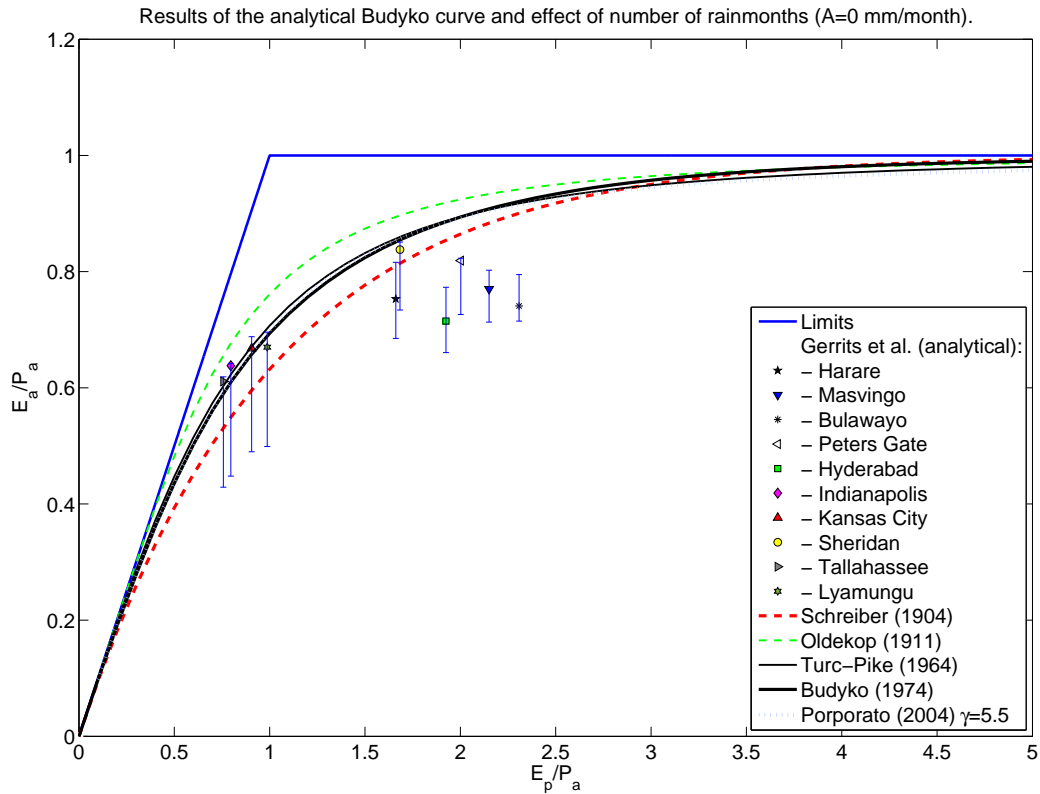


Figure 5.13: Results of the analytical model for the ten locations and the different classical Budyko curves, as well as the effect of number of rain months on the Budyko curve. The lower bound represents a number of rain months of 6 and the upper bound a number of rain months of 12.

5.6 Discussion

The results presented in Figure 5.13 deviate from the classical Budyko curves. For some locations our results yield more evaporation than predicted by the existing curves, while others yield less. In general, locations with a distinct monsoon season, like southern Africa, underestimate evaporation and are closer to Schreiber [1904]’s curve, while others are closer to Budyko [1974]’s curve. In order to explain this discrepancy, we looked at the possible effect of the most sensitive parameter: $n_{r,m}$, the number of rain months per year. This is the indicator for a climate with a distinct dry and wet season (see Figure 5.8). In Figure 5.13 the range of possible outcomes is presented. The upper bound corresponds with 12 rain months per year and the lower bound represents 6 rain months per year. It is clear that the monsoon effect can not explain the discrepancy. However, it is clear that the outliers are from stations with a clear dry season.

Another possible explanation was mentioned by Budyko [1974] and Potter et al. [2005]. They found systematic deviations for certain catchments and they explained the effect by seasonality. They observed that locations where monthly potential evaporation and precipitation rates are in phase, in general are overestimated the classical Budyko curves. Locations where the potential evaporation and precipitation are out of phase, are generally underestimated. Milly [1994] investigated this process in more detail. He developed a model where he incorporated season-

ality and demonstrated that he could explain the deviations. In our locations we see the same: the locations that are out of phase plot below the curves, and those that are in phase plot higher.

A possible reason for this effect could be vegetation as also suggested by Milly and Dunne [1994]. In areas where potential evaporation and precipitation are out of phase, for example in semi-arid regions, vegetation has been adapted to the rainfall pattern. In times of droughts, plants can withdraw water from deeper layers by developing a deep root system. Hence they still can transpire even during the dry season. This process can be modeled by the carry-over factor A of Equation 5.23. If we estimate a reasonable value for this water consumption from deeper layers (see Table 5.3), our results improve significantly. In Figure 5.14 the results are shown. These results should be seen as an indication of the amount of the annual carry-over required to compensate for seasonality, and not as a confirmation of this process. Further research is required to test this hypothesis.

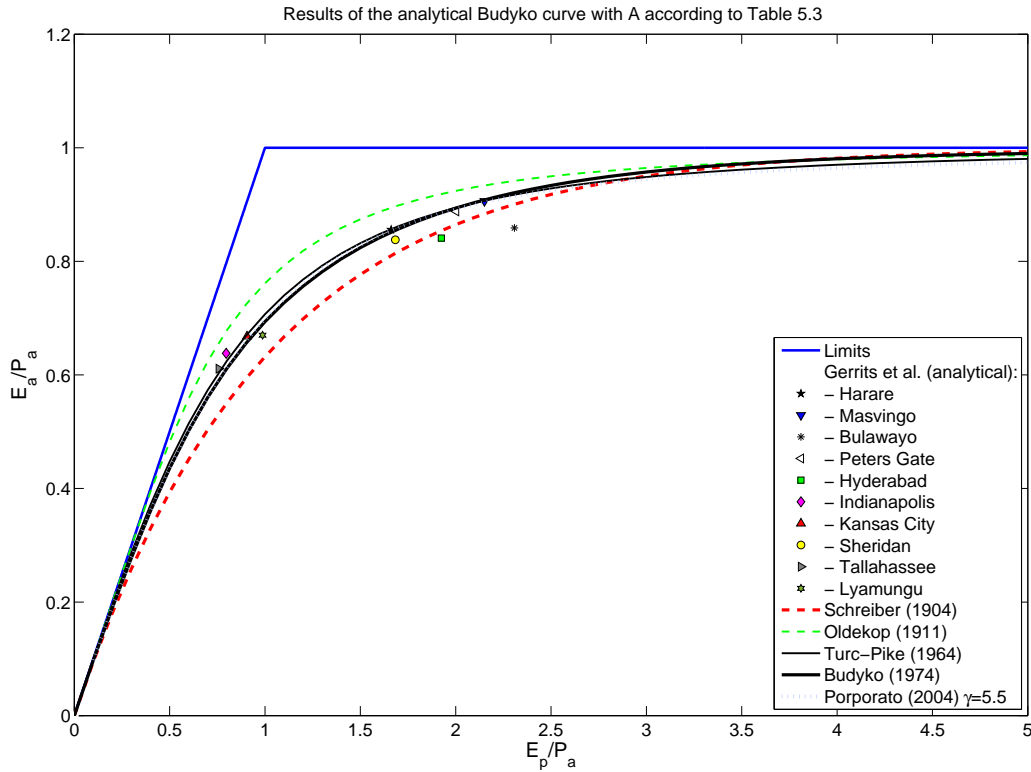


Figure 5.14: Results of the analytical model for the ten locations and the different classical Budyko curves when taking deep root systems into account.

Another seasonality effect is the change in interception threshold, $D_{i,d}$ and transpiration threshold, $D_{t,m}$ throughout the seasons. In our approach, we use a constant value. By neglecting the seasonality of the transpiration threshold an error is made, since most vegetation has a distinct growing and dormant period. However, one may question if this is a wrong assumption for the interception process. Often it is concluded that the interception capacity changes throughout the year (e.g., Link et al. [2004] and Loustau et al. [1992]). During summer time higher canopy

storage capacity values are observed, because deciduous trees still have leaves. During fall, the trees drop their leaves, so the canopy storage capacity is less. However, in our model interception is not only defined as canopy interception, but as the sum of canopy and forest floor interception. When a tree loses its leaves, they fall on the ground and stay there for a long time. Hence, one might expect that the total interception capacity remains the same (or does not differ much) over the year.

This effect is observed by our field measurements in the Huewelerbach. The storage capacity of the canopy has a coefficient of variation of 54% (Figure 3.6) and the forest floor a c_v of 28% (Figure 3.8). When the two are added the total c_v is 32%. Hence a large reduction in the seasonal variation compared to the case when only canopy storage was considered. Furthermore, our Budyko model uses a daily threshold with the dimension $[L T^{-1}]$ and not the storage capacity with dimension $[L]$. The used threshold is thus equal to S_i times the mean number of rain events per day. Since the mean number of rain events is often inversely related to the seasonal pattern in S_i this dampens the seasonal effect even more.

5.7 Conclusions

A lot of research has been done on finding the relation between the aridity index and actual evaporation as a function of annual precipitation. Although observations do not fully agree with empirical relationships, all these curves have similar shapes. The model presented in this paper lies within the range of these curves and the scatter plots generated by observations. The evaporation model distinguishes between interception and transpiration. Interception is modeled as a threshold process on daily time scale. It is upscaled by Equation 5.11 making use of the daily rainfall characteristics and the expected rain days per month. Successively, monthly interception is upscaled to annual interception, making use of the rainfall distribution of monthly rainfall. Also transpiration can be modeled as a threshold process on a monthly timescale and successively upscaled to annual transpiration. For the expected rain days per month two equations are used. One where the number of rain days is considered proportional to the monthly rainfall and one where the Markov properties of daily rainfall are used. The first equation can be solved analytically and is summarized in Table 5.4. The equation with Markov properties could not be solved analytically, hence it is solved numerically.

The analytical and numerical solutions differ for interception and transpiration, but when added up, the difference in the total evaporation is less. If the model output is compared with measured data from Harare, we can conclude that the annual evaporation model performs quite well for this location.

Since the analytical and the numerical solutions do not differ much, we applied the analytical model for ten locations around the world in different climates. The results look promising and do

not deviate much from the classical Budyko curves. Remarkable is the fact that locations with a distinct rainy season are below the existing curves and the others are on the formula found by Budyko [1974], yielding highest evaporation to precipitation ratios. Budyko [1974], Potter et al. [2005], and Milly [1994] gave a possible explanation for this. They claim that this can be caused by the phase difference between potential evaporation and rainfall. When a carry-over factor, A , is used for semi arid areas (which takes into account that plants can withdraw water from deeper layers by developing a deep root system) the results improve significantly.

Concluding, the analytical model, with only five (measurable) parameters, is capable of representing the Budyko curve. However, further research is necessary on the seasonality of the thresholds for interception and transpiration.

	Interception	Transpiration
Daily	[Eq. 5.8]: $E_{i,d} = \min(D_{i,d}, P_d)$	-
Monthly	[Eq. 5.12]: $E_{i,m} = P_m (1 - \exp(-\phi_{i,m}))$	[Eq. 5.18]: $E_{t,m} = \min(A + B \cdot (P_m - E_{i,m}), D_{t,m})$
Annual	[Eq. 5.16]: $E_{i,a} = P_a \left(1 - 2\phi_{i,a} K_0 \left(2\sqrt{\phi_{i,a}} \right) - 2\sqrt{\phi_{i,a}} K_1 \left(2\sqrt{\phi_{i,a}} \right) \right)$	[Eq. 5.23]: $E_{t,a} = 2BP_a \left(\phi_{i,a} K_0 \left(2\sqrt{\phi_{i,a}} \right) + \sqrt{\phi_{i,a}} K_1 \left(2\sqrt{\phi_{i,a}} \right) \right) \times \left(\frac{A}{\kappa_n B} + 1 - \exp(-\phi_{t,a}) \left(\frac{A}{\kappa_n B} + 1 + \phi_{t,a} - \frac{1}{B} \phi_{t,a} \right) \right)$

$$\text{with } \phi_{i,m} = \frac{D_{i,d}}{\beta}, \phi_{i,a} = \frac{n_{r,d} D_{i,d}}{\kappa_m} \text{ and } \phi_{t,a} = \frac{D_{t,m}}{\kappa_n}$$

Table 5.4: Summary of the solution of the analytical evaporation model without Markov properties.

Chapter 6

Conclusions and Recommendations

6.1 The role of interception in the hydrological cycle

Interception has mainly three roles in the hydrological cycle: interception as a rainfall reducer, interception as a spatial redistributor, and interception as a temporal redistributor. The three roles are described in the following sections.

Interception as a rainfall reducer

The most widely known effect of interception is that interception causes less water to be available for infiltration. A part of the rainfall is intercepted and directly fed back to the atmosphere. On our three experimental plots we observed that a significant amount was intercepted, especially if one takes into account that interception can occur in multiple layers. In the beech forest (Huewelerbach) the canopy intercepted on average 7% in winter and 15% in summer. Subsequently, the forest floor intercepted 22% of throughfall, causing that in total 27-34% of the rainfall evaporated, which is about 34-43% of actual evaporation. The Cedar forest floor (Botanical Garden) intercepted 18% of throughfall on average and showed little seasonal variation: in summer 20% evaporated and in winter 16% of throughfall. The setup in Westerbork showed a larger variation throughout the year. The moss/grass floor intercepted 25% of rainfall in summer and 15% in winter when corrected for transpiration. Table 6.1 presents an overview of all setups.

Species	Location	Season	P	$E_{i,c}$	$E_{i,f}$	E_i
Beech	Huewelerbach	Summer	100%	15%	19% (22% of T_f)	34%
		Winter	100%	7%	20% (22% of T_f)	27%
Moss/Grass	Westerbork	Summer	100%	-	25%	25%
		Winter	100%	-	15%	15%
Cedar	Botanical Garden	Summer	100%	-	- (20% of T_f)	-
		Winter	100%	-	- (16% of T_f)	-

Table 6.1: Overview of interception evaporation as percentage of gross precipitation (average over observation period). Canopy interception has not been measured for the cedar trees.

The amount of interception depends on three factors:

- Available storage,
- Precipitation characteristics, and
- Potential evaporation;

The first factor is most widely recognized. Many interception studies focus on the determination of storage capacities of different vegetation species, since the storage is considered to be the most dominant feature of the process of interception. This appears not to be true. We found in Chapter 3 that a variation in storage capacity of $\pm 100\%$ only resulted in a change of 11% in evaporation when a Rutter model is applied. Especially, canopy interception is not dominated by the storage, but more by the evaporative demand caused by wind fluxes. On the other hand, storage is more important for the forest floor, most probably as a result of the low wind speed at ground level. In Table 6.2 we present the storage capacities we determined.

Species	Location	Season	S_c [mm]	S_f [mm]
Beech	Huewelerbach	Summer	0.9 ± 0.5 ($c_v = 54\%$)	1.8 ± 0.4 ($c_v = 19\%$)
		Winter	0.4 ± 0.2 ($c_v = 46\%$)	1.8 ± 0.8 ($c_v = 50\%$)
Moss/Grass	Westerbork	Summer	-	4.1 ± 1.0 ($c_v = 24\%$)
		Winter	-	2.0 ± 0.9 ($c_v = 45\%$)
Cedar	Botanical Garden	Summer	-	1.0 ± 0.3 ($c_v = 35\%$)
		Winter	-	1.0 ± 0.3 ($c_v = 35\%$)

Table 6.2: Overview of interception storage in mm with coefficient of correlation. Canopy interception is not measured for the cedar trees.

The second important factor is the rainfall characteristic. Firstly, the storm depth determines the possible amount of interception, but even more important is the temporal distribution of rain events. This is also confirmed by the sensitivity analysis in Chapter 5, where the number of rain days per month and the number of rain months per year are the most sensitive parameters for interception.

The third factor determines the maximum possible interception. In temperate climates, potential evaporation is often a limiting factor. The potential evaporation is higher for the canopy, due to turbulent wind fluxes, compared to low wind fluxes at the forest floor. Combined with the relatively higher storage capacity of the forest floor, this results in longer time scales for the forest floor than for the canopy.

By combining the three main factors we developed an annual interception model as a function of rainfall. The model is based on a simple daily threshold model for interception and successively integrated over time by taken into account the temporal rainfall frequency distribution. In Figure 6.1 an example is given of the annual interception model. It shows the importance of interception and the reduced amount of precipitation that is available for infiltration (and superficial runoff).

By combining this model with a monthly threshold transpiration model, we derived an annual evaporation model that shows the total influence of interception in the water balance and provides a physical explanation for the empirical Budyko curve.

Interception as a spatial redistributor

It is true that on average interception acts as a rainfall reducer; however, locally this is not necessarily the case. Although on most locations throughfall is less than gross precipitation, at some locations throughfall can exceed gross precipitation by a factor two or three. This is caused by funneling of tree branches and is often observed in interception studies. The locally high concentration of throughfall is compensated by the remaining area where throughfall is largely reduced.

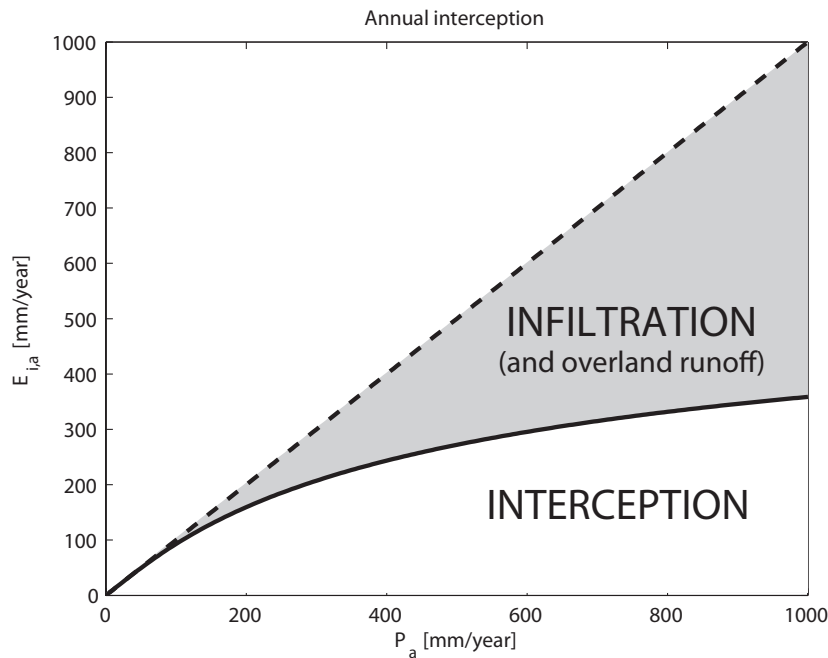


Figure 6.1: Interception as a function of precipitation (from Figure 5.2C).

The importance of branch structure also becomes evident when looking at spatial patterns in time. For the experimental site in Luxembourg it appeared that the hot spot remained throughout the seasons; however, the general persistence of the spatial pattern is weak.

Due to the canopy, the spatial pattern in summer is slightly more heterogeneous than in winter, although this is not a clear relation when analysed with semi-variograms. In summer and winter the correlation length (range) varies between 6 and 7 m. However, in the transition seasons the correlation length is significantly lower.

The spatial distribution of throughfall is important because it has a large impact on subsurface storm flow (SSF) behaviour. It appears that the spatial pattern affects both the SSF generation and the spatial variability along a hillslope, but only marginally the total SSF amount. Main cause for the differences in SSF-outflow is likely the relation between throughfall pattern and fill and spill areas.

Throughfall patterns also have an influence on soil moisture patterns during and shortly after a rain event. With a semi-variogram analysis we showed that throughfall patterns are especially important with large storms and gentle slopes. However this conclusion is based on a virtual experiment and should be confirmed with real soil moisture observations.

Interception as a temporal redistributor

Interception causes rainfall to be delayed before it reaches the ground where it can infiltrate.

This is the reason that one can shelter under a tree for a while to avoid becoming wet; however, only for a short period of time. After the storage capacity is reached, drainage starts and a subsequent interception process can start (e.g., forest floor interception). Depending on the number of interception storages the delay between rainfall and infiltration increases. This delay equals the total interception storage ($\sum S_c, S_f, \dots$) divided by the average rain intensity. We stated earlier that the storage capacity and the rain intensity are heterogeneous in space, which implies that delay time is not the same at every location.

6.2 Outlook

More than 2000 articles have been published on interception studies (source: Scopus and ISI Web of Knowledge SM) and still new articles are being published. Most of these articles focus on canopy interception and describe in detail the process for different tree species in different climates, resulting in long reference tables, as for example presented in Table 1.1 and by Breuer et al. [2003]. Although this information is of high value for modelling purposes it would have been more logical if these tables had also been available for the other types of interception, such as described in Section 1.3.

Although a more balanced database on interception values will help, it is not the complete solution for hydrological modelling. Often experimental results are site and time specific. Therefore it is difficult to upscale literature values on interception for catchment modelling.

Moreover, canopy and forest floor interception interact and strengthen each other, but this has not been much investigated so far. Generally, the two are considered in isolation, even where they occur jointly. Where the canopy is dense, less water is available for the forest floor, but also less radiation, while turbulence is reduced. This results in a reduction of forest floor evaporation. On the other hand, in dense forests the forest floor layer is thicker, and thus more water can be intercepted. This feedback interaction should be taken into account in future interception studies and therefore it is recommended to measure canopy and forest floor jointly.

In the past, several methods have been investigated and applied to quantify and study the interception process. Most techniques focused on the determination of the storage capacity, while the evaporation from interception remained underemphasized. Lysimeter set-ups in the field are the best solution to quantify both the flux and the storage. However, they often have problems with the artificial layer underneath the forest floor (so-called interface effect). A way forward could be to measure forest floor evaporation by use of tracers, such as stable isotopes. The recent improvement in isotope analysers will push forward this way of determining evaporation, although the challenge remains in figuring out a good (continuous) sampling method. Furthermore, isotope fractionation can also be used to separate interception from transpiration, since

interception fractionates while transpiration does not change the isotopic ratio. This can be helpful for interception studies on small vegetation like creeping bushes, grasses, and mosses.

Measuring interception evaporation through the energy balance may also overcome the interface effect. Knowing how the available energy is partitioned over the different fluxes and compartments, evaporation by interception can be derived. However, this would require intensive field experiments where both the energy fluxes and the evaporation processes are measured simultaneously. Flux towers will be needed to measure temperature, humidity, and wind profiles under the unstable canopy layer. Although these are complex (and therefore expensive) measurements, the biggest advantage of energy balance measurements is that the forest floor is not disturbed.

In the future, the information on energy partitioning can also be obtained from remote sensing data. Remote sensing could provide the necessary spatial and temporal information, however it is probably not able to distinguish between canopy and forest floor interception, which for most hydrological applications is not so important. Through a combination of methods interception could be more adequately incorporated in hydrological models.

References

- Allen, R. G., Pereira, L. S., Raes, D., Smith, M., 1998. Crop evapotranspiration - Guidelines for computing crop water requirements. Vol. 56. FAO - Food and Agriculture Organization of the United Nations.
- Amiro, B., 2009. Measuring boreal forest evapotranspiration using the energy balance residual. *Journal of Hydrology* 366, 112 – 118.
- Arora, V. K., 2002. The use of the aridity index to assess climate change effect on annual runoff. *Journal of Hydrology* 265, 164–177.
- Aston, A., 1979. Rainfall interception by eight small trees. *Journal of Hydrology* 42, 383–396.
- Atlas2004, 2004. Atlas hydro-climatologique du Grand-Duché de Luxembourg 2004. Tech. rep.
- Atlas2005, 2005. Atlas hydro-climatologique du Grand-Duché de Luxembourg 2005. Tech. rep.
- Atlas2006, 2006. Atlas hydro-climatologique du Grand-Duché de Luxembourg 2006. Tech. rep.
- Aussenac, G., 1968. Interception des précipitations par le couvert forestier. *Annals of Forest Science* 25, 135–156.
- Aussenac, G., Boulangeat, C., 1980. Interception des précipitations et évapotranspiration réelle dans des peuplements de feuillu (*Fagus sylvatica* L.) et de résineux (*Pseudotsuga menziesii* (Mirb) Franco). *Annals of Forest Science* 37, 91–107.
- Baird, A. J., Wilby, R. L., 1999. Eco-hydrology - Plants and water in terrestrial and aquatic environments. Routledge.
- Beard, J. S., 1956. Results of the mountain home rainfall interception and infiltration project on black wattle, 1953-1954. *Journal of South African Forestry* 27, 72–85.
- Bernard, J. M., 1963. Forest floor moisture capacity of the new jersey pine barrens. *Ecology* 44 (3), 574–576.
- Beven, K., Germann, P., 1982. Macropores and water flow in soils. *Water Resources Research* 18 (5), 1311–1325.
- Bouten, W., Heimovaara, T. J., Tiktak, A., 1992. Spatial patterns of throughfall and soil water dynamics in a Douglas fir stand. *Water Resources Research* 28, –.
- Bouten, W., Swart, P. J. F., De Water, E., 1991. Microwave transmission, a new tool in forest hydrological research. *Journal of Hydrology* 124 (1-2), 119–130.
- Brechtel, H. M., 1969. Wald und Abfluss-Methoden zur Erforschung der Bedeutung des Waldes für das Wasserdargebot. *Deutsche Gewässerkundliche Mitteilungen* 8, 24–31.
- Bréda, N. J. J., 2003. Ground-based measurements of leaf area index: a review of methods, instruments and current controversies. *Journal of Experimental Botany* 54 (392), 2403–2417.
- Breuer, L., Eckhardt, K., Frede, H.-G., 2003. Plant parameter values for models in temperate climates. *Ecological Modelling* 169 (2-3), 237 – 293.
- Bruijnzeel, L. A., 2005. Tropical montane cloud forest: a unique hydrological case. *Forests, Water and People in the Humid Tropics*, 462–483.
- Bruijnzeel, L. A., Eugster, W., Burkard, R., 2005. Encyclopedia of hydrological sciences. John Wiley & Sons, Ch. 38: Fog as a hydrologic input, pp. 559–582.
- Bruijnzeel, L. A., Wiersum, K. F., 1987. Rainfall interception by a young acacia auriculiformis

- (a.cunn) plantation forest in West Java, indonesia: application of Gash's analytical model. *Hydrological Processes* 1, 309–319.
- Bryant, M. L., Bhat, S., Jacobs, J. M., 2005. Measurements and modeling of throughfall variability for five forest communities in the southeastern US. *Journal of Hydrology* 312, 95–108.
- Budyko, M. I., 1974. *Climate and life*. Academic Press, Orlando.
- Bultot, F., Dupriez, G. L., Bodeux, A., 1972. Interception de la pluie par la végétation forestière estimation de l'interception journalière à l'aide d'un modèle mathématique. *Journal of Hydrology* 17, 193–223.
- Burghouts, T. B. A., Van Straalen, N. M., Bruijnzeel, L. A., 1998. Spatial heterogeneity of element and litter turnover in a Bornean rain forest. *Journal of Tropical Ecology* 14, 477–505.
- Burns, D. A., McDonnell, J. J., Hooper, R. P., Peters, N. E., Freer, J. E., Kendall, C., Beven, K., 2001. Quantifying contributions to storm runoff through end-member mixing analysis and hydrologic measurements at the Panola Mountain Research Watershed (Georgia, USA). *Hydrological Processes* 15 (10), 1903–1924.
- Buttle, J., 2006. Mapping first-order controls on streamflow from drainage basins: the T³ template. *Hydrological Processes* 20, 3415–3422.
- Buttle, J. M., McDonald, D. J., 2002. Coupled vertical and lateral preferential flow on a forested slope. *Water Resources Research* 38, –.
- Calder, I. R., 1986. A stochastic model of rainfall interception. *Journal of Hydrology* 89, 65–71.
- Calder, I. R., 1990. *Evaporation in the uplands*. John Wiley & Sons.
- Calder, I. R., Rosier, P. T. W., 1976. The design of large plastic-sheet net-rainfall gauges. *Journal of Hydrology* 30 (4), 403 – 405.
- Calder, I. R., Wright, I. R., 1986. Gamma ray attenuation studies of interception from Sitka Spruce: some evidence for an additional transport mechanism. *Water Resources Research* 22, 409–417.
- Calder, I. R., Wright, I. R., Murdiyarso, D., 1986. A study of evaporation from tropical rain forest - West Java. *Journal of Hydrology* 89, 13–31.
- Chilès, J. P., Delfiner, P., 1999. *Geostatistics. Modeling spatial uncertainty*. John Wiley & Sons.
- Choudhury, B. J., 1999. Evaluation of an empirical equation for annual evaporation using field observations and results from a biophysical model. *Journal of Hydrology* 216 (1-2), 99–110.
- Clark, O. R., 1940. Interception of rainfall by prairie grasses, weeds and certain crop plants. *Ecological Monographs* 10, 243–277.
- Cressie, N. A. C., 1993. *Statistics for spatial data*. John Wiley & Sons.
- Cuartas, L. A., Tomasella, J., Nobre, A. D., Hodnett, M. G., Waterloo, M. J., Múnera, J. C., 2007. Interception water-partitioning dynamics for a pristine rainforest in Central Amazonia: Marked differences between normal and dry years. *Agricultural and Forest Meteorology* 145 (1-2), 69 – 83.
- De Groen, M. M., 2002. *Modelling interception and transpiration at monthly time steps: introducing daily variability through Markov chains*. Swets & Zeitlinger BV, Lisse, the Netherlands.
- De Groen, M. M., Savenije, H. H. G., 2006. A monthly interception equation based on the statistical characteristics of daily rainfall. *Water Resources Research* 42.

- Deguchi, A., Hattori, S., Park, H., 2006. The influence of seasonal changes in canopy structure on interception loss: Application of the revised Gash model. *Journal of Hydrology* 318, 80–102.
- Dolman, A. J., Gregory, D., 1992. The parametrization of rainfall interception in GCMs. *Quarterly Journal of the Royal Meteorological Society* 118 (505), 455–467.
- Donohue, R. J., Roderick, M. L., McVicar, T. R., 2007. On the importance of including vegetation dynamics in Budyko's hydrological model. *Hydrology and Earth System Sciences* 11, 983–995.
- Dunne, T., 1978. *Hillslope Hydrology*. John Wiley & Sons, Ch. Field studies of hillslope flow processes, pp. 227–294.
- Edwards, W. R. N., 1986. Precision weighing lysimetry for trees, using a simplified tared-balance design. *Tree Physiology* 1, 127–144.
- Fenicia, F., Savenije, H. H. G., Avdeeva, Y., 2008a. Anomaly in the rainfall-runoff behaviour of the Meuse catchment. Climate, land use, or land use management? *Hydrology and Earth System Sciences Discussion* 5, 1787–1819.
- Fenicia, F., Savenije, H. H. G., Matgen, P., Pfister, L., 2008b. Understanding catchment behavior through stepwise model concept improvement. *Water Resources Research* 44, 1–13.
- Freer, J., McDonnell, J. J., Beven, K. J., Peters, N. E., Burns, D. A., Hooper, R. P., Aulenbach, B., Kendall, C., 2002. The role of bedrock topography on subsurface storm flow. *Water Resources Research* 38, –.
- Friesen, J., van Beek, C., Selker, J., Savenije, H. H. G., van de Giesen, N., 2008. Tree rainfall interception measured by stem compression. *Water Resources Research* 44, –.
- Fritschen, L. J., L. C., Kinerson, R., 1973. A 28-meter Douglas-fir in a weighing lysimeter. *Forest Science* 19, 256–261.
- Gash, J. H. C., 1979. An analytical model of rainfall interception by forests. *Quarterly Journal of the Royal Meteorological Society* 105, 43–55.
- Gash, J. H. C., Lloyd, C. R., Lauchaud, G., 1995. Estimation sparse forest rainfall interception with an analytical model. *Journal of Hydrology* 170, 79–86.
- Gash, J. H. C., Morton, A. J., 1978. An application of the Rutter model to the estimation of the interception loss from Thetford Forest. *Journal of Hydrology* 38 (1-2), 49–58.
- Gash, J. H. C., Rosier, P. T. W., Ragab, R., 2008. A note on estimating urban roof runoff with a forest evaporation model. *Hydrological Processes* 22 (8), 1230–1233.
- Gash, J. H. C., Stewart, J. B., 1975. The average surface resistance of a pine forest derived from bowen ratio measurements. *Boundary Layer Meteorol* 8, 453–464.
- Gash, J. H. C., Wright, I. R., Lloyd, C. R., 1980. Comparative estimates of interception loss from three coniferous forests in Great Britain. *Journal of Hydrology* 48 (1-2), 89–105.
- Germer, S., Elsenbeer, H., Moraes, J. M., 2006. Throughfall and temporal trends of rainfall redistribution in an open tropical rainforest, south-western Amazonia (Rondonia, Brazil). *Hydrology and Earth System Sciences* 10, 383–393.
- Gerrits, A. M. J., Hopp, L., McDonnell, J. J., Savenije, H. H. G., Pfister, L., 2010 (work in progress). The effect of spatial throughfall patterns on soil moisture patterns and the generation of subsurface stormflow. *Journal of Hydrology*.

- Gerrits, A. M. J., Pfister, L., Savenije, H. H. G., 2010 (in press). Spatial and temporal variability of canopy and forest floor interception in a beech forest. *Hydrological Processes* doi: 10.1002/hyp.7712, –.
- Gerrits, A. M. J., Savenije, H. H. G., 2010 (in press)a. *Forest Hydrology and Biogeochemistry*. Springer-Verlag, Ch. Forest floor interception.
- Gerrits, A. M. J., Savenije, H. H. G., 2010 (in press)b. *Treatise on Water Science*. Elsevier, Ch. Interception.
- Gerrits, A. M. J., Savenije, H. H. G., Hoffmann, L., Pfister, L., 2007. New technique to measure forest floor interception - an application in a beech forest in Luxembourg. *Hydrology and Earth System Sciences* 11, 695–701.
- Gerrits, A. M. J., Savenije, H. H. G., Pfister, L., 2008. Forest floor interception measurements. *IHP-VI Technical Documents in Hydrology* 81, 81–86.
- Gerrits, A. M. J., Savenije, H. H. G., Pfister, L., 2009a. Canopy and forest floor interception and transpiration measurements in a mountainous beech forest in Luxembourg. *IAHS Redbook* 326, 18–24.
- Gerrits, A. M. J., Savenije, H. H. G., Veling, E. J. M., Pfister, L., 2009b. Analytical derivation of the Budyko curve based on rainfall characteristics and a simple evaporation model. *Water Resources Research* 45, –.
- Grayson, R. B., Western, A. W., Chiew, F. H. S., Blöschl, G., 1997. Preferred states in spatial soil moisture patterns: Local and nonlocal controls. *Water Resources Research* 33, –.
- Grimmond, C. S. B., Oke, T. R., 1991. An evapotranspiration-interception model for urban areas. *Water Resources Research* 27, –.
- Guevara-Escobar, A., Gonzalez-Sosa, E., Ramos-Salinas, M., Hernandez-Delgado, G. D., 2007. Experimental analysis of drainage and water storage of litter layers. *Hydrology and Earth System Sciences* 11 (5), 1703–1716.
- Hall, R. L., Calder, I. R., 1993. Drop size modification by forest canopies: Measurements using a disdrometer. *J. Geophys. Res.* 98 (D10), 18465–18470.
- Hancock, N. H., Crowther, J. M., 1979. A technique for the direct measurement of water storage on a forest canopy. *Journal of Hydrology* 41, 105–122.
- Haynes, J. L., 1940. Ground rainfall under vegetation canopy of crops. *Journal of the American Society of Agronomy* 32, 176–184.
- Heijboer, D., Nellestijn, J., 2002. *Klimaatatlas van Nederland: de normaalperiode 1971-2000*. Elmar, Rijswijk.
- Helvey, J. D., 1964. Rainfall interception by hardwood forest litter in the southern Appalachians. *U.S. Forest Service Research Paper SE* 8, 1–8.
- Helvey, J. D., Patric, J. H., 1965. Canopy and litter interception of rainfall by hardwoods of Eastern United States. *Water Resources Research* 1 (2), 193–206.
- Herbst, M., Rosier, P. T., McNeil, D. D., Harding, R. J., Gowing, D. J., 2008. Seasonal variability of interception evaporation from the canopy of a mixed deciduous forest. *Agricultural and Forest Meteorology* 148 (11), 1655–1667.
- Hildebrandt, A., Al Aufi, M., Amerjeed, M., Shammass, M., Eltahir, E. A. B., 2007. Ecohydrology of a seasonal cloud forest in Dhofar: 1. field experiment. *Water Resources Research* 43, –.

- Hölscher, D., Köhler, L., van Dijk, A. I. J. M., Bruijnzeel, L. A. S., 2004. The importance of epiphytes to total rainfall interception by a tropical montane rain forest in Costa Rica. *Journal of Hydrology* 292 (1-4), 308–322.
- Hoover, M. D., Lunt, H. A., 1952. A key for the classification of forest humus types. *Soil Science Society Proceedings* 16, 368–371.
- Hopp, L., McDonnell, J. J., 2009. Connectivity at the hillslope scale: Identifying interactions between storm size, bedrock permeability, slope angle and soil depth. *Journal of Hydrology* 376, 378–391.
- Hörmann, G., Branding, A., Clemen, T., Herbst, M., Hinrichs, A., Thamm, F., 1996. Calculation and simulation of wind controlled canopy interception of a beech forest in Northern Germany. *Agricultural and Forest Meteorology* 79 (3), 131–148.
- Horton, R. E., 1919. Rainfall interception. *Monthly Weather Review* 47 (9), 603–623.
- Huang, Y. S., Chen, S. S., Lin, T. P., 2005. Continuous monitoring of water loading of trees and canopy rainfall interception using the strain gauge method. *Journal of Hydrology* 311, 1–7.
- Hursh, C. R., Pereira, H. C., 1953. Field moisture balance in the Shimba Hills, Kenya. *East African Agricultural Journal* 18, 139–148.
- Hutley, L. B., Dole, D. J., Y., Boonsaner, A., 1997. Water balance of an Australian subtropical rainforest at altitude: the ecological and physiological significance of intercepted cloud and fog. *Australian Journal of Botany* 45, 311–329.
- IWRMS, 2001. The Mupfure catchment. http://www.geogr.uni-jena.de//fileadmin/Geoinformatik/projekte/iwrms/www/download/other-reports/mupfure_catchment_description.pdf, (accessed on 14-10-2008).
- Jothityangkoon, C., Sivapalan, M., 2009. Framework for exploration of climatic and landscape controls on catchment water balance, with emphasis on inter-annual variability. *Journal of Hydrology* 371, 154–168.
- Keim, R., Skaugset, A., Link, T., Iroum, A., Nov. 2004. A stochastic model of throughfall for extreme events. *Hydrology and Earth System Sciences* 8 (1), 23–34.
- Keim, R. F., Skaugset, A. E., Weiler, M., 2005. Temporal persistence of spatial patterns in throughfall. *Journal of Hydrology* 314, 263–274.
- Keim, R. F., Skaugset, A. E., Weiler, M., 2006a. Storage of water on vegetation under simulated rainfall of varying intensity. *Advances in Water Resources* 29, 974–986.
- Keim, R. F., Tromp-van Meerveld, H. J., McDonnell, J. J., 2006b. A virtual experiment on the effects of evaporation and intensity smoothing by canopy interception on subsurface stormflow generation. *Journal of Hydrology* 327, 352–364.
- Kittredge, J., 1948. *Forest influences*. McGraw-Hill Book Co, New York.
- Klaassen, W., Bosveld, F., de Water, E., 1998. Water storage and evaporation as constituents of rainfall interception. *Journal of Hydrology* 212-213, 36–50.
- Klaassen, W., Lankreijer, H. J. M., Veen, A. W. L., 1996. Rainfall interception near a forest edge. *Journal of Hydrology* 185, 349–361.
- Levia, D. F., Frost, E. E., 2003. A review and evaluation of stemflow literature in the hydrologic and biogeochemical cycles of forested and agricultural ecosystems. *Journal of Hydrology* 274, 1–29.

- Li, X. Y., Gong, J. D., Gao, Q. Z., Wei, X. H., 2000. Rainfall interception loss by pebble mulch in the semiarid region of China. *Journal of Hydrology* 228, 165–173.
- Link, T. E., Unsworth, M., Marks, D., 2004. The dynamics of rainfall interception by a seasonal temperate rainforest. *Agricultural and Forest Meteorology* 124 (3-4), 171–191.
- Liu, S., 2001. Evaluation of the liu model for predicting rainfall interception in forests world-wide. *Hydrological Processes* 15, 2341–2360.
- Llorens, P., Gallart, F., 2000. A simplified method for forest water storage capacity measurement. *Journal of Hydrology* 240, 131–144.
- Lloyd, C. R., Marques, A. D. O., 1988. Spatial variability of throughfall and stemflow measurements in Amazonian rainforest. *Agricultural and Forest Meteorology* 42 (1), 63 – 73.
- Loustau, D., Berbigier, P., Granier, A., Oct. 1992. Interception loss, throughfall and stemflow in a maritime pine stand. II. An application of Gash's analytical model of interception. *Journal of Hydrology* 138 (3-4), 469–485.
- Lundberg, A., Eriksson, M., Halldin, S., Kellner, E., Seibert, J., 1997. New approach to the measurement of interception evaporation. *Journal of Atmospheric and Oceanic Technology* 14, 1023–1035.
- Manfroi, O. J., Kuraji, K., Suzuki, M., Tanaka, N., Kume, T., Nakagawa, M., Kumagai, T., Nakashizuka, T., 2006. Comparison of conventionally observed interception evaporation in a 100-m² subplot with that estimated in a 4-ha area of the same Bornean lowland tropical forest. *Journal of Hydrology* 329, 329–349.
- Mazvimavi, D., 1998. Water resources management in the water catchment board pilot areas, phase 1: data collection. Tech. rep., CASS, University of Zimbabwe.
- McIntosh, J., McDonnell, J. J., Peters, N. E., 1999. Tracer and hydrometric study of preferential flow in large undisturbed soil cores from the Georgia Piedmont, USA. *Hydrological Processes* 13 (2), 139–155.
- Miller, H. D., 1966. Transport of intercepted snow from trees during snowstorms. US Forest Service - Research paper 33, 1–30.
- Miller, J. D., Anderson, H. A., Ferrier, R. C., Walker, T. A. B., 1990. Comparison of the hydrological budgets and detailed hydrological responses in two forested catchments. *Forestry* 63 (3), 251–269.
- Milly, P. C. D., 1993. An analytic solution of the stochastic storage problem applicable to soil water. *Water Resources Research* 29, 3755–3758.
- Milly, P. C. D., 1994. Climate, soil water storage, and the average annual water balance. *Water Resources Research* 30 (7), 2143–2156.
- Milly, P. C. D., Dunne, K. A., 1994. Sensitivity of the global water cycle to the water-holding capacity of land. *Journal of Climate* 7, 506–526.
- Mitchell, T. D., Jones, P. D., 2005. An improved method of constructing a database of monthly climate observations and associated high-resolution grids. *International Journal of Climatology* 25 (6), 693–712.
- Mosley, M. P., 1979. Streamflow generation in a forested watershed, New Zealand. *Water Resources Research* 15, 795–806.

- Murakami, S., 2006. A proposal for a new forest canopy interception mechanism: Splash droplet evaporation. *Journal of Hydrology* 319, 72–82.
- Murakami, S., 2007. Application of three canopy interception models to a young stand of Japanese cypress and interpretation in terms of interception mechanism. *Journal of Hydrology* 342, 305–319.
- Muzylo, A., Llorens, P., Valente, F., Keizer, J., Domingo, F., Gash, J., 2009. A review of rainfall interception modelling. *Journal of Hydrology* 370, 191–206.
- Nakayoshi, M., Moriwaki, R., Kawai, T., Kanda, M., 2009. Experimental study on rainfall interception over an outdoor urban-scale model. *Water Resources Research* 45, –.
- Nash, J. E., Sutcliffe, J. V., 1970. River flow forecasting through conceptual models. Part I: a discussion of principles. *Journal of Hydrology* 10, 282–290.
- Navar, J., Charles, F., Jurado, E., 1999. Spatial variations of interception loss components by Tamaulipan thornscrub in northeastern Mexico. *Forest Ecology and Management* 24, 231–239.
- Nooren, C. A. M., van Breemen, N., Stoorvogel, J. J., Jongmans, A. G., 1995. The role of earthworms in the formation of sandy surface soils in a tropical forest in Ivory Coast. *Geoderma* 65, 135–148.
- Nyberg, L., 1996. Spatial variability of soil water content in the covered catchment at Gardsjön, Sweden. *Hydrological Processes* 10, 89–103.
- Oberhettinger, F., Badii, L., 1973. *Tables of Laplace Transformations*. Springer-Verlag Berlin Heidelberg, New York.
- Oke, T. R., 1982. The energetic basis of the urban heat island. *Quarterly Journal of the Royal Meteorological Society* 108 (455), 1–24.
- Ol'dekop, E. M., 1911. On evaporation from the surface of river basins. *Transactions on Meteorological Observations*. University of Tartu 4, 200.
- Onda, Y., Komatsu, Y., Tsujimura, M., Ichi Fujihara, J., 2001. The role of subsurface runoff through bedrock on storm flow generation. *Hydrological Processes* 15 (10), 1693–1706.
- Pathak, P. C., Pandey, A. N., Singh, J. S., 1985. Apportionment of rainfall in central Himalayan forests (India). *Journal of Hydrology* 76, 319–332.
- Penman, H. L., 1948. Natural evaporation from open water, bare soil and grass. *Proceedings of the Royal Society of London* 193, 120–146.
- Perrin, C., Oudin, L., Andreassian, V., Rojas-Serna, C., Michel, C., Mathevet, T., 2007. Impact of limited streamflow data on the efficiency and the parameters of rainfall-runoff models. *Hydrological Sciences Journal* 52, 131–151.
- Pfister, L., Wagner, C., Vansuypeene, E., Drogue, G., Hoffmann, L., 2005. *Atlas climatique du Grand-Duché de Luxembourg*. Johnen-Druck GmbH & Co, Bernkastel-Kues.
- Pike, J. G., 1964. The estimation of annual runoff from meteorological data in a tropical climate. *Journal of Hydrology* 2, 116–123.
- Pitman, J. I., 1989. Rainfall interception by bracken litter - relationship between biomass, storage and drainage rate. *Journal of Hydrology* 111, 281–291.
- Pitman, W. V., 1973. A mathematical model for generating monthly river flows from meteorological data in Southern Africa. University of Witwatersrand, Department of Civil Engineering, Hydrological Research Unit, South Africa 2/73.

- Porporato, A., Daly, E., Rodriguez-Iturbe, I., 2004. Soil water balance and ecosystem response to climate change. *The American Naturalist* 164 (5), 625–632.
- Potter, N. J., Zhang, L., Milly, P. C. M., McMahon, T. A., Jakeman, A. J., 2005. Effects of rainfall seasonality and soil moisture capacity on mean annual water balance for Australian catchments. *Water Resources Research* 41.
- Priestley, C. H. B., Taylor, R. J., 1972. On the assessment of surface heat flux and evaporation using large-scale parameters. *Monthly Weather Review* 100, 81–91.
- Putuhen, W., Cordery, I., 1996. Estimation of interception capacity of the forest floor. *Journal of Hydrology* 180, 283–299.
- Pypker, T. G., Unsworth, M. H., Bond, B. J., 2006. The role of epiphytes in rainfall interception by forests in the Pacific Northwest. I. laboratory measurements of water storage. *Canadian Journal of Forest Research* 36, 808–818.
- Ragab, R., Bromley, J., Rosier, P., Cooper, J. D., Gash, J. H. C., 2003. Experimental study of water fluxes in a residential area: 1. rainfall, roof runoff and evaporation: the effect of slope and aspect. *Hydrological Processes* 17 (12), 2409–2422.
- Raupach, M. R., Finnigan, J. J., Mar. 1997. The influence of topography on meteorological variables and surface-atmosphere interactions. *Journal of Hydrology* 190 (3-4), 182–213.
- Roberts, M. C., Klingeman, P. C., 1970. The influence of landform and precipitation parameters on flood hydrograph. *Journal of Hydrology* 11, 393–411.
- Rodríguez-Iturbe, I., Porporato, A., 2004. *Ecohydrology of water-controlled ecosystems*. Cambridge University Press.
- Rowe, L., 1983. Rainfall interception by an evergreen beech forest, Nelson, New Zealand. *Journal of Hydrology* 66, 143–158.
- Rutter, A. J., Kershaw, K. A., Robins, P. C., Morton, A. J., 1971. A predictive model of rainfall interception in forests. I. Derivation of the model and comparison with observations in a plantation of Corsican pine. *Agricultural Meteorology* 9, 367–384.
- Rutter, A. J., Morton, A. J., Robins, P. C., 1975. A predictive model of rainfall interception in forests. II Generalization of the model and comparison with observations in some coniferous and hardwood stands. *Journal of Applied Ecology* 12, 367–380.
- Samuel, J. M., Sivapalan, M., Struthers, I., 2008. Diagnostic analysis of water balance variability: A comparative modeling study of catchments in Perth, Newcastle, and Darwin, Australia. *Water Resources Research* 44.
- Sato, Y., Kumagai, T., Kume, A., Otsuki, K., Ogawa, S., 2004. Experimental analysis of moisture dynamics of litter layers - the effect of rainfall conditions and leaf shapes. *Hydrological Processes* 18, 3007–3018.
- Savenije, H. H. G., 1997. Determination of evaporation from a catchment water balance at a monthly time scale. *Hydrology and Earth System Sciences* 1, 93–100.
- Savenije, H. H. G., 2003. *Lecture notes Delft University of Technology: Hydrology of Catchments, Rivers and Deltas*.
- Savenije, H. H. G., 2004. The importance of interception and why we should delete the term evapotranspiration from our vocabulary. *Hydrological Processes* 18, 1507–1511.

- Savenije, H. H. G., 2005. Water Encyclopedia: Surface and Agricultural Water. Wiley Publishers, Ch. Interception.
- Schaap, M. G., Bouten, W., 1997. Forest floor evaporation in a dense Douglas fir stand. *Journal of Hydrology* 193, 97–113.
- Schellekens, J., Bruijnzeel, L. A., Scatena, F. N., Bink, N. J., Holwerda, F., 2000. Evaporation from a tropical rain forest, Luquillo Experimental Forest, eastern Puerto Rico. *Water Resources Research* 36 (8), 2183–2196.
- Schreiber, P., 1904. Über die Beziehungen zwischen dem Niederschlag und der Wasserführung der Flüsse in Mitteleuropa. *Zeitschrift für Meteorologie* 21(10), 441–452.
- Scott, R., Koster, R. D., Entekhabi, D., Suarez, M. J., 1995. Effect of a canopy interception reservoir on hydrological persistence in a General Circulation Model. *Journal of Climate* 8, 1917–1921.
- Shuttleworth, W. J., 1993. Handbook of Hydrology. McGraw-Hill, Ch. 4, pp. 4.1–4.53.
- Shuttleworth, W. J., Calder, I. R., 1979. Has the Priestley-Taylor equation any relevance to forest evaporation. *Journal of Applied Meteorology* 18, 639–646.
- Shuttleworth, W. J., Gash, J. H. C., Lloyd, C. R., Moore, C. J., Roberts, J. M., et.al, 1984. Eddy correlation measurements of energy partition for Amazonian forest. *Quarterly Journal of the Royal Meteorological Society* 110, 1143–1162.
- Simunek, J., van Genuchten, M. T., Sejna, M., 2006. The HYDRUS Software Package for Simulating the Two- and Three-Dimensional Movement of Water, Heat, and Multiple Solutes in Variably-Saturated Media: Technical Manual. Version 1.0. PC Progress, Prague, Czech Republic.
- Sivapalan, M., Blöschl, G., 1998. Transformation of point rainfall to areal rainfall: Intensity-duration-frequency curves. *Journal of Hydrology* 204 (1-4), 150–167.
- Staelens, J., De Schrijver, A., Verheyen, K., Verhoest, N. E. C., 2006. Spatial variability and temporal stability of throughfall water under a dominant beech (*Fagus sylvatica* L.) tree in relationship to canopy cover. *Journal of Hydrology* 330, 651–662.
- Stewart, J. B., 1977. Evaporation from the wet canopy of a pine forest. *Water Resources Research* 13 (6), 915–921.
- Storck, P., Lettenmaier, D. P., Bolton, S. M., 2002. Measurement of snow interception and canopy effects on snow accumulation and melt in a mountainous maritime climate, Oregon, United States. *Water Resources Research* 38, –.
- Thamm, F., Widmoser, P., 1995. Zur hydrologischen Bedeutung der organischen Auflage im Wald: Untersuchungsmethoden und erste Ergebnisse. *Zeitschrift für Pflanzenernährung und Bodenkunde* 158, 287–292.
- Thurow, T. L., Blackburn, W. H., Warren, S. D., Taylor jr, C. A., 1987. Rainfall interception by midgrass, shortgrass, and live oak mottes. *Journal of Range Management* 40 (5), 455–460.
- Toba, T., Ohta, T., 2005. An observational study of the factors that influence interception loss in boreal and temperate forests. *Journal of Hydrology* 313, 208–220.
- Tobón-Marin, C., Bouten, I. W., Dekker, S., 2000. Gross rainfall and its partitioning into throughfall, stemflow and evaporation of intercepted water in four forest ecosystems in western Amazonia. *Journal of Hydrology* 237, 40–57.

- Todorovic, P., Woolhiser, D. A., 1975. A stochastic model of n -day precipitation. *Journal of Applied Meteorology* 14, 17–24.
- Tromp-van Meerveld, H. J., McDonnell, J. J., 2006a. Threshold relations in subsurface stormflow: 1. A 147-storm analysis of the Panola hillslope. *Water Resources Research* 42, –.
- Tromp-van Meerveld, H. J., McDonnell, J. J., 2006b. Threshold relations in subsurface stormflow: 2. the fill and spill hypothesis. *Water Resources Research* 42, –.
- Tromp-van Meerveld, H. J., Peters, N. E., McDonnell, J. J., 2007. Effect of bedrock permeability on subsurface stormflow and the water balance of a trenched hillslope at the Panola Mountain Research Watershed, Georgia, USA. *Hydrological Processes* 21 (6), 750–769.
- Turc, L., 1954. Le bilan d'eau des sols. Relation entre la précipitation, l'évaporation et l'écoulement. *Annals of Agronomy* 5, 491–569.
- Valente, F., David, J. S., Gash, J. H. C., 1997. Modelling interception loss for two sparse eucalypt and pine forest in central Portugal using reformulated Rutter and Gash analytical models. *Journal of Hydrology* 190, 141–162.
- Van Dijk, A. I. J. M., Bruijnzeel, L. A., 2001. Modelling rainfall interception by vegetation of variable density using an adapted analytical model. part 1. model description. *Journal of Hydrology* 247, 230–238.
- Van Genuchten, M. T., 1980. A closed-form equation for predicting the hydraulic conductivity of unsaturated soils. *Soil Science Society of America Journal* 44, 892–898.
- Viville, D., Biron, P., Granier, A., Dambrine, E., Probst, A., 1993. Interception in a mountainous declining spruce stand in the Strengbach catchment (Vosges, France). *Journal of Hydrology* 144, 273–282.
- Wallace, J., McJannet, D., 2006. On interception modelling of a lowland coastal rainforest in northern queensland, australia. *Journal of Hydrology* 329, 477–488.
- Walsh, R. P. D., Voigt, P. J., 1977. Vegetation litter: an underestimated variable in hydrology and geomorphology. *Journal of Biogeography* 4, 253–274.
- Wang, A., Diao, Y., Pei, T., Jin, C., Zhu, J., 2007. A semi-theoretical model of canopy rainfall interception for a broad-leaved tree. *Hydrological Processes* 21 (18), 2458–2463.
- Ward, A. D., Trimble, S. W., 2004. *Environmental Hydrology*, 2nd Edition. Lewis Publishers.
- Weiler, M., McDonnell, J., Jan. 2004. Virtual experiments: a new approach for improving process conceptualization in hillslope hydrology. *Journal of Hydrology* 285 (1-4), 3–18.
- Western, A. W., Blöschl, G., Grayson, R. B., 1998. How well do indicator variograms capture the spatial connectivity of soil moisture? *Hydrological Processes* 12, 1851–1868.
- Western, A. W., Grayson, R. B., Blöschl, G., Willgoose, G. R., McMahon, T. A., 1999. Observed spatial organization of soil moisture and its relation to terrain indices. *Water Resources Research* 35, –.
- Western, A. W., Zhou, S.-L., Grayson, R. B., McMahon, T. A., Blöschl, G., Wilson, D. J., 2004. Spatial correlation of soil moisture in small catchments and its relationship to dominant spatial hydrological processes. *Journal of Hydrology* 286, 113–134.
- Whipkey, R. Z., Kirkby, M. J., 1978. *Hillslope Hydrology*. John Wiley & Sons, Ch. Flow within the soil, pp. 121–144.

- Woods, R., Rowe, L., 1996. The changing spatial variability of subsurface flow across a hillside. *Journal of Hydrology NZ* 35, 49–84.
- Woolhiser, D. A., Keefer, T. O., Redmond, K. T., 1993. Southern oscillation effects on daily precipitation in the southwestern United States. *Water Resources Research* 29 (4), 1287–1295.
- Yang, D., Sun, F., Liu, Z., Cong, Z., Lei, Z., 2006. Interpreting the complementary relationship in non-humid environments based on the Budyko and Penman hypotheses. *Geophysical Research Letters* 33.
- Yang, H., Yang, D., Lei, Z., Sun, F., 2008. New analytical derivation of the mean annual water-energy balance equation. *Water Resources Research* 44.
- Zhang, G., Zeng, G. M., Jiang, Y. M., Huang, G. H., Li, J. B., Yao, J. M., Tan, W., Xiang, R. J., Zhang, X. L., 2006. Modelling and measurement of two-layer-canopy interception losses in a subtropical mixed forest of central-south China. *Hydrology and Earth System Sciences* 10, 65–77.
- Zhang, G. P., Savenije, H. H. G., 2005. Rainfall-runoff modelling in a catchment with a complex groundwater flow system: application of the Representative Elementary Watershed (REW) approach. *Hydrology and Earth System Sciences* 9, 243–261.
- Zhang, L., Dawes, W. R., Walker, G. R., 2001. Response of mean annual evapotranspiration to vegetation changes at catchment scale. *Water Resources Research* 37, 701–708.
- Zhang, L., Hickel, K., Dawes, W. R., Chiew, F. H. S., Western, A. W., Briggs, P. R., 2004. A rational function approach for estimating mean annual evaporation. *Water Resources Research* 40.
- Ziegler, A. D., Giambelluca, T. W., Nullet, M. A., Sutherland, R. A., Tantasarin, C., Vogler, J. B., Negishi, J. N., 2009. Throughfall in an evergreen-dominated forest stand in northern Thailand: Comparison of mobile and stationary methods. *Agricultural and Forest Meteorology* 149 (2), 373 – 384.
- Zimmermann, A., Germer, S., Neill, C., Krusche, A. V., Elsenbeer, H., 2008. Spatio-temporal patterns of throughfall and solute deposition in an open tropical rain forest. *Journal of Hydrology* 360 (1-4), 87–102.
- Zinke, P. J., 1967. *Forest Hydrology*. Pergamon Press, Oxford, Ch. Forest interception studies in the United States, pp. 137–161.

Acknowledgements

People often think that doing a PhD-study is a lonely business; however, every PhD candidate knows that the opposite is true. Although there is always one name on the cover of a PhD-thesis, it should completely be filled with co-authors. The disadvantage of this ‘method’ is that you will get long Nature-like lists of authors and that you can not specify *why* and *how* those people have contributed. Luckily, this chapter allows me to do so.

First of all, I would like to thank my supervisors Huub Savenije and Laurent Pfister. Huub, thank you for all the discussion time, for always having an open office door, for your infinite effort to explain me the difference between the past tense and the present perfect (I think I owe you a new red pen), and thank you for all the opportunities you gave me. Laurent, thank you for making me feel home at the CRP in Luxembourg, for always making time in your busy schedule to discuss my progress and give me helpful feedback. Thank you for arranging my difficult administrative requests and thank you for all the joy during conferences.

Referring to joy, I would also like to thank Wim Luxemburg. Wim, thank you for introducing me into the field of hydrology and showing me the fun of fieldwork in Luxembourg. Thank you for helping me constructing my measuring devices, without you my ‘bakkies’ would not be constructed as on the drawing! Thank you for always helping me with solving my 563 equipment problems and filling the time between the 32 exits of highway E411 with your funny jokes and riddles (I think by now I know your entire repertoire).

My ‘bakkies’ would also not exist without the help of Kees van Beek and Paul Vermeulen from the electronic laboratory. Soldering and gluing strain gauges is still not my specialty, but I enjoyed the time in your workshop.

I am also grateful to the people of the Botanical Garden and ASTRON-Westerbork. All gardeners, thank you for your continuous quick, friendly and good help. observers@astron.nl thank you for regularly cleaning my tipping bucket. You saved me a lot of extra trips to Westerbork, although it was always a pleasure to visit you.

Jean François Iffly and Cyrille Tailliez: Merci beaucoup pour l’entretien de la Placette! I know how labour intensive the Huewelerbach site is and combined with all the other measuring sites

you have to maintain in Luxembourg I am very very grateful for your dedication!

I also would like to thank Jeff McDonnell, Luisa Hopp and all people from the Hillslope and Watershed Hydrology group in Oregon. I really liked the two months in Corvallis and to participate in the field course to HJ Andrews. Luisa and Mathias, thank you for showing me around in the beautiful diverse state of Oregon. I really want to come back!

Many thanks to room A0.05 of the CRP. Núria, Sebastian, Guy, Bob, Saskia, Mara, Hugo, and Fabrizio: I hope that I did not distract you too much from your work with my talking. I really enjoyed all the field trips, bowling matches, Christmas markets and pub trips. You really let me feel home in Luxembourg: thank you all!

I am also very grateful to the Water Resources Section, with whom I spend most of my time. I really appreciate the positive and informal working environment at our department, which was essential for finishing this thesis. Although I am grateful to everybody for the pleasant time, I would like mention some colleagues in specific. Hanneke de Jong and Betty Rothfusz, thank you both for taking care of all administrative paper work and for hosting the morning coffee breaks. Hessel Winsemius, Marloes Mul, Martijn Westhoff and Tatenda Tsiko, thank you for the good discussions, the fun in Luxembourg and Vienna, and for letting me win Pictionary. Nico de Vos, Guouping Zhang and Jehanzeb Cheema for putting up with my talking for a long time. I know it was not easy, but I hope you also liked it a bit. Thanks!

Finally, I would like to thank the person who is responsible for the start of my PhD study in the first place. Jeroen, with your trust you convinced me to start a PhD and gave me the confidence to finish it. You gave me a family, love, and continuous support. For you I am most grateful.

Curriculum Vitae

Miriam Gerrits was born in Haarlem, the Netherlands, on the 15th of March 1980. In 1998 she started to study Civil Engineering at Delft University of Technology, the Netherlands. During her studies she was a board member of the study association of Civil Engineering ‘Practische Studie’ with education as her field of expertise. From 2002 onwards, she was a student assistant at the Chair of Hydrology, Department of Water Managements. In 2005 Miriam graduated at this chair on the topic ‘Hydrological modelling of the Zambezi catchment for gravity measurements’.

After her MSc-degree Miriam started a PhD-study at the Public Research Center Gabriel Lippmann, Luxembourg, and Delft University of Technology on the role of interception in the hydrological cycle. She carried out field experiments in Luxembourg, the Netherlands, and Zimbabwe and developed an interception model based on only measurable parameters. Miriam presented her work on several international conferences: EGU, AGU, ERB, IAHS, and WaterNet and won the best poster award of the Water Research Center Delft in 2006. During her PhD study Miriam visited Oregon State University, USA, for two months, where she worked on a scientific paper and developed an interception module for their fieldwork course in HJ Andrews.

During her PhD, Miriam was actively involved in BSc and MSc courses and supervised several students. For the courses ‘Hydrological Measurements’, and ‘Hydrological modelling’, she wrote lecture notes, gave lectures, and guided practicals. Since 2002 Miriam was also involved in the yearly field course to Luxembourg, where MSc-students learn how to do hydrological experiments. Miriam also organized a symposium on ‘Water management in fast developing urban areas in Asia’, and was web-master of the Water Resources Section and the Boussinesq Center, the Netherlands.

The findings of her PhD study resulted in publications in peer-reviewed journals and invited book chapters.

Publications related to this thesis:

Gerrits, A. M. J., Hopp, L., McDonnell, J. J., Savenije, H. H. G., Pfister, L., 2010 (work in progress). The effect of spatial throughfall patterns on soil moisture patterns and the generation of subsurface stormflow. *Journal of Hydrology*

Gerrits, A. M. J., Savenije, H. H. G., 2010 (in press)a. *Forest Hydrology and Biogeochemistry*. Springer-Verlag, Ch. Forest floor interception

Gerrits, A. M. J., Pfister, L., Savenije, H. H. G., 2010 (in press). Spatial and temporal variability of canopy and forest floor interception in a beech forest. *Hydrological Processes* doi: 10.1002/hyp.7712, –

Gerrits, A. M. J., Savenije, H. H. G., 2010 (in press)b. *Treatise on Water Science*. Elsevier, Ch. Interception

Gerrits, A. M. J., Savenije, H. H. G., Veling, E. J. M., Pfister, L., 2009b. Analytical derivation of the Budyko curve based on rainfall characteristics and a simple evaporation model. *Water Resources Research* 45, –

Gerrits, A. M. J., Savenije, H. H. G., Pfister, L., 2009a. Canopy and forest floor interception and transpiration measurements in a mountainous beech forest in Luxembourg. *IAHS Redbook* 326, 18–24

Gerrits, A. M. J., Savenije, H. H. G., Pfister, L., 2008. Forest floor interception measurements. *IHP-VI Technical Documents in Hydrology* 81, 81–86

Gerrits, A. M. J., Savenije, H. H. G., Hoffmann, L., Pfister, L., 2007. New technique to measure forest floor interception - an application in a beech forest in Luxembourg. *Hydrology and Earth System Sciences* 11, 695–701